A THESIS FOR THE DEGREE OF DOCTOR OF PHILOSOPHY

Molecular Signaling Cascade of Indirubin-3′-monoxime in Apoptosis, Paraptosis and Inflammation

MATHARAGE GAYANI DILSHARA

Department of Marine Life Sciences
SCHOOL OF BIOMEDICAL SCIENCE
JEJU NATIONAL UNIVERSITY
REPUBLIC OF KOREA

February 2017

Molecular signaling cascade of indubin-3-monoxime in apoptosis, paraptosis and inflammation

Matarage Gayani Dilshara

(Supervised by Professor Gi-Young Kim)

A thesis submitted in partial fulfillment of the requirement of the degree of Doctor of Philosophy

2017.2

This thesis has been examined and approved by

....
Sang Rul Park, Associate Professor of Jeju National University
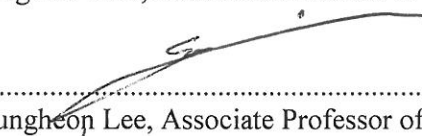
....
Seungheon Lee, Associate Professor of Jeju National University

....
Moon-Soo Heo, Professor of Jeju National University

....
Kil-Nam Kim, Senior Researcher of Korea Basic Science Institute
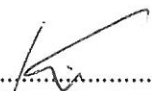
....
Gi-Young Kim, Professor of Jeju National University

February 2017
....
Date

Department of Marine Life Science

GRADUATE SCHOOL

JEJU NATIONAL UNIVERSITY

Table of Contents

Chapter 5

List of figures

v

Chapter 1

An introduction to anti-cancer mechanisms *in vitro*

1.1. Indirubin-3′-monoxime as anticancer drug

Indirubin, a 3,2-bisindole is the active ingredient of Dang Gui Long Hui Wan, from a mixture of herbal medicines customarily used in traditional Chinese medicine to treat chronic myelocytic leukemia (CML) (Kim et al., 2011). The anti-leukemic activity of this ingredient has been attributed to the red-colored indigo isomer indirubin (Perabo et al., 2006). Indirubin isolated from Chinese medicinal herbs such as *Strobilanthes cusia, Isatis indigotica, Polygonum tinctorium,* and *Isatis tinctoria* (Zhu et al., 2012). Moreover, indirubin may also derived from various natural sources such as mollusks, belonging to the Muricidae family, urine of healthy and diseased patients and different natural or recombinant bacterial species (Knockaert et al., 2004). Over the last half century, a number of indirubin analogs have been synthesized to optimize this promising drug scaffold. The commercially available analogue of indirubin, indirubin-3′-monoxime (I3M), one of the indirubin analogue strongly inhibit the growth of various human cancer cells, mainly via the apoptosis.
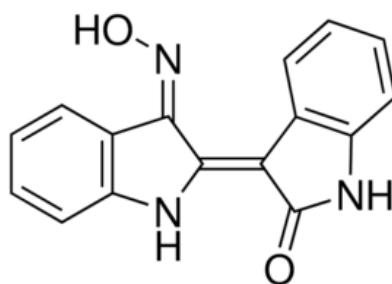
Fig. 1. Chemical structure of Indirubin-3′-monoxime

In the attempt to reveal the mechanism of action of I3M, various biological activities of I3M have been discovered. Previous studies have demonstrated that I3M is a promising anti-cancer

agent based on the capability of selectively induce apoptotic cell death in a wide spectrum of human cancer cells with minimal toxicity on normal cells and potentiates to arrest tumor growth in rat model *in vivo* (Kim et al., 2007). It has been reported to induce apoptosis in human cervical cancer HeLa cells, hepatoma HepG2 cells, colon cancer HCT116 cells (Shi and Shen, 2008), human laryngeal carcinoma Hep-2 cells (Kameswaran et al., 2009 and Paulkumar et al., 2010) prostate (Wei et al., 2015 and Rivest et al., 2011) oral (Lo and Chang., 2013) and lung (Lee et al., 2005 and Ahn et al., 2015) cancers and renal cell cancer cell lines in a time- and dose-dependent manner (Perabo et al.,2011). *In vivo* study carried out in rat tumor model provides further evidence for the anti-cancer activity of I3M.

Ravichandran *et al*. was shown indirubin-3'-monoxime exhibited anticancer effect against [B(α)P] induced lung cancer by its apoptotic action in A/J mice (Ravichandran et al., 2010). Moreover, indirubin-3'-monoxime enhances mitochondrial dysfunction and triggers growth inhibition and G_0/G_1 phase cell cycle arrest in human neuroblastoma cells (Liao and Leung., 2013). I3M induced cell cycle arrest and apoptosis in Hep-2 human laryngeal carcinoma cells associated with induction of Cdk inhibitor p21, inhibition of cyclin D1, and activation of caspase-3 (Kameswaran and Ramanibai, 2009). I3M enhances block of cancer cell growth and induced apoptosis independent up-regulation of surviving in transitional cell cancer (Perabo et al., 2006). Moreover, antiangiogenic activity of I3M was reported against human umbilical vein endothelial cells (HUVECs). Further this study has been shown that I3M inhibited proliferation, migration and tube formation of HUVEC cells (Kim et al., 2011).

1.2. Paraptosis as a cell death mechanism of cancers

Paraptosis is a new type of PCD that is specified by cytoplasmic vacuolization derived

from the swelling of endoplasmic reticulum and/or mitochondria (Wei et al., 2014). Paraptosis is distinguished from apoptosis by its non-response to caspase inhibitors (that inhibit apoptosis) and exhibit lack of apoptotic morphology including apoptotic bodies formation, caspases activation, chromatin condensation and fragmented nuclei formation (Wang et al., 2013 and Wang et al., 2014). The cell death occurred via paraptosis is also insensitive to autophagic inhibitors and overexpression of Bcl-2-like anti-apoptotic proteins (Yoon et al., 2014). Despite, investigation of compounds that potential to enhance paraptosis by targeting ER and the mitochondria may provide rational approaches towards eliminate of tumor cells effectively that evade apoptosis. However, the molecular mechanisms underlying paraptosis, specially signaling pathways involve for the progressive swelling of mitochondria and ER remain poorly understood. Recent studies have been shown that mitogen-activated protein kinases (MAPKs) are effectively involve for the paraptosis. Treatment with protein biosynthesis inhibitors like cycloheximide blocked paraptosis process by indicating requirement of active protein synthesis in paraptosis process (Yoon et al., 2014). Curcumin-induced paraptosis on malignant breast cancer cells through proteasomal dysfunction (Yoon et al., 2010). Another study regarding the curcumin-induced paraptosis trigger by sustaining overload of Ca^{2+} into mitochondria via inhibition of the mitochondrial Na^+/Ca^{2+} exchanger (mNCX) and proteasomes (Yoon et al., 2012). Furthermore, Wang *et al* reported that caspase-independent paraptosis induced by honokiol via reactive oxygen spieces in leukemia cells (Wang et al., 2013). Observations that curcumin-induced paraptosis could be inhibit by well-known proteasome inhibitors such as MG132, lactacystin, or ALLN (Yoon et al., 2012)

1.3. Apoptosis cell death as an anticancer target

Apoptosis was described in terms of characteristic changes in cell morphology, including cell shrinkage, chromatin condensation, nuclear fragmentation, and membrane blebbing (Indran et al., 2011). Apoptosis is implicated in a variety of biological processes, such as embryogenesis, regulation of the immune system, and elimination of damaged cells (Guicciardi et al., 2013). The importance of apoptosis has been emphasized by recent demonstrations involving various chemotherapeutic anti-cancer agents. Indeed, current anti-cancer therapy using many chemotherapeutic agents as well as ionizing radiation therapy activated the apoptotic machinery to kill cancer cells (Zhang et al., 2015). The last decade has shown an extraordinary development in investigation of apoptosis and cancer treatments by regulating the redox system (Circu and Aw, 2010). Furthermore, the molecular mechanisms that control and execute apoptotic cell death are being identified. In the future, it seems likely that rational strategies to manipulate cell apoptosis will be focused novel therapies that are more beneficial than current treatment regimens. Importantly, many attempts have been made to develop a new generation of anti-cancer agents from naturally derived compounds because of their fewer side effects.

p53 is a transcription factor that binds to DNA in a sequence-specific manner to activate transcription of target genes. The pathway through which p53 induces apoptosis involves regulation of transcription of target genes as well as transcription-independent mechanisms of p53, possibly reflecting distinct mechanisms of p53 action in different cell types. p53-dependent apoptosis is dependent on the Apaf-1/caspase-9 pathway and requires mitochondrial cytochrome *c* release. A number of p53-regulated genes containing p53 responsive elements have been identified, and some of these represent potential downstream mediators of p53-

dependent apoptosis including Bax, Noxa, PERP, PUMA etc:

1.4. Anti-invasive mechanism of cancer cells

Metastasis and invasion are key factors that determine the malignant behavior of cancer cells. In particular, extracellular proteinases are essential for the metastasis and invasion processes that degrade the components of the extracellular matrix (ECM) and facilitate the disconnection of intercellular adhesions and separation of single cells from solid tumor tissue to metastatic colonies at distant sites (Herszényi et al., 2014). Previous studies have shown that most of cancer cells have high metastatic ability because of the constitutive expression of several angiogenic genes including vascular endothelial growth factor (VEGF) and matrix metalloproteinase-9 (MMP-9) (Sharma et al., 2011). Matrix metalloproteinases (MMPs) are important zinc-dependent endopeptidases responsible for the degradation of major components of ECM, including type IV and V gelatin, and collagen. Thus, its role is closely related to the metastasis and invasion of cancer cell (Sekhon., 2010). Among the MMP family, which consists of 24 members, MMP-9 is known to be significantly upregulated in almost all tumor type (Löffek et al., 2011). Furthermore, MMP-9 expression positively correlates with cancer stage, grade, and prognosis (Aglund et al., 2004). Several studies have shown that cancer cells that were attributable to metastasis to distant organs, including the lungs, liver, lymph nodes, and adrenal medulla expressed high levels of MMP-9 (Löffek et al., 2011 and Minn et al., 2005). This suggests that MMP-9 is not only important in identifying invasion symptoms and its diagnosis, but also a promising strategy to prevent cancer invasion and metastasis. Therefore, MMP-9 expression may prove an important therapeutic target for preventing the invasion and metastasis of a broad-spectrum of cancers.

1.5. Aims of this study

The main purpose of this thesis was to establish the molecular signaling cascade for the anti-cancer mechanism in human cancer cells based on the I3M treatment. The consecutive signaling molecules involved in anticancer mechanism are investigated from the transcription and translation levels. The main objectives of the study were

➢ To characterized the molecules involved in cell death pathways to response I3M in human breast, prostate and hepatoma cancer cells

➢ To identify the effect of I3M as anti-invasive agent in prostate cancer cells

➢ To develop the effect of I3M as anticancer drug for the cancer patient

➢ To develop the effect of I3M as an anti-inflammatory agent to treat various types of anti-inflammatory diseases

Chapter 2

Indirubin-3′-monoxime induces cell death via paroaptosis

in MDA-MB-231 breast cancer cells: Involvement of

CHOP-mediates ER stress, ROS, and

proteasome dysfunction

Abstract

The indirubin derivative, indirubin 3′-monoxime (I3M) has already exhibited its anticancer effects by leading to cell death in different cancer cell lines and may be a novel therapeutic approach for treatment-resistant cancers. Since many cancers resistant to apoptosis, the present study reports for the first time that I3M-induced cell death by targeting paraptosis as a nonapoptotic programmed cell death mechanism. I3M significantly inhibited the cell viability in different types of cancer cell lines. However, H_2O_2-induced apoptosis was attenuated by pretreatment of z-VAD-fmk, a pan-caspase inhibitor; however, this inhibition was not observed for I3M-treated MDA-MB-231 cells. The expression of LC3-I, LC3-II, p62, and ATG-7 was not upregulated upon I3M treatment and also I3M did not induced Beclin 1 protein expression level by indicating autophagy process may not involve to cell death in MDA-MB-231 cells. As a key feature of paraptosis, I3M enhanced formation of vacuoles which are derived from mitochondria and/or the ER. Nevertheless, exposure to I3M remarkably increased ER stress protein markers such as ATF4 and p-eIF2α by activating mitogen-activated protein kinase (MAPK) signaling pathway. Moreover, I3M treatment significantly enhanced CHOP protein and m-RNA expression level, indicating that one of the major roles of CHOP is to increase I3M-mediated paraptosis. In concentration dependent treatment of I3M subsequently enhanced accumulation of poly-ubiquitinated proteins confirming I3M-induced paraptosis occurred via proteasome dysfunction. More importantly, we have shown that involvement of intra-mitochondrial Ca^{2+} in I3M-induced paraptosis in MDA-MB-231 cells. Our results demonstrate that mitochondrial Ca^{2+} accumulation possesses induction of ROS generation thus induced paraptosis followed by I3M treatment. Flow cytometry analysis showed that pretreatment with 4 μM ruthenium red remarkably decreased I3M-induced mitochondrial Rhod-2 staining intensity suggesting that Ca^{2+} accumulation into mitochondria mediate via mitochondrial

channel uniporters. Collectively, our results show that accumulation of Ca^{2+} into mitochondria via mitochondrial channel uniporters through ER stress which regulate by proteasome dysfunction mainly involved in I3M-induced paraptosis in MDA-MB-231 breast cancer cells.

Key words: paraptosis; proteasome; mitochondrial channel uniporters; poly-ubiquitinated proteins; ER stress

2.1. Introduction

Indirubin has been identified as the main active ingredient of a traditional Chinese medicinal recipe, Danggui Longhui Wan, used to treat various diseases including chronic myelocytic leukemia and certain autoimmune conditions and anti-inflammatory agent (Lee et al., 2014 and Zhang et al., 2015). Indirubin is the purple component of blue indigo dye, isolated from Chinese medicinal herbs such as *Strobilanthes cusia, Isatis indigotica, Polygonum tinctorium,* and *Isatis tinctoria* (Zhu et al., 2012). Nevertheless, indirubin may also derived from various natural sources such as mollusks, belonging to the Muricidae family, urine of healthy and diseased patients and different natural or recombinant bacterial species (Knockaert et al., 2004). However, chemically, indirubin is a 3,2′-bisindole, a stable isomer of indigo (Kim et al., 2013). It has been shown to inhibit cell growth and induce apoptosis and differentiation of human cancer cells. Recent studies have revealed that indirubin and indirubin derivatives induce the apoptosis in several human cancer cells including breast (Nicolaou et al., 2012 and Shi et al., 2012), laryngeal (Kameswaran et al., 2009), thyroid (Broecker-Preuss et al., 2015), salivary gland adenocarcimona (Yoon et al., 2010), colon (Liu et al., 2012 and Gandin et al., 2012), prostate (Wei et al., 2015 and Rivest et al., 2011), oral (Lo and Chang., 2013), and lung (Lee et al., 2005 and Ahn et al., 2015) cancers, has been suggested to possess potential in the

prevention of cancer. Since past decades, it has been used as a beneficial anti-cancer agent, because it has been exhibited to inhibit progression and suppress the initiation, proliferation and invasiveness of cancers in a wide range of models *in vivo* and *in vitro* (Williams et al., 2011).

Research on anticancer activity of I3M has so far mainly focused on its apoptosis induction potential. In contrast, in the present study we have shown that I3M inhibits proliferation of breast and hepatoma cancer cell lines through induction of paraptosis. Since inherent or acquired cellular resistance to various pro-apoptotic treatments often leads to therapeutic failure, a better understanding of alternative non-apoptotic pathways may facilitate the design of novel therapeutics against cancers. Paraptosis is a novel type of PCD that is characterized by cytoplasmic vacuolization derived from the swelling of endoplasmic reticulum and/or mitochondria (Wei et al., 2014). Paraptosis is distinguished from apoptosis by its non-response to caspase inhibitors (that block apoptosis) and lack of apoptotic morphology including formation of apoptotic bodies, activation of caspases, chromatin condensation and formation of fragmented nuclei (Wang et al., 2013 and Wang et al., 2014). This cell death occurred via paraptosis is also insensitive to autophagic inhibitors and overexpression of Bcl-2-like anti-apoptotic proteins (Yoon et al., 2014). Despite, investigation of compounds that potential to enhance paraptosis by targeting ER and the mitochondria may provide rational approaches towards eliminate of tumor cells effectively that evade apoptosis. However, the molecular mechanisms underlying paraptosis, specially signaling pathways involve for the progressive swelling of mitochondria and ER remain poorly understood. Recent studies have been shown that mitogen-activated protein kinases (MAPKs) are effectively involve for the paraptosis. Treatment of protein biosynthesis inhibitors like cycloheximide blocked paraptosis process by

indicating requirement of active protein synthesis in paraptosis process (Yoon et al., 2014). Curcumin-induced paraptosis on malignant breast cancer cells through proteasomal dysfunction (Yoon et al., 2010). Another study regarding the curcumin-induced paraptosis trigger by sustaining overload of Ca^{2+} into mitochondria via inhibition of the mitochondrial Na^+/Ca^{2+} exchanger (mNCX) and proteasomes (Yoon et al., 2012). Further, Wang *et al* reported that caspase-independent paraptosis induced by honokiol via reactive oxygen spieces in leukemia cells (Wang et al., 2013). Observations that curcumin-induced paraptosis could be inhibit by well-known proteasome inhibitors such as MG132, lactacystin, or ALLN (Yoon et al., 2010). In the current study, we have shown that I3M-induced paraptosis by accumulation of Ca^{2+} into mitochondria via mitochondrial channel uniporters through proteasome dysfunction regulate ER stress in MDA-MB-231 breast cancer cells. Moreover, the role of CHOP in I3M-mediated paraptosis was observed in MDA-MB-231 cells. These observations expand our understanding on the mechanism of action of I3M on human breast cancer cells and will facilitate further investigations into the development of new therapies for breast cancers.

2.2. Materials and method

2.2.1. Chemical reagents

Antibodies against Bid, Bax, caspase-8, CHOP, Bcl2, PERK, phospho (p)-PERK, ATF4, Becline 1, p38, phospho (p)-p38 and LC3 were purchased from Santa Cruz Biotechnology (Santa Cruz, CA). Antibodies against JNK, phospho (p)-JNK, PARP, LC3, Atg7, p62, Beclin 1, eIF2α, p-eIF2α and GAPDH were purchased from Cell Signaling (Beverly, MA). 3-(4,5-dimethyl-2-thiazolyl)-2,5-diphenyl-2H-tetrazolium bromide (MTT), *N*-acetyl-L-cysteine (NAC), glutathione (GSH), and 4′6′-diamidino-2-phenylindole (DAPI), catalase and EGTA were purchased from Sigma Chemical Co. (St. Louis, MO). PD98059, SB203580, and SP600125 were obtained from Calbiochem (San Diego, CA). Peroxidase-labeled donkey anti-rabbit and sheep anti-mouse immunoglobulin were purchased from KOMA Biotechnology (Seoul, Republic of Korea). Bafilomycin A1, Rapamycin, 3MA, MG132, Ruthenium red and RHOD 2/AM were purchased from Santa Cruz Biotechnology (Santa Cruz, CA). ER-Tracker-FITC and MitoTracker Green FM™ (MTG) were purchased from Molecular Probes (Eugene, OR). z-VAD-fmk purchased from Calbiochem (San Diego, CA). Calcium staining dye, Fluo-4AM, was purchased from Invitrogen (Carlsbad, CA).

2.2.2. Cell lines and cell culture

Human breast cancer MDA-MB-231, human prostate cancer PC3, human hepatoma Hep3B cell and human colorectal carcinoma HCT116 were obtained from the American Type Culture Collection (Manassas, VA). Cells were maintained in RPMI-1640 medium supplemented with 10% heat-inactivated FBS and 1% penicillin–streptomycin (Sigma) in 5% CO_2 at 37°C.

2.2.3. Western blot analysis

Total cell extracts were prepared using a 100 μl ice-cold PROPREP protein extraction kit (iNtRON Biotechnology). Lysates were centrifuged and protein concentrations were determined by the Bio-Rad protein assay kit (Bio-Rad, Hercules, CA). The protein was applied to a 10% to 15% SDS-polyacrylamide gel, transferred to a nitrocellulose membrane, and then detected by the proper primary and secondary antibodies before visualization by chemiluminescence kit (Amersham).

2.2.4. Reverse transcriptase-polymerase chain reaction (RT-PCR)

The total RNA was extracted from the cells using Easy-blue reagent (iNtRON Biotechnology, Sungnam, Republic of Korea), 24 h after treatment with or without different concentrations of I3M. The subsequent procedures for conducting reverse transcription were exactly the same as those in the instruction manual (RT-PCR Premix, iNtRON Biotechnology). The reverse transcription products from total RNA served as a template for PCR. Master mix (containing buffer, dNTP mix, $MgCl_2$, Taq polymerase, and nuclease-free water) to each PCR tube with appropriate primer. PCR tubes were placed in thermal cycler for amplification program, which includes three steps: denaturation, annealing, elongation. Synthesized single strand cDNA was amplified by RT-PCR with the following primer pairs: CHOP sense 5′-CAA CTG CAG AGA TGG CAG CTG A-3′ and CHOP antisense 5′-CTG ATG CTC CCA ATT GTT CAT-3′, glyceraldehyde-3-phosphate dehydrogenase (GAPDH) sense 5′-GTC TTC ACC ACC ATG GAG-3′ and GAPDH antisense 5′-CCA CCC TGT TGC TGT AGC-3′. The reaction sequence consisted of 50°C for 30 min, 94°C for 2 min, and 94 °C for 29 cycles of 15 s each;

14

60°C for 30 s; and 72°C for 45 s with an extension at 72°C for 10 min. The reaction products were analyzed on 1.2% agarose gels with ethidium bromide run at 110 V for 20 min.

2.2.5. MTT tetrazolium assay

The MTT (3-(4,5-dimethyl-2-thiazolyl)-2,5-diphenyl-2H-tetrazolium bromide) tetrazolium reduction was used to assayed viability of cells. The MTT was prepared in PBS usually at final concentration of 5mg/ml. Cells were seeded into the wells of a 24 well plate at a density of 1×10^4 cells/well and then allowed to adhere for 24 h at 37°C in a 5% CO_2. After incubation, the cells were treated with desired concentrations of I3M (0, 5, 10, 15, 20, and 25 μM) for 24 h. Tetrazolium dye (MTT; 5 mg/ml in PBS) was added to each well, again cells were incubated at 37°C for 30 min. The quantity of formazan (presumably directly proportional to the number of viable cells) was measured by recording changes in absorbance at 540 nm using a microplate reader (Thermo Electron Corporation, Marietta, OH). Triplicate experiments were performed at each concentration and the results were presented as mean ± SE.

2.2.6. Immunofluorescent Confocal Laser Microscopy

For Beclin 1 detection, cells were fixed with 4% paraformaldehyde/phosphate buffered saline (PBS) at room temperature for 20 min, permeabilized with 0.1% Triton X-100 in PBS for 10 min on ice, and then blocked with 3% bovine serum albumin/PBS for 2 h at room temperature. The fixed cells were incubated with the anti-Beclin 1antibody at 4°C for 2 h, washed with PBS, incubated for another 1 h with FITC-conjugated goat anti-rabbit IgG, and washed well with PBS. Then cells were observed by fluorescence microscopy. For nuclear

staining fixed cells were washed with PBS and nuclei stained with DAPI solution. For detection of ER and mitochondrial derived vacuoles, after incubation, the cells were treated with desired concentrations of I3M (0, 5, 10, and 15 μM) for 24 h and then 1% formaldehyde was added to each well for 30 min. Cells were permeabilized with 1% Triton X-100 for 5 min and washed twice in PBS.

2.2.7. ROS generation

MDA-MB-231 cells were seeded on 24-well plate at a density of 1×10^5 cells/ml and preincubated with florescence dye 6-carboxy-2′,7′-dichlorofluorescein diacetate (H$_2$DCFDA, Molecular Probes, Eugene, OR) for 1 h and then treated the indicated concentrations of I3M, NAC, GSH, and catalase for 24 h. The cells were lysed with triton and the sample was centrifuged and supernatant was analyzed for ROS production using GLOMAX luminometer (Promega).

2.2.8. Flow cytometry

Rhod-2 fluorescence intensity was measured with a flow cytometer (Becton Dickinson San Jose, CA). At least 10,000 cells for each sample were analyzed. The Cellquest software (Becton Dickinson San Jose, CA) was used for data analysis. To analyze the CHOP expression MDA-MB-231 cells were exposure with or without varying doses of I3M for 24 h. The cells were washed in phosphate-buffered saline (PBS) simultaneously incubated with FITC-conjugated anti-human CHOP and Beclin1 monoclonal antibodies. For negative control, cells were staining with mouse IgG$_1$ (BD Bioscience). Immunofluorecence measurements were obtained using FACSCalibur (Becton Dickinson San Jose, CA).

16

2.2.9. Transfection of CHOP and eIF2α small interfering RNS (siRNA)

CHOP and *eIF2α*-specific silencing RNA was purchased from Santa Cruz Biotechnology (Santa Cruz, CA). RPMI medium was added to 20 nM siRNA duplex with the transfection reagent G-Fectin (Genolution Pharmaceuticals, Inc., Seoul, Republic of Korea) in each transfection according to the manufacture′s recommendations.

2.2.10. Statistical analysis

All data from MTT assay, FACS analysis, RT-PCR, western blot analysis and ROS generation were derived from at least three independent experiments. Images were captured using Chemi-Capt (Vilber Lourmat) and transported into Photoshop. All bands were quantified by the Scion Imaging software (http://www.scioncorp.com). Statistical analyses were conducted using SigmaPlot software (version 12.0). Values were presented as mean ± S.E. Significant differences between the groups were determined using the one-way ANOVA. Statistical significance was regarded at [*] and [#], $p < 0.05$.

2.3. Results

2.3.1. I3M effectively induces cell death on human cancer cells

To evaluate the anticancer activity of I3M on various human cancer cells, we first examined its cytotoxic effects with different concentrations of curcumin for 24 h and performed cell viability assay. We found that I3M treatment more potently induced cell death in various cancer cell lines (Fig. 2A). Moreover, dose-dependent manner pretreatment of z-VAD-fmk did

17

not remarkably blocked I3M-induced cell death in MDA-MB-231 cells and moderately compensate in Hep3B cells; however, this z-VAD-fmk-attenuated cell death was not observed in PC-3 and HCT-116 cells (Fig. 2B). To determine whether I3M induced cell death occurred through apoptosis, cells were treated with a positive control, H_2O_2. Treatment of H_2O_2 for 24 h induced cell death on both MDA-MB-231 cells and Hep3B cells (Fig. 2C). H_2O_2-induced apoptosis was attenuated by pretreatment of z-VAD-fmk, a pan-caspase inhibitor; however, the inhibition was not observed for I3M-treated cells (Fig. 2C). Further, H_2O_2-induced apoptosis was confirmed by proteolytic cleavage of PARP, caspase-8 (Fig. 2D). In particular, with respective to the positive control H_2O_2 treatment, I3M did not induce PARP, caspase-8 cleavage. Nevertheless, treatment with I3M did not downregulated H_2O_2-attenuated Bcl-2 expression level (Fig. 2D). Phase-contrast microscopy images further revealed that PC-3 and HCT-116 cells treated with I3M displayed typical morphological features of apoptosis (Fig. 2E). Although, MDA-MB-231 cells did not show such characteristics changes related to apoptosis while Hep3B cells slightly exhibited such typical morphological features of apoptosis. Furthermore, morphological observation in the cell nuclei of MDA-MB-231 cells for 24 h after treatment of I3M did not showed any significant morphological alterations in the nuclei when compared to untreated control (Fig. 2F). However, fragmented nuclei were observed in positive control H_2O_2 treatment (Fig. 2F). Taken together these results indicate that I3M potentiate to induce apoptosis in cell type dependent manner in human cancer cells.
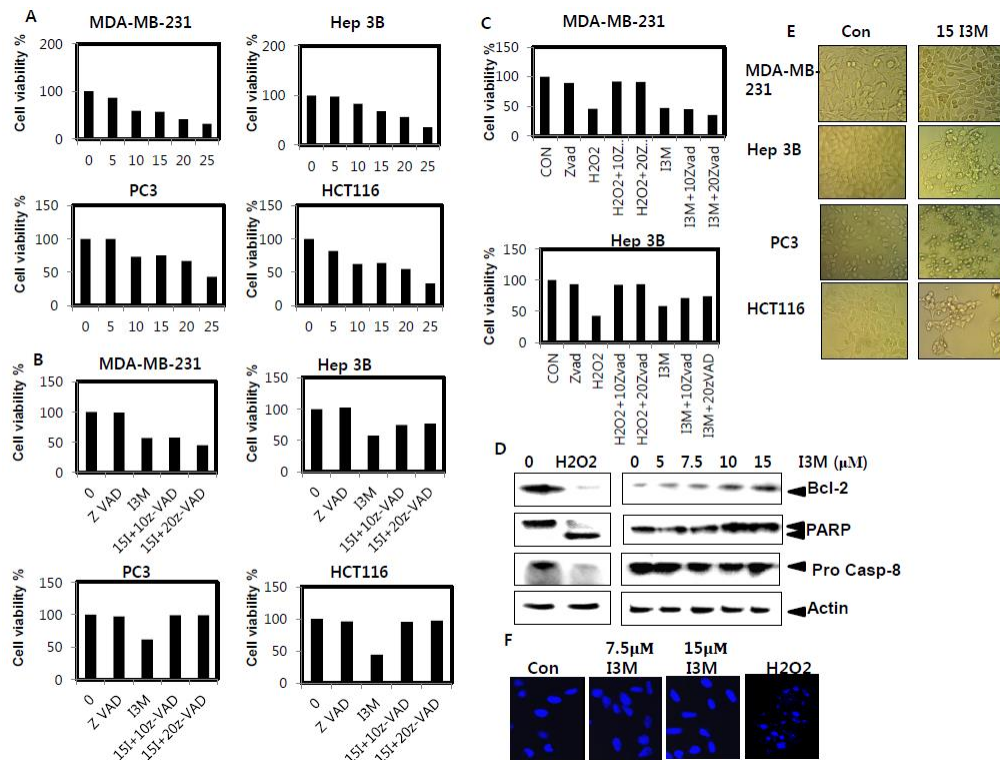
Fig. 2. Effects of I3M on the viability of cancer cells. (A) MDA-MB-231, Hep3B, PC3, and HCT116 cancer cells were treated with the indicated concentrations of I3M for 24 h. (B) MDA-MB-231, Hep3B, PC3 and HCT116 cancer cells were pretreated with the indicated concentrations of z-VAD-fmk for 1 h and further treated with 15 μM I3M for 24 h. Cell viability was measured by an MTT assay following 24 h. (C) MDA-MB-231 and Hep3B cells were pretreated with the indicated concentrations of z-VAD-fmk for 1h and further treated with 500 μM H_2O_2 or 15 μM I3M for 24 h. Cell viability was measured by an MTT assay following 24 h. (D) MDA-MB-231 cells were treated with 500 μM H_2O_2 or various concentrations of I3M. Equal amount of cell lysates was resolved on SDS–polyacrylamide gels, transferred to nitrocellulose membranes, and probed with antibodies against Bcl-2, PARP, and caspase-8. (E) The morphology of cells treated with or without I3M was examined under light microscopy (×400). (F) MDA-MB-231 cells were treated with indicated concentrations of I3M for 24 h.

Cells were stained with cell-permeable DNA-binding dye DAPI for 10 min at room temperature, visualized and analyzed by fluorescence microscopy. β-Actin was used as an internal control for western blot analyses.

2.3.2. Autophagy may not regulate by I3M

To investigate whether the caspase-independent cell death was mediated through autophagy, next we examined the expression of several proteins known to be participated in the induction of autophagy, including LC3-I, LC3-II, p62, and Atg-7, in MDA-MB-231 cells treated with I3M in concentration dependent manner. The upregulation of expression of LC3-II, Atg-7 and downregulation of p62 were not observed upon treatment with I3M (Fig. 3A). The induction of these proteins was significantly counteracted by the addition of 3MA, a known inhibitor of autophagy by indicating I3M did not induced autophagy in MDA-MB-231 cells (Fig. 3A). Next we detected the expression of Beclin 1, an important marker of autophagy, in MDA-MB-231 cells upon treatment with I3M, Rapamycin, inducer of autophagy, and 3MA, an inhibitor of autophagy. We found that pretreatment of Rapamycin enhanced the Beclin 1 protein level while 3MA treatment completely blocked expression of Beclin 1 (Fig. 3B). Similar to the data of 3MA treatment, I3M did not induced Beclin 1 protein expression level in MDA-MB-231 cells. For further examine the role of autophagy in I3M-induced cell death, we treated MDA-MB-231 cells with I3M before treatment with anti-Beclin1 antibody and assayed for Beclin1 expression. Our data showed that similar to the untreated group, treatment with I3M could not induce the Beclin 1 protein expression level in MDA-MB-231 cells (Fig. 3C). Collectively these results suggested that autophagy process may not involve as a cell death program in I3M-mediated cell death in MDA-MB-231 cells.
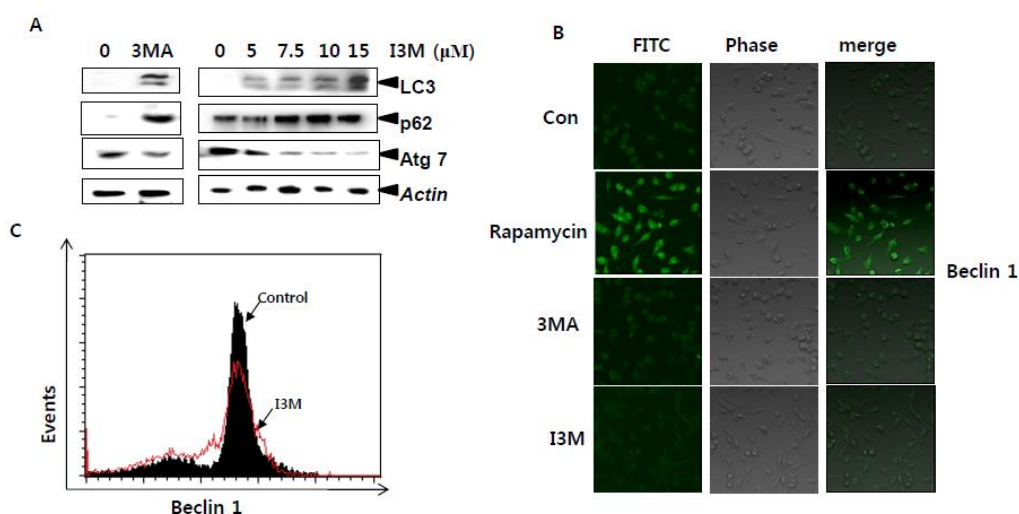
Fig. 3. I3M inhibits autophagy in MDA-MB-231 cells. (A) MDA-MB-231 cells were treated with 5mM 3MA or various concentrations of I3M for 24 h. Equal amount of cell lysates were resolved on SDS–polyacrylamide gels, transferred to nitrocellulose membranes, and probed with antibodies against LC3, p62, and Atg7. (B) MDA-MB-231 cells were pretreated with 1Mm Rapamycin and 0.6 mM 3MA for 1h and then incubated with 15 μM I3M for 24h. Cells were fixed, permeabilized, and stained with Beclin 1 monoclonal antibody. The monoclonal antibody was detected using an antimouse secondary antibody conjugated with Alexa Fluor® 488. Stained-Beclin 1 then observed under a fluorescent microscope (×400). (C) MDA-MB-231 cells were treated with 15 μM I3M for 24 h. Flow cytometry was conducted to analyze the expression level of Beclin 1. β-Actin was used as an internal control for western blot analyses.

2.3.3. Involvement of ER and mitochondria in I3M induce paraptosis

Investigation of the cellular morphologies showed that marked cellular vacuolation commonly preceded cell death in MDA-MB-231 cells. In concentration and time dependent

manner treatment of I3M significantly induced vacuolated cells percentage as ~20-67 % and ~18-68 % respectively (Fig. 4A). After I3M treatment for 12 h, vacuoles were clearly discernible by phase-contrast microscopy. Next, to examine whether the I3M-enhanced vacuoles may derive from mitochondria and/or the ER, cells were exposure to ER-tracker and Mito-tracker. Compared with the untreated group, at 24 h after I3M treatment increased numerous small both ER and mitochondria derived fluorescent vacuoles (Fig. 4B). Treatment of I3M in concentration dependent manner significantly accumulated polyubiquitinated proteins. Consequently, I3M significantly increased priteins levels of ATF4 and p-eIF2α at 24 h by indicating that I3M treatment induced the ER stress in MDA-MB-231 cells (Fig. 4C, upper panel). Moreover, time-dependent treatment of 15μM I3M remarkably increased ATF4 and p-eIF2α protein levels (Fig. 4C, lower panel). To determine the importance of ER stress proteins in paraptosis, sieIF2α were transfected into MDA-MB-231 cells and transfection efficiency was analyzed by western blot (Fig. 4D). Cell viability assay shown transient knockdown of eIF2α markedly attenuated I3M-induced cell death (Fig. 4E). Research has indicated that mitogen-activated protein kinase (MAPK) signaling pathways have a role in the response to ER stress. Based on that next, we examined the protein expression level of p-ERK, p-p38, and p-JNK after the exposure to I3M. We found that 24 h of I3M treatment upregulated the phosphorylation of JNK protein level while enhanced the phosphorylation of p38 protein level in constant manner (Fig. 4F). According to our results, phosphorylated ERK activated only in between 6-9 h. Moreover, when further examine the activation differences of these proteins we detected the pretreatment of JNK inhibitor SP600125, markedly enhanced I3M-decreased cell viability (Fig. 4G). However, I3M-downregulated cell viability did not affect by the pretreatment of p38 inhibitor SB203580 and ERK inhibitor PD98059 (Fig. 4G). Collectively,

our results show that involvement of ER and mitochondria in I3M-induced paraptosis accomplished by MAPK signaling pathway in MDA-MB-231 breast cancer cells.
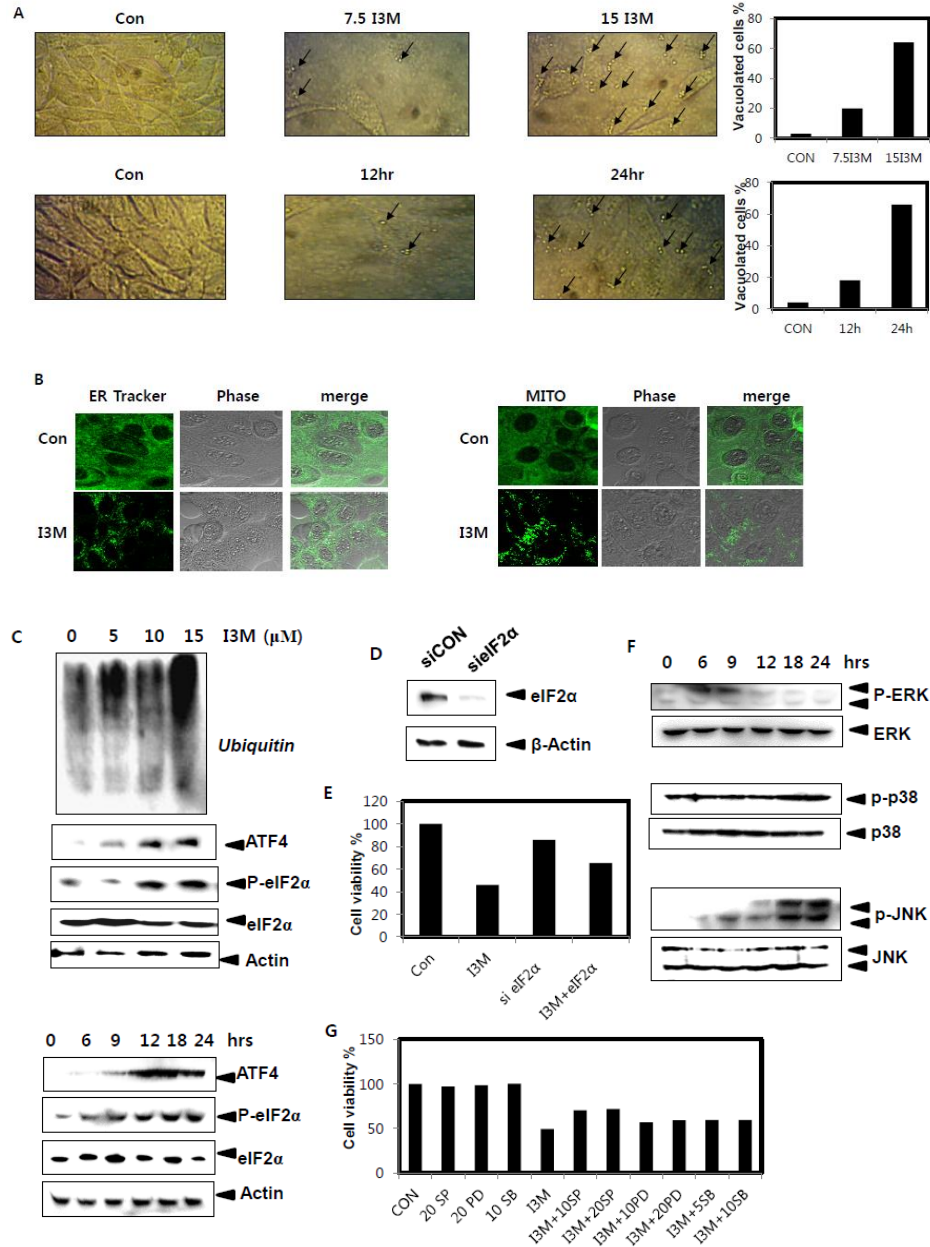
Fig. 4. I3M induced vaculization and ER stress in MDA-MB-231 breast cancer cells. (A) MDA-MB-231 cells were seeded at 2×10^5 cells/ml and incubated with 15 μM I3M for the indicated time (0-24 h) and/or cells were incubated with indicated concentrations of I3M (0-15

μM) for 24 h. Cells were examined under light microscopy (×400) and percentage of vacuolated cells were calculated. (B) Cells were stained with ER Tracker and Mito Tracker followed by with or without I3M treatment for 24 h. Cells were observed under a fluorescent microscope (×400). (C) Cells were seeded at 2×10^5 cells/ml and incubated with 15 μM I3M for the indicated time (0-24 h) and/or cells were incubated with indicated concentrations of I3M (0-15 μM) for 24 h. Cells were harvested and the indicated proteins were detected by Western blot analysis. (D) Cells were transiently transfected with *eIF2α* siRNA for 24 h. The transfection efficiency was assayed by western blot analysis. (E) Cells were transiently transfected with *eIF2α* for 24 h and then treated with or without before treatment with15 μM I3M for 24 h. Cell viability was determined using an MTT assay. (F) Cells were incubated with 15 μM I3M for the indicated time (0-24 h) and the indicated proteins were detected by Western blot analysis. (G) MDA-MB-231 cells were pretreated with the specific inhibitors, SP600125, PD98059, and SB203580 at the indicated concentrations for 1 h and further treated with 15 μM I3M for 24 h. The viability of cells was determined using an MTT assay.

2.3.4. Involvement of CHOP in I3M-induced paraptosis

In order to investigate the importance of CHOP in regulation of I3M-mediated paraptosis we knockdown CHOP using small interfering RNA (siRNA) and examined the vacuoles derived by ER and mitochondria. A specific siCHOP were transfected into MDA-MB-231 cells and transfection efficiency was analyzed by western blot (Fig. 5A). As shown in Fig. 5B, knockdown of CHOP blocked I3M-induced ER and mitochondrial vacuoles formation (Fig. 5B). In a parallel experiment we examined the cell viability using MTT assay. Pretreatment of siCHOP significantly blocked I3M-induced cell death in MDA-MB-231 cells (Fig. 5C).

24

Immunocytochemistry analysis of CHOP shown that treatment with 10 μM I3M resulted in enhanced the CHOP expression level (Fig. 5D). Further, the expression level of CHOP significantly increased with the treatment of I3M in concentration dependent manner (Fig. 5E). Nevertheless, to further confirmation, time dependent manner treatment of I3M-remarkably enhanced m-RNA and protein expression level of CHOP reached its peak at 12h of the I3M treatment. Then, we assessed the mRNA and protein expression level of CHOP in the presence of I3M. Treatment of I3M significantly enhanced CHOP protein and m-RNA expression level, indicating that one of the major roles of CHOP is to increase I3M-mediated paraptosis (Fig. 5F). These data indicate that in the presence of I3M, increased levels of CHOP enhanced paraptosis in MDA-MB-231 cells.
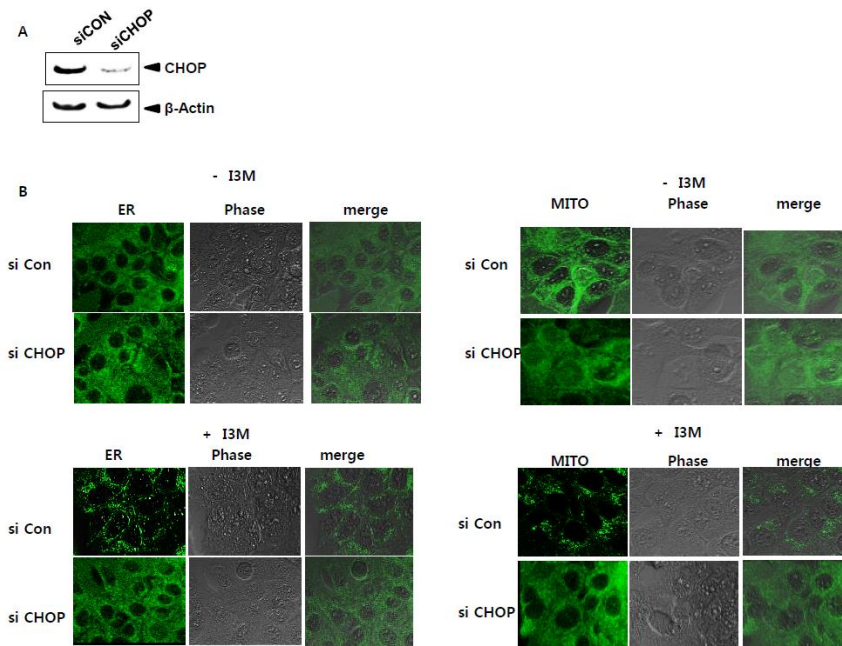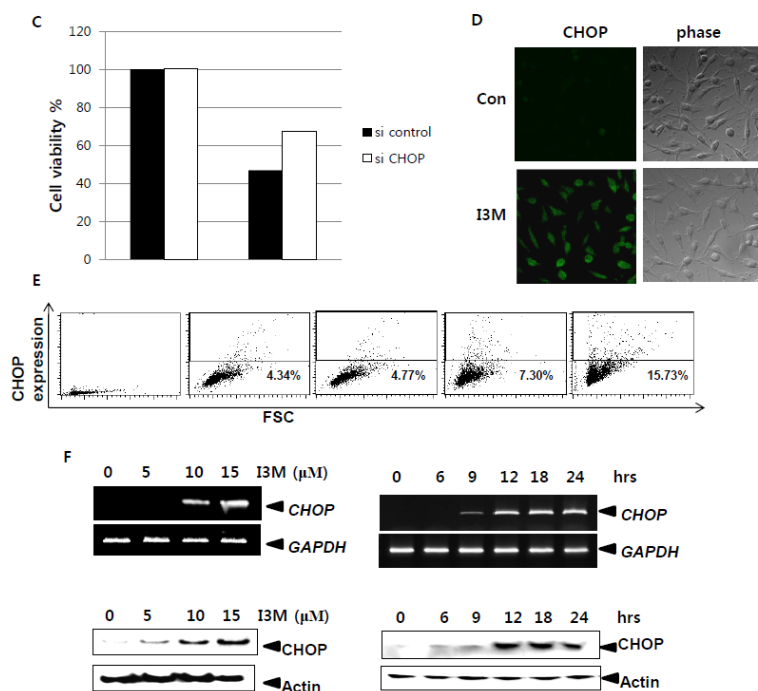
Fig. 5. I3M-induces CHOP expression in MDA-MB-231 cells. (A) Cells were transiently transfected with *CHOP* siRNA for 24 h and then treated with or without before treatment with 15 μM I3M for 24 h. The transfection efficiency was assayed by western blot analysis. (B) Cells were stained with ER Tracker and Mito Tracker followed by with or without I3M treatment for 24 h. Cells were observed under a fluorescent microscope (×400). (C) The viability of cells was determined using an MTT assay. (D) Cells were fixed, permeabilized, and stained with the CHOP monoclonal antibody. The monoclonal antibody was detected using an antimouse secondary antibody conjugated with Alexa Fluor® 488. Stained-CHOP then observed under a fluorescent microscope (×400). (E) Cells were seeded at 2×10^5 cells/ml and incubated with indicated I3M concentrations (0-15 μM) for 24h. Flow cytometry was conducted to analyze the expression level of CHOP. (F) Cells were incubated with indicated concentrations of I3M (0-15 μM) for 24 h and/or 15 μM I3M for indicated time points. RT-PCR and western blot analyses of CHOP was performed at 24 h.

26

2.3.5. Proteasome dysfunction and accumulation of poly ubiquitinylate proteins are critically involved for paraptosis

Next, we examined the importance of accumulation of poly ubiquitinated proteins through proteasome dysfunction by I3M treatment in paraptosis. Pretreatment with known proteasome inhibitor MG132, enhanced I3M-induced formation of ER and mitochondrial vacuoles formation in MDA-MB-231 cells (Fig. 6A). Next, we assayed the effect of MG132 in cell death of MDA-MB-231 cells. Interestingly, compared with the control treatment, combined treatment with I3M and MG132 significantly enhanced I3M-induced cell death at 24 h (Fig. 6B). Immunocytochemistry analysis shown treatment of 15μM of I3M significantly enhanced poly-ubiquitin at 24 h by indicating that I3M-induced paraptosis occurred via proteasome dysfunction (Fig. 6C). In a parallel experiment, we examined the levels of poly-ubiquitin proteins using flow cytometry analysis. The data also revealed that poly-ubiquitin level remarkably enhanced with the treatment of I3M (Fig. 6D). Then to analyze the effect of proteasome dysfunction on ER stress, MDA-MB-231 cells pretreated with I3M for 2 h, followed by exposure to MG132 for 24 h, before preparation of protein concentration detected cells supernatants for western blot analysis. Treatment of I3M remarkably increased CHOP level in MDA-MB-231 cells (Fig. 6E). In particular, pretreatment with MG132 synergistically increased I3M-induced CHOP expression. We also examined that phosphorylation of JNK level comparatively induced by combined treatment of MG132 and I3M (Fig. 6E). These data indicate that accumulation of poly ubiquitinated proteins via proteasome dysfunction into the endoplasmic reticulum (ER) by I3M is critically involved for the paraptosis in MDA-MB-231 breast cancer cells.
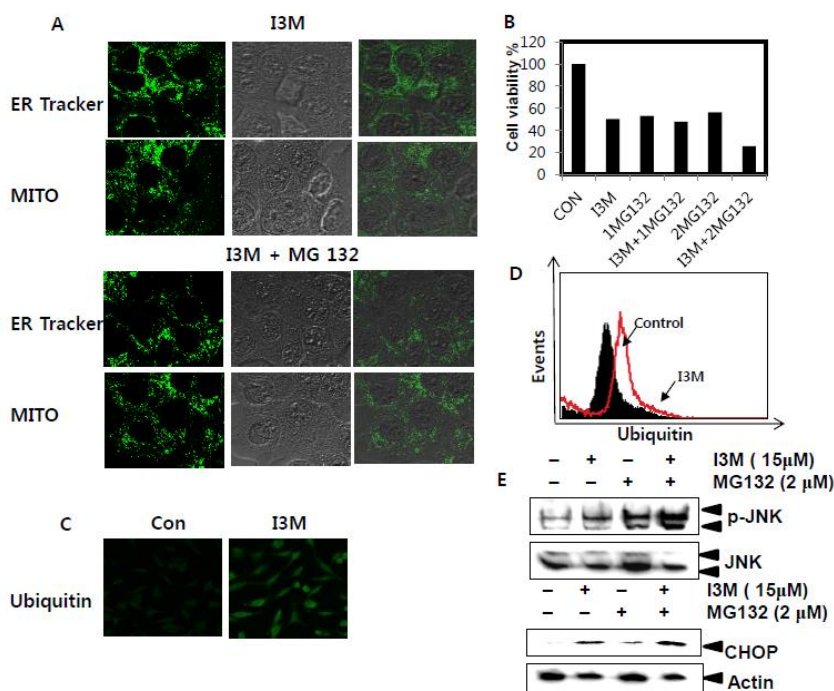
Fig. 6. I3M-induces proteasome dysfunction and accumulation of poly ubiquitinated proteins MDA-MB-231 cells. (A) MDA-MB-231 cells were pretreated with the 2 µM MG132 for 1h and further treated with 15 µM I3M for 24 h. Cells were stained with ER Tracker and Mito Tracker and observed under a fluorescent microscope (×400). (B) MDA-MB-231 cells were pretreated with the indicated concentrations of MG132 for 1h and further treated with 15 µM I3M for 2 4h. Cell viability was measured by an MTT assay following 24 h. (C) Cells were fixed, permeabilized, and stained with the ubiquitin monoclonal antibody. The monoclonal antibody was detected using an antimouse secondary antibody conjugated with Alexa Fluor® 488. Stained-ubiquitin then observed under a fluorescent microscope (×400). (D) Flow cytometry was conducted to analyze the expression level of ubiquitin. (E) MDA-MB-231 cells were pretreated with 2µM of MG132 for 1h and further treated with 15 µM I3M for 24 h. Equal amount of cell lysates were resolved on SDS–polyacrylamide gels, transferred to nitrocellulose membranes, and probed with antibodies against p-JNK, JNK, and CHOP. β-Actin was used as

28

a loading control.

2.3.6. I3M enhanced mitochondrial calcium uptake

In order to determine the involvement of Ca^{2+} uptake by mitochondria in I3M-induced paraptosis we next performed flow cytometry analysis after exposure to mitochondrial Ca^{2+} indicator dye, Rhod-2. Concentration dependent treatment of I3M gradually increased the mitochondrial Ca^{2+} levels (Fig. 7A). As shown in Fig. 7B, the mitochondrial Rhod-2 staining intensity was highly detected in I3M treated cells, contrary to that observed for the untreated control group (Fig. 7B). In particular, treatment of 15 μM I3M significantly increased the mitochondrial Ca^{2+} levels in MDA-MB-231 cells; however, this upregulation did not reach the level observed for PC3 prostate cancer cells and HCT116 colon cancer cells (Fig. 6C). On the other hand, 15 μM I3M treatment slightly increased the mitochondrial Ca^{2+} levels in Hep 3B hepatocellular carcinoma cells (Fig. 7C). Since the ER involve for the upload of Ca^{2+} to the mitochondria then we treated sieIF2α to examine the relationship between ER and mitochondria in regulation of intracellular calcium homeostasis. Using fluorescence microscopy, we found that treatment of sieIF2α completely blocked I3M-induced mitochondrial Ca^{2+} levels in MDA-MB-231 cells at 24 h (Fig. 7D). Taken together these data shown that I3M has influence on increase of mitochondrial Ca^{2+} levels in MDA-MB-231 cells.
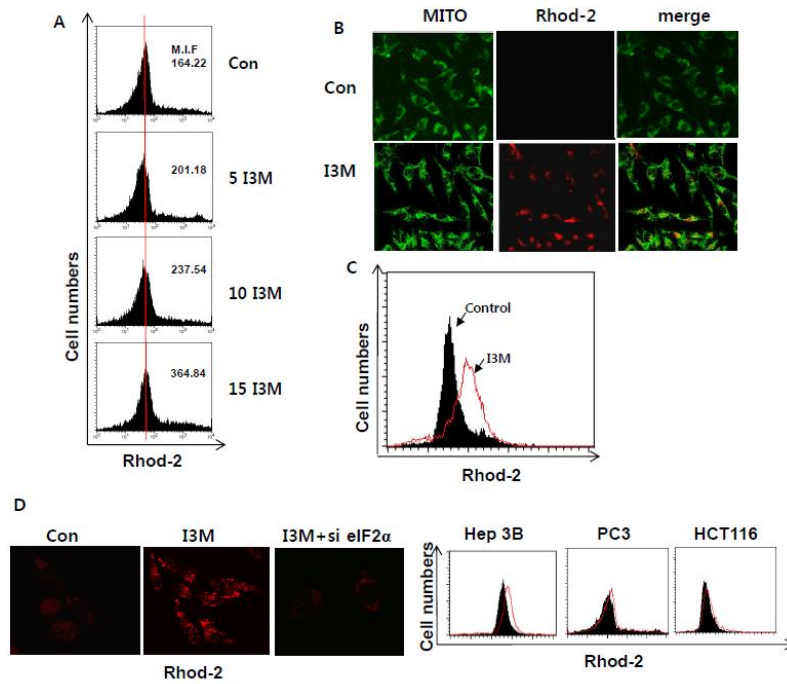
Fig. 7. I3M-induces mitochondrial Ca^{2+} uptake in MDA-MB-231 cells. (A) MDA-MB-231 cells treated with indicated concentrations of I3M (0-15 μM) for 24 h and then stained with 2.5 μM Rhod-2. Rhod-2 fluorescence intensity was measured using flow cytometry. (B) MDA-MB-231 cells were stained with 2.5μM Rhod-2 followed by the treatment of 15 μM I3M for 24h. Fluorescence intensity of Rhod-2 was observed under a fluorescent microscope (×400). (C) MDA-MB-231, Hep3B, PC3, and HCT116 cancer cells were treated with 15 μM I3M for 24 h. Rhod-2 fluorescence intensity was measured using flow cytometry. (D) Cells were transiently transfected with si*IF2α* for 24 h and then treated with or without before treatment with 15 μM I3M for 24 h. Cells were stained with Rhod-2 followed by with or without I3M treatment for 24 h. Cells were observed under a fluorescent microscope (×400).

2.3.7. Overloaded Ca²⁺ into mitochondria via ER induced ROS production induced paraptosis by I3M

Compelling evidence supports a mutual relationship between calcium and ROS, next we focus on whether I3M-induced paraptosis occurred via ROS production by accumulated Ca^{2+} in MDA-MB-231 cells (Voccoli et al., 2014). Data obtained using fluorescence microscopy, showed that of the I3M-treated MDA-MB-231 cells induced mitochondrial Rhod-2 staining intensity; however, treatment of calcium chelator EGTA completely inhibited the staining intensity of Rhod-2, thereby suggesting that EGTA has effect to mitochondrial calcium uptake (Fig. 8A). Further, the number of vacuolated cells percentage reduced from ~60% to 30% in I3M and I3M with EGTA treatment respectively (Fig. 8B). In a parallel experiment, then we analyzed I3M cytotoxicity using MTT assay. The concentration dependent pretreatment of calcium chelator EGTA, significantly reduced I3M-induced cell death (Fig. 8C). Then, to examine the link between the calcium and ROS production, cells treated with EGTA for 2 h prior to treatment with I3M. Then ROS generation was assayed by the fluorescence spectrophotometer. As shown in Fig. 8D, I3M-induced ROS production remarkably reduced by the pretreatment of EGTA (Fig. 8D). Moreover, dose dependent manner treatment of ROS inhibitors such as NAC, GSH, and catalase, induced I3M-decreased cell viability percentage (Fig. 8E). Past reports shown that induction of ROS have potential to induce ER stress also. Though, ER stress is a crucial step in I3M-induced paraptosis therefore, next we examined the effect of ER stress protein CHOP, after treatment with NAC using western blot analysis. Treatment of 10 μM of NAC comparatively inhibited that I3M-induced expression of CHOP protein level in MDA-MB-231 cells (Fig. 8F, upper panel). On the other hand, NAC treatment remarkably decreased the I3M-induced JNK phoporylation at 24 h (Fig. 8F, lower panel). In

31

particularly, as shown in western blot data, pretreatment of EGTA notably downregulated I3M-induced protein expression levels of CHOP and pJNK in MDA-MB-231 cells (Fig. 7G). These results demonstrate that I3M possesses induction of ROS generation via mitochondrial Ca^{2+} accumulation thus induced paraptosis followed by ER stress in MDA-MB-231 cells.
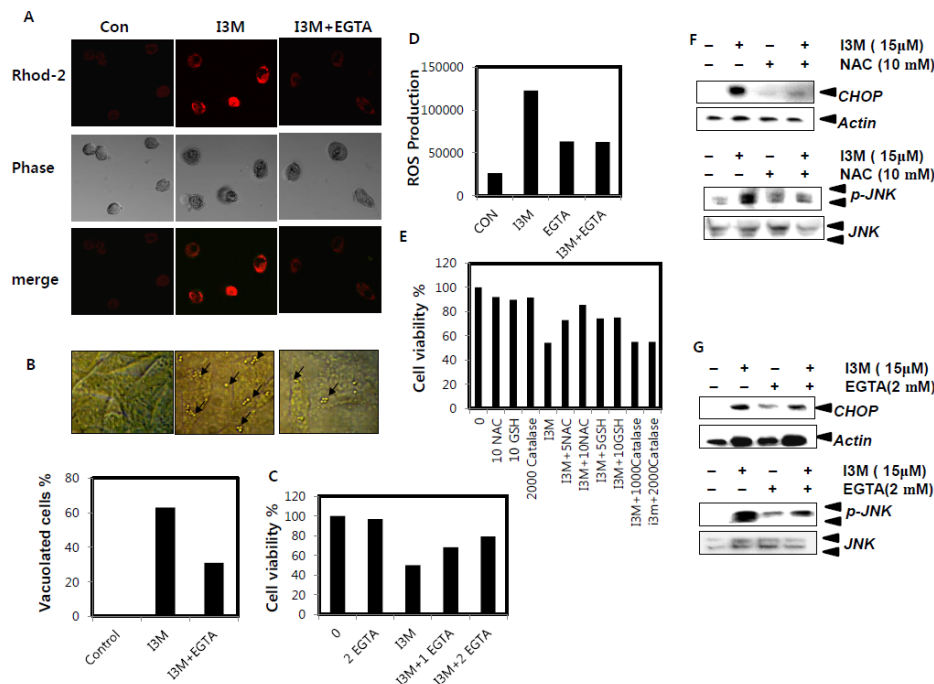
Fig. 8. I3M-induces Ca^{2+} uptake by mitochondria via ER induced ROS production. (A and B) MDA-MB-231 cells were pretreated with 2 mM of EGTA for 1h and further treated with 15 μM I3M for 24 h. Rhod-2 fluorescence intensity was measured using flow cytometry and light microscopy respectively. Percentage of vacuolated cells were denoted in the graph. (C) MDA-MB-231 cells were pretreated with the indicated concentrations of z-EGTA for 1 h and further treated with 15 μM I3M for 24 h. Cell viability was measured by an MTT assay following 24 h. (D) MDA-MB-231 cells were pretreated with 20 μM DCFDA for 1 h and then incubated with 2mM of EGTA for 1h and further treated with 15 μM I3M for 24 h. ROS generation was analyzed by a fluorometer. (E) MDA-MB-231 cells were pretreated with the indicated

concentrations of NAC, GSH and catalase for 1 h and further treated with 15 μM I3M for 24 h. Cell viability was measured by an MTT assay following 24 h. (F) MDA-MB-231 cells were incubated with 10 mM NAC for 1h and then treated with 15 μM I3M for 24 h. Equal amount of cell lysates were resolved on SDS–polyacrylamide gels, transferred to nitrocellulose membranes, and probed with antibodies against JNK, p-JNK, and CHOP. (G) Cells were incubated with 2 mM EGTA for 1h and then treated with 15 μM I3M for 24 h. Equal amount of cell lysates were resolved on SDS–polyacrylamide gels, transferred to nitrocellulose membranes, and probed with antibodies against JNK, p-JNK, and CHOP. β-Actin was used as an internal control for western blot analysis.

2.3.8. Blocking of mitochondrial channel uniporters reduced I3M induced parapotosis

To confirmed that overloaded Ca^{2+} into the mitochondria from ER, mediate via mitochondrial channel uniporters next cells were treated with I3M for 2 h followed by treatment with an inhibitor of uniporter-mediated mitochondrial Ca^{2+} uptake, ruthenium red (RR), before examine the cytotoxic effect using MTT assay. Compared to the control group, I3M treatment markedly reduced the cell viability (Fig. 9A). However, 1-3 μM dose-dependent manner pretreatment of RR significantly inhibited the reduction of viability of cells (Fig. 9A). Additionally, we investigated whether I3M regulates Ca^{2+} overload into mitochondria through mitochondrial channel uniporters. Fluorescence microscopic analysis showed that pretreatment of 4 μM ruthenium red remarkably decreased I3M-induced ER and mitochondrial derived vacuoles at 24 h (Fig. 9B). Flow cytometry data confirmed that ruthenium red treatment notably reduced mitochondrial Rhod-2 staining intensity compared with untreated control group in MDA-MB-231 cells (Fig. 9C). In addition, as shown in Fig. 9D, fluorescence microscopy using

Rhod-2 staining indicated that blocking of mitochondrial channel uniporters by ruthenium red completely inhibited I3M-induced mitochondrial Rhod-2 staining intensity (Fig. 9D). Nevertheless, as shown in ubiquitination assay, ruthenium red treatment sharply decreased the I3M-upregulated ubiquitination of ER stress protein in MDA-MB-231 cells (Fig. 9E). The western blot analysis indicated that I3M-enhaced the expression level of CHOP, phosphorylated JNK, and eIF2α remarkably downregulated with the treatment of RR by indicating mitochondrial channel uniporters play an important role in mediation of ER stress via ubiquitin (Ub)-proteasome pathway in I3M-induced paraptosis in MDA-MB-231 breast cancer cells (Fig. 9E). These results suggest that I3M mediates Ca^{2+} accumulation into mitochondria through mitochondrial channel uniporters in MDA-MB-231 breast cancer cells.
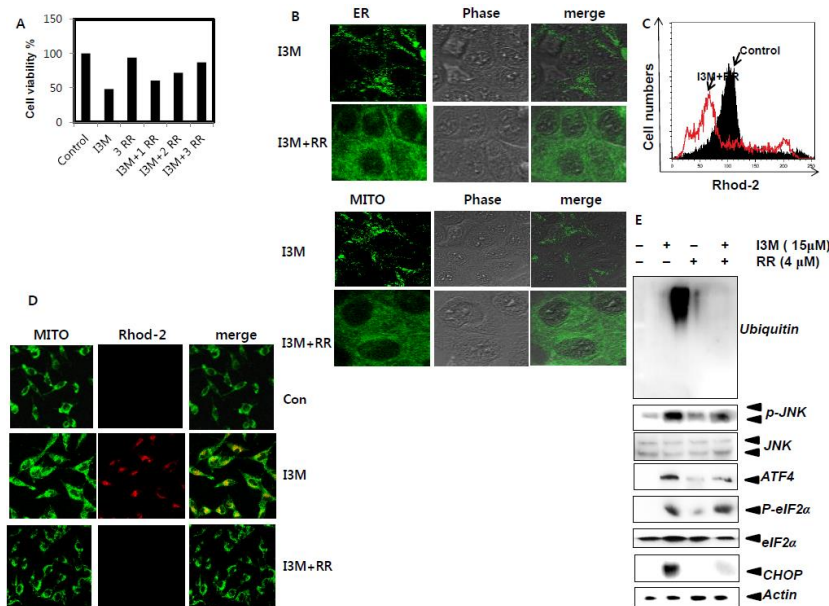
Fig. 9. I3M-enhances blocking of mitochondrial channel unireporters. (A) MDA-MB-231 cells were pretreated with the indicated concentrations of ruthenium red (RR) for 1h and further treated with 15 μM I3M for 24 h. Cell viability was measured by an MTT assay following 24 h. (B, C and D) MDA-MB-231 cells were pretreated with 3 μM ruthenium red for 1h and

further treated with 15 μM I3M for 24 h. Cells were stained with ER Tracker and Mito Tracker followed by with or without I3M treatment for 24 h. Cells were observed under a fluorescent microscope (×400) (B). Rhod-2 fluorescence intensity was measured using flow cytometry and fluorescent microscope (×400) respectively (C and D). (E) Cells were harvested and the indicated proteins were detected by Western blot analysis. β-Actin was used as an internal control for western blot analysis.

2.4. Discussion

The main obstruction to effective and efficient breast cancer therapy is development of intrinsic (de novo) or acquired resistance (García-Becerra et al., 2013). Decades of research have sequentially revealed that resistance to apoptosis is frequent mechanism by which these cancer cells prevent death (Fulda., 2010). Therefore, investigation of alternative approaches that triggering cell death is mostly required to improving efficiency of the treatments. Paraptosis can be served as one of crucial alternative cell death mechanism pathway but still it has not been well characterized. The present study reports for the first time that I3M can induce non-apoptotic programmed cell death via paraptosis in MDA-MB-231 breast cancer cells and Hep3B hepatocellular carcinoma cells. Here we provide convincing evidence demonstrating that I3M-induced paraptosis by extensive vacuolization that occurred through excessive dilation of endoplasmic reticulum (ER) and mitochondria. Further, we have shown that the contribution of CHOP protein via proteasome dysfunction to I3M-induced paraptosis in MDA-MB-231 breast cancer cells.

Specifically, I3M treatment significantly did not exhibited apoptotic characteristics such as

35

nuclear fragmentation, activation of caspases, PARP cleavage and apoptotic bodies formation by indicating that I3M-induced cell death in MDA-MB-231 cells different from apoptotic mechanism. However, that apoptotic remarks partially observed in Hep 3B cells. The loss of mitochondrial membrane potential (MMP) can be check point of apoptosis because, release of cytochrome c from the intermembrane space to cytosol involves to activation apoptotic signaling (Wang et al., 2014). According to our results the marked reduction of MMP observed in MDA-MB-231 cells, however; lack of caspase activation indicates loss of MMP not regulate apoptosis in I3M-induced cell death. The reduction of MMP also examined in Jurkat cells without inducing apoptosis (Jambrina et al., 2003). Nevertheless, the induction of cell death by I3M did not associate with the autophagy process. Since, LC3 has been characterized as an autophagosomal marker in mammalian autophagy we examined the LC3 expression level in MDA-MB-231 cells. Nevertheless, p62 also known to be an autophagy marker as it forms link between polyubiquitinated proteins and autophagy we analyzed changes of p62 expression level with the I3M treatment. Indeed, I3M treatment did not increased LC3-II or decreased p62 generation by indicating autophagy process did not involve in I3M-induced cell death in MDA-MB-231 cells. Interestingly, rapamycin but not I3M similar as 3MA induced Beclin 1 expression level. Hence, these facts indicate that I3M induces paraptosis cell death in MDA-MB-231 cells.

As a key feature of paratosis process, vacuoles formed by magamitochondria due to subsequent fusion of excessive swelled ER and mitochondria (Yoon et al., 2010). In particularly, as a result of I3M treatment, vacuolation was examined that triggers cell death in MDA-MB-231 cells. Based on that we further interested to investigate the molecular mechanism which regulate I3M-induced paraptosis. Aside from the induction of accumulation of poly-

36

ubiquitinated proteins with markers of ER stress including ATF4, peIF2α and CHOP by I3M, the proteasome inhibitor MG132 also found to further induce ER stress markers with enhanced the formation of ER and mitochondrial derived vacuoles in MDA-MB-231 cells. Therefore, these results indicate that poly-ubiquitinated proteins accumulation via proteasome dysfunction is crucial event in I3M-mediated paraptosis in MDA-MB-231 cells.

Cumulative data supported that interaction of mitochondria with Ca^{2+} store in the ER crucially involves the efficient respond to the Ca^{2+} signaling with in the internal organelles (Romagnoli et al., 2007). However, as a result of upregulation of free Ca^{2+} in the cytoplasm may loss of Ca^{2+} homeostasis thereby potently induces cell death via apoptosis process (Tasheva et al., 2013). There are several mechanisms that induced the cell death via disrupted Ca^{2+} homeostasis including nitric oxide synthases (iNOS), Ca^{2+} dependent protease activation and Ca^{2+}-dependent transcription factor-cAMP response element-binding protein (CREB) (Tasheva et al., 2013). In particularly, disruption of Ca^{2+} homeostasis by I3M may leading to the cell death regulate via paraptosis process. In our study, exposure to EGTA, an extracellular calcium chelator some extent induced I3M-reduced cell viability, by indicating aside from the involvement of intracellular calcium, extracellular calcium also found to involve in I3M-induced cell death. More importantly, Voccoli *et al* was reported downregulation of extracellular calcium using a chelating agent can reduce mitochondrial ROS production thereby induce cell viability in human oligodendrocyte MO3.13 cells (Voccoli et al., 2014). Consequently, exposure to EGTA significantly attenuated I3M-induced ROS production in MDA-MB-231 cells. Researches have been indicated that Ca^{2+} influx from the extracellular space via the plasma membrane or by release of Ca^{2+} from endoplasmic (ER), sarcoplasmic (SR) like intracellular Ca^{2+} stores affect to the elevation in intracellular Ca^{2+} concentration

(Patergnani et al., 2011). Hence, Rhod-2 staining of MDA-MB-231 cells shown that I3M-induced Rhod-2 staining intensity remarkably decreased by the EGTA treatment. Therefore, these results suggest that I3M-induced intra-mitochondrial Ca^{2+} level via the extracellular Ca^{2+} concentration that release by ER due to ER stress.   The accumulation of Ca^{2+} in the mitochondria from the cytoplasm regulate by the mitochondrial Ca^{2+} uniporter (MCU) which is located in the inner membrane of the mitochondria (Kirichok et al., 2004). To test this hypothesis, we treated inhibitor of mitochondrial Ca^{2+} unireporter RR, on I3M-treated MDA-MB-231 cells. Interestingly, treatment of RR significantly inhibited I3M-induced mitochondrial Ca^{2+} accumulation indicating that accumulation of Ca^{2+} in the mitochondria from the cytoplasm mainly regulated by MCU.

Investigation of effective and efficient paraptosis enhancing agents and the underline the particular molecular mechanisms in this alternative cell death form may promote the development of novel therapeutics against malignant cancer cells that harbor defective apoptotic machineries. In this study, we demonstrated that I3M induces an inhibition of cell growth in MDA-MB-231 cells. Moreover, we demonstrated crucial role of mitochondria and ER regulate Ca^{2+} homeostatis and proteasomal dysfunction in paraptosis. However, further research is needed on investigation of chemosensitizing effects of I3M on cancers and *in vivo* cancer models to further verify the clinical relevance of I3M as a potent anticancer agent.

2.5. Conclusion

I3M induces an inhibition of cell growth in MDA-MB-231 cells. The inhibition of cell growth by I3M did not occurred via apoptosis or autophagy. I3M induces proteasome dysfunction and

accumulation of ER stress related proteins in to the ER lumen. Due to overload of proteins in the ER, its increases ER stress, release Ca^{2+} ions into the cytoplasm. The Ca^{2+} ions enter to the mitochondria via mitochondrial channel unireporters causes unequal distribution of Ca^{2+} ions with in the cellular organells resulting paraptosis cell death.

Chapter 3

Indirubin-3′-monoxime induces p53-mediated cell death via apoptosis and paraptosis in

Hep3B hepatoma cancer cells

Abstract

Indirubin-3′-monoxime (I3M) is a derivative of indirubin which is the active component of Danggui-Long-Hui-Wan, a traditional Chinese recipe used exhibits promising anticancer effects in wide range of cancers. I3M exhibits anticancer properties by modulating cell cycle arrest, apoptosis, cell invasion and metastasis, lack of understanding of their mode of action. Therefore, in this study, we present the I3M as a promising anticancer agent based on the induction of the cell death via apoptosis and paraptosis in Hep3B hepatocarcinoma cells. Also, we investigated the role of p21 and ROS regulate NFκB signaling pathway in I3M-midiated cell death in Hep3B cells. I3M treatment significantly reduced viability of Hep3B cells and gradually upregulated Bax, and Bid protein expression level by indicating I3M-induced apoptosis in Hep3B cells. Nevertheless, treatment of I3M-increased numerous small ER and mitochondria derived fluorescent vacuoles and enhanced the Rhod-2 staining intensity suggested that I3M-induced cell death in Hep3B cells partially enhanced via paraptosis. We observed that I3M-enhanced the expression of p53 and p21 protein and mRNA level in Hep3B cells. The cells transfection with sip53 markedly decreased I3M-induced p21 fluorescence intensity, demonstrate that I3M mediate p21 expression regulate by p53 in Hep3B cells. Further, we investigated that I3M-induced expression of p21 mediate the ROS accumulation in Hep3B cells. Treatment with 15μM I3M significantly induced NFκB luciferase activity, whereas treatment of NAC downregulated I3M-induced NFκB luciferase reporter activity in Hep3B cells. Therefore, ROS play an important role in activation of NFκB thereby reduced apoptosis in Hep3B cells. Nevertheless, our results demonstrate that I3M mediate p53 regulate both apoptosis and paraptosis processes in Hep3B cells. Taken together, our findings illustrate the anticancer activity of I3M basis of its ability to simultaneously induce apoptosis and paraptosis

41

in Hep3B hepatoma cancer cells, proving the potential of I3M in developing as an anticancer drug in near future.

3.1. Introduction

Cell death is the event of a biological cell ceasing to carry out its functions, might be the result of the natural process to eliminate existing old cells by new cells, or may be resulted due to different kind of factors such as disease, injury or death of the particular organism of which the cells are part (Suzanne and Steller., 2013 and Zong and Thompson., 2006). Cell death is a crucial terminal mechanism for cells of multicellular organisms, and it is mainly regulated by programmed cell death (PCD) (Huang et al., 2014). However, expanding body of evidence indicate eventhough, independence of caspases cell death can be occurred (Baraz et al., 2014). Therefore, alternative modes of PCD have been suggested, such as autophagy, mitotic catastrophe, paraptosis, apoptosis-like PCD and necrosis-like PCD (Kaiser et al., 2008). The intracellular organelles like endoplasmic reticulum (ER), mitochondria and lysosomes can lead individually or mutual interaction with one another to regulated PCD with the involvement of endonucleases, proteases, calpains, and catepsins other than the caspases (Bröker et al., 2005 and Orrenius et al., 2011). However, investigation of caspase independence pathways is essential for the field of oncology, because those can potentially be manipulated to development of novel cancer treatments in future.

Of these, apoptosis is the well categorized type of PCD, being clarified by predominant signatures such as internucleosomal DNA fragmentation, nuclear condensation, membrane

blebbing, cell shrinkage, global mRNA decaying and formation of numerous spherical bodies (Sahu et al., 2013 and Thomas et al., 2015). Cumulative data supported that proteolytic cleavage of different kind of proteins via activated caspase proteases involve in the accomplishment of apoptotic morphology (Bae et al., 2008). Despite, the process of proteolytic cleavage of these proteins development in apoptotic morphology remains unknown. Aside from the induction of cell death via apoptosis, researchers have investigated that cell death also enhance by paraptosis, a novel type of nonapoptotic cell death and can serve as emerging strategy to induce death of cancer cells thus has potential to utilize caspase-independent apoptotic pathways for the development of new anticancer therapies. Paraptosis is characterized by a process of vacuolation that begins with physical enlargement of mitochondria and the endoplasmic reticulum (ER) (Jia et al., 2015 and Wang et al., 2012). Although the mechanisms underlying paraptosis, in particular, biochemical signaling pathways that responsible for the triggering mitochondrial and ER dilatation, have not yet been fully investigated, it may be associated with the loss of calcium ion homeostatis or uneven distribution of calcium ion within the intracellular organelles (Yoon et al., 2014).

In past decades, it has been a dramatic resumption of the interest in indirubin, a red-colored 3,2′-bisindole isomer due to the investigation of its great pharmacological potential (Varela et al., 2008). The pharmacological properties of indirubin have been known for ancient times. Indeed, Indirubin-3′-monoxime is a derivative of indirubin which is the active component of Danggui-Long-Hui-Wan, a traditional Chinese recipe used for the treatment of various diseases in particular chronic myelogenous leukemia (Kritsanida et al., 2009). Indirubin and its derivatives, a group of bis-indole alkaloids, have shown strong cytotoxic effect on wide range of human cancer cell lines, manifested by either cell death mainly via apoptosis or cell cycle

arrest (Lucas et al., 2010). Moreover, in vivo studies using rat tumor models provides further evidence for the anticancer mechanisms of indirubin (Kim et al., 2007). In the attempt to investigate the mechanism of action of indirubins, different biological activities of indirubin and its derivatives have been discovered. It has been well documented that indirubin and its derivatives shown anticancer activity in various human cancer cells. Consequently, indirubin and its derivatives exhibit its anticancer activities in thyroid (Broecker-Preuss et al., 2015), lung (Ahn et al., 2015), oral (Lo and Chang., 2013), pancreatic (Nam et al., 2013), human acute lymphoblastic leukemia (Lee et al., 2013), breast, and bladder (Braig et al., 2014 and Shi et al., 2011) cancers.

Our previous study demonstrated that I3M-induced paraptosis in human breast cancer cell line MDA-MB-231 and its partially induced paraptosis in human hepatocellular carcinoma Hep 3B cells. Consequently, in the present study, we report that the I3M regulates its anticancer properties via apoptosis and paraptosis in Hep3B hepatocellular carcinoma cells. We further, investigated the involvement of p21 in I3M-induced apoptosis by regulating ROS production and nuclear factor κB activity. Nevertheless, our results further demonstrated that the role of tumor suppressor p53 gene in I3M-induced apoptosis and paraptosis in Hep3B cells.

3.2. Materials and methods

3.2.1. Antibodies and reagents

Antibodies against Bid, Bax, caspase-8, Bcl2, and β-actin were purchased from Santa Cruz Biotechnology (Santa Cruz, CA). Antibodies against p21 and p53 were purchased from Cell Signaling (Beverly, MA). 3-(4,5-dimethyl-2-thiazolyl)-2,5-diphnyl-2H-tetrazolium bromide

(MTT) were purchased from Sigma (St. Louis, MO) and Roswell Park Memorial Institute Medium (RPMI), antibiotics mixture, and fetal bovine serum (FBS) were obtained from WelGENE Inc. (Daegu, Republic of Korea). Peroxidase-labeled goat anti-rabbit immunoglobulin was purchased from KOMA Biotechnology (Seoul, Republic of Korea). Other chemicals were purchased as Sigma grades.

3.2.2. Cell line and cell growth assay

Human hepatocellular carcinoma cell line, Hep3B was obtained from the American Type Culture Collection. Cells were cultured at 37°C in a 5% CO_2-humidified incubator and maintained in RPMI 1640 culture medium containing 10% heat-inactivated fetal bovine serum (Life Technologies Bethesda Research Laboratories and 1% penicillin-streptomycin (Sigma). The cells were seeded (5×10^4 cells/ml), grown for 24 h, and then incubated for up to 24 h with I3M. MTT assays were done to assess cell viability.

3.2.3. Flow cytometric analysis

Flow cytometer was used to analyze the cell cycle distribution. Cells grown overnight were treated with I3M for 24 h in complete media. Whole Hep3B cells were harvested and fixed with 70% ethanol for 1 h at 4°C. Fixed cells were washed in phosphate-buffered saline (PBS). Cells were then incubated with 5 μg/ml propidium iodide (PI; Sigma–Aldrich) for 30 min at 4°C in the dark. FACS Calibur flow cytometer (BD Biosciences, Franklin Lakes, NJ) was used to analyze the cell cycle distribution. Approximately 10000 cells were analyzed for each sample. For Rhod-2 and HE staining, live cells were incubated with Rhod-2 and HE. For p21 expression

analysis, cells were trypsinized, washed once with PBS, fixed with ice-cold 70% ethanol for overnight and immunostained with a rabbit anti-p21 antibody followed by a FITC-conjugated goat anti-rabbit antibody. The p21 expression level was analyzed using a fluorescence-activated cell sorting cater-plus flow cytometry.

3.2.4. Western blot analysis

Cell lysates were prepared using PRO-PREP protein extraction solution (iNtRON Biotechnology, Sungnam, Republic of Korea). Aliquots of protein were electrophoresed on SDS/PAGE. The proteins were separated by electrophoresis prior to transfer to nitrocellulose membranes and incubated with primary antibodies overnight at 4°C, followed by incubation with horseradish-peroxidase-conjugated goat anti-rabbit secondary antibody at a dilution of 1:3000 for 1 h at room temperature. The antigen–antibody complex was detected with the ECL Prime Western Blotting Detection Kit (Amersham, Arlington Heights, IL). The intensity of the blots was quantified by densitometry analysis using chemiluminescence system.

3.2.5. Real-time polymerase chain reaction (RT-PCR)

Total RNA was extracted from cells using Trizol reagent (Invitrogen) following the manufacturer′s instruction. The transcription level of p21 gene was evaluated by the use of real-time RT-QPCR technique according to the producer′s specifications (One-Step RT-PCR Premix, Bioneer, Daejeon, Republic of Korea). The sequences of the sense and antisense primers for p21 were 5′-CTC AGA GGA GGC GCC ATG-3′ and 5′-GGG CGG ATT AGG GCT TCC-3′, respectively. For glyceraldehyde-3-phosphate dehydrogenase (GAPDH), the sense primer 5′-CGT CTT CAC CAT GGA GA-3′ and the anti-sense primer 5′-CGG CCA TCA CGC CCA

46

CAG TTT-3′ were used (corresponding to a 310-bp region of GAPDH). The thermal profile for one-step RT-PCR was as follows: For p21, 30 cycles of denaturation at 94°C for 30 s, annealing at 59°C for 30 s and extended at 72°C for 30 s; and for GAPDH, 28 cycles of denaturation at 94°C for 30 s, annealing at 62°C for 30 s and extended at 72°C for 30 s. Each gene analysis was performed in triplicate. Additionally, the RT-PCR products were separated on 2% polyacrylamide gels and staining with ethidium bromide.

3.2.6. Electrophoretic mobidity shift assay (EMSA)

Nuclear extracts were prepared according to the protocol of Nuclear Extraction kit (Pierce, Rockford, IL, USA). Synthetic complementary NF-κB (5′-AGT TGA GGG GAC TTT CCC AGG C-3′) binding oligonucleotides (Santa Cruz Biotechnology) were 3′-biotinylated using the biotin 3′-end DNA labeling kit (Pierce) according to the manufacturer's instructions, and annealed for 30 min at room temperature. DNA/nuclear protein complexes were separated by electrophoresis on a native 4% polyacrylamide gels pre-electrophoresed for 60 min in 0.5× Tris borate/EDTA before being transferred onto a positively charged nylon membrane (HybondTM-N^+) in 0.5 × Tris borate/EDTA at 100 V for 30 min. The transferred DNAs were cross-linked to the membrane at 120 mJ/cm^2. Horseradish peroxidase-conjugated streptavidin was used according to the manufacturer's instructions to detect the transferred DNA.

3.2.7. Immunofluorescent Confocal Laser Microscopy

After treatment with I3M for 24 h, cells were fixed with 4% paraformaldehyde /phosphate buffered saline (PBS) at room temperature for 20 min, permeabilized with 0.1% Triton X-100 in PBS for 10 min on ice, and then blocked with 3% bovine serum albumin/PBS for 2 h at room

47

temperature for the detection of p53 and p21 expression. Before the observe cells from confocal microscopy, fixed cells were incubated with the anti-p53 and p21 antibodies at 4°C for 2 h, washed with PBS, incubated for another 1 h with FITC-conjugated goat anti-rabbit IgG, and washed well with PBS. For DAPI staining fixed cells were washed with PBS and nuclei were stained with DAPI solution. For detection of ER and mitochondrial derived vacuoles, after incubation, the cells were treated with desired concentrations of I3M for 24 h and then 1% formaldehyde was added to each well for 30 min. Cells were permeabilized with 1% Triton X-100 for 5 min and washed twice in PBS. The stained cells were detected by fluorescence microscopy.

3.2.8. ROS generation

Cells were transiently transfected with *p21* siRNA for 24 h and then treated with or without 15 μM I3M for an additional 24 h followed by exposure to florescence dye 6-carboxy-2′,7′-dichlorofluorescein diacetate (H_2DCFDA, Molecular Probes, Eugene, OR) for 1 h. The cells were lysed with triton and the sample was centrifuged and supernatant was analyzed for ROS roduction using GLOMAX luminometer (Promega).

3.2.9. Luciferase activity assay

For luciferase activity assay, Lipofectamine method was used to cell transfection. In brief, Hep3B cells were seeded at a density of 1×10^4 cells/well. After 24 h, cells were transfected with 2 μg each plasmid construct according to the Lipofectamine method. The cells were incubated with 5 mM NAC 1 h before 15 μM I3M treatment for 24 h and then cells were harvested. Luciferase activity was measured by according to the manufacture′s protocol and

detected by GLOMAX luminometer (Promega, Madison, WI, USA).

3.2.10. Transient knockdown of p53 and p21

P53 and p21 siRNA was purchased from Santa Cruz Biotechnology. The transfection reagent G-Fectin (Genolution Pharmaceuticals, Inc., Seoul, Republic of Korea) was added to each well with 450 µl RPMI1640 plus 20 nM siRNA duplex into the cells and incubated for 24 h.

3.2.11. Statistical analysis

All results were presented as at least three independent experiments. The images were visualized with Chemi-Smart 2000 (Vilber Lourmat, Cedex, France). Images were captured using Chemi-Capt (Vilber Lourmat) and transported into Adobe Photoshop (version 8.0). All data are presented as mean ± SE. Significant differences between the groups were determined using one-way ANOVA test. When $P < 0.05$, the values were considered to be significantly different.

3.3. Results

3.3.1. I3M induces cell death on Hep3B cells via apoptosis and paraptosis

In order to investigate whether I3M has anti-proliferative or cytotoxic effects, human hepatoma Hep3B cells was treated with indicated concentrations of I3M for 24 h and the resulting number of viable cells remaining were assessed. I3M treatment significantly reduced viability of Hep3B cells in concentration dependent manner. According to MTT assay results, treatment with 15 µM I3M remarkably reduced viable cell percentage in Hep3B cells (Fig.

10A). In a parallel experiment, the expression levels of Bax, Bid, and Bcl2 protein were determined by western blot analysis at 24 h. Dose dependent manner treatment of I3M gradually upregulated Bax, and Bid protein expression level while decreasing protein expression level of Bcl2 by indicating apoptosis is involved in death of Hep3B cells regulate by I3M (Fig. 10B). Treatment of 10 μM I3M for 24 h also partially induced nuclear fragmentation when compared with positive control H_2O_2 group, as illustrated by fluorescent staining of nuclei (Fig. 10C). Next, we attempt to reveal whether or not I3M induced cell death completely occurred via apoptosis, then Hep3B cells we pretreated with I3M for 2h, followed by treatment with pan caspase inhibitor, z-VAD-fmk for 24 h. Interestingly, treatment with z-VAD-fmk slightly attenuated I3M-induced cell death suggesting rather than apoptosis another cell death mechanism is involved in I3M-mediated cell death of Hep3B cells (Fig. 10D). In this regards, when examine the cell morphology under the light microscope, I3M-treated cells exhibited numerous small vacuoles as a key feature of paraptosis process. In 7.5 μM and 10 μM treatment with I3M significantly induced vacuolated cells percentage as ~36 % and ~78% respectively (Fig. 10E). Next, to examine whether the I3M-enhanced vacuoles may derive from mitochondria and/or the ER, cells were exposure to ER-tracker and Mito-tracker and examined by immunofluorescent confocal microscopy. Compared with the untreated group, at 24 h after I3M treatment increased numerous small ER and mitochondria derived fluorescent vacuoles (Fig. 10F). To further confirm the I3M-induced paraptosis in Hep3B cells, next we examined the Ca^{2+} uptake by mitochondria after exposure to mitochondrial Ca^{2+} indicator dye, Rhod-2. Flow cytometry analysis showed that treatment with I3M markedly increased mitochondrial Ca^{2+} levels at 24 h (Fig. 10G). Since it is indicated, in paraptosis, overloaded Ca^{2+} into the mitochondria from ER, mediate via mitochondrial channel uniporters next cells were treated

with I3M for 2 h followed by treatment with an inhibitor of uniporter-mediated mitochondrial

Ca^{2+} uptake, ruthenium red (RR), then Rhod-2 staining intensity was measured by flow

cytometry analysis. According to the Fig. 1H, ruthenium red treatment notably reduced

mitochondrial Rhod-2 staining intensity compared with I3M treated group in Hep3B cells (Fig.

1H). Taken together these results indicated that I3M induce cell death in Hep3B cells via

apoptosis and paraptosis processes.
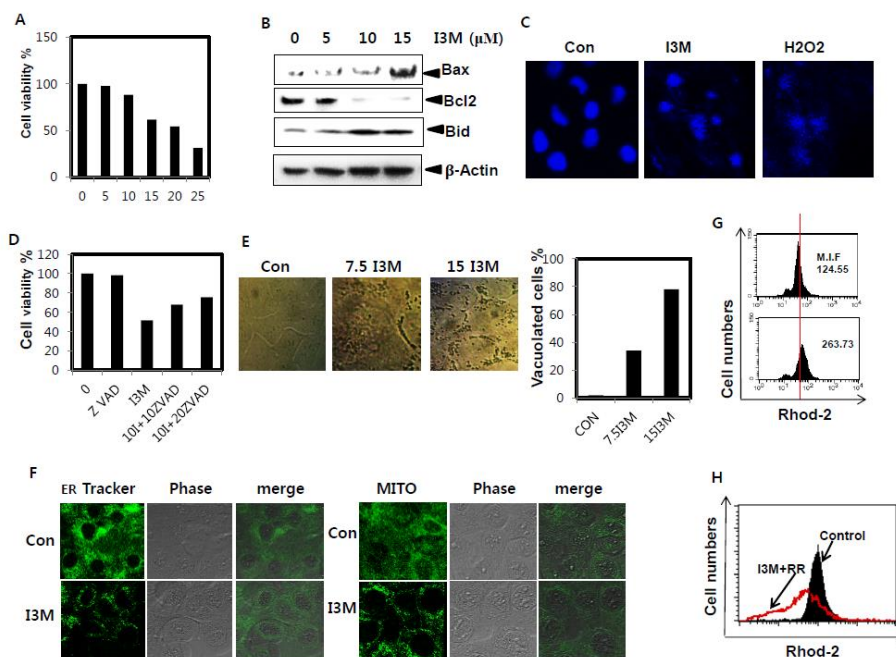
Fig. 10. Effects of I3M on the apoptosis and paraptosis in Hep3B cancer cells. (A and B) Hep3B

cells were seeded at 2×10^5 cells/ml and incubated with indicated concentrations of I3M (0-25

μM) for 24 h. Cell viability was measured by an MTT assay (A). Equal amount of cell lysates

was resolved on SDS–polyacrylamide gels, transferred to nitrocellulose membranes, and

probed with antibodies against Bax, Bcl-2, and Bid. β-Actin was used as an internal control for

western blot analyses (B). (C) The cells were treated for the indicated concentrations of I3M

and cells were fixed, permeabilized, and nuclei were stained with DAPI solution. Stained-

nuclei were then observed under a fluorescent microscope. (D) Hep3B cells were pretreated with the indicated concentrations of z-VAD-fmk for 1 h and further treated with 15 μM I3M for 24 h. Cell viability was measured by an MTT assay following 24 h. (E) Hep3B cells were incubated with indicated concentrations of I3M (0-15 μM) for 24 h. Cells were examined under light microscopy (×400) and percentage of vacuolated cells were calculated. (F) Cells were stained with ER Tracker and Mito Tracker followed by with or without I3M treatment for 24 h. Cells were observed under a fluorescent microscope (×400). (G) Hep3B cells treated with 15 μM I3M for 24 h and then stained with 2.5 μM Rhod-2. Rhod-2 fluorescence intensity was measured using flow cytometry. (H) Cells were treated with 4 μM Ruthenium red (RR), prior treatment with 15 μM I3M for 24 h. Rhod-2 fluorescence intensity was measured using flow cytometry.

3.3.2. I3M enhances p53 and p21 expression

We examined the effects of I3M on p53 expression in Hep3B cells because p53 mainly involved in Bax expression in apoptosis. The upregulation of Bax protein level induced by treatment of cells with I3M raised the possibility that I3M treatment activates the p53 tumor suppressor. In particular, western blot analysis show, I3M induced p53 expression in dose and time dependent manner, however markedly increased p53 expression was observed 24 h after the treatment of I3M (Fig. 11A). Next, we examined the p53 expression by immunocytochemistry. Compared with untreated control group, exposure to 15μM I3M at 24 h significantly enhanced the p53 expression level in Hep3B cells (Fig. 11B). Nevertheless, p53 controls the apoptosis via transcription regulation of p21, next we focused whether or not I3M regulates p21 expression. According to the RTPCR analysis, I3M induced p21 expression in

dose dependent manner (Fig. 11C, top). Similar to the mRNA expression, expression of protein level of p21, significant higher in dose dependent manner treatment of I3M at 24h (Fig. 2C, bottom). In a parallel experiment, we also analyzed p21 expression in time dependent manner with the treatment of I3M. Time dependent manner treatment of 10 μM I3M remarkably enhanced m-RNA and protein level of p21 in Hep3B cells with the starting point at 18 h and clearly at 24 h (Fig. 11D). Nevertheless, flow cytometry analysis confirmed that concentration dependent treatment of I3M gradually increased the p21 expression level (Fig. 11E). It has been proposed that p21 attributes with functions of the cell cycle regulatory proteins. Therefore, we were interested to investigate I3M regulate cell cycle arrest via p21 in Hep3B cells. We observed that I3M treatment remarkably induced G_2/M phase arrest in Hep3B cells. According to the flow cytometry analysis, treatment of 0, 5, 10, and 15 μM I3M significantly induced G2/M phase cell population as 9.77%, 15.59%, 20.52%, and 31.66% (Fig. 11F). Collectively these results indicate that I3M enhances the expression of p53 and p21 protein and mRNA level in Hep3B cells.
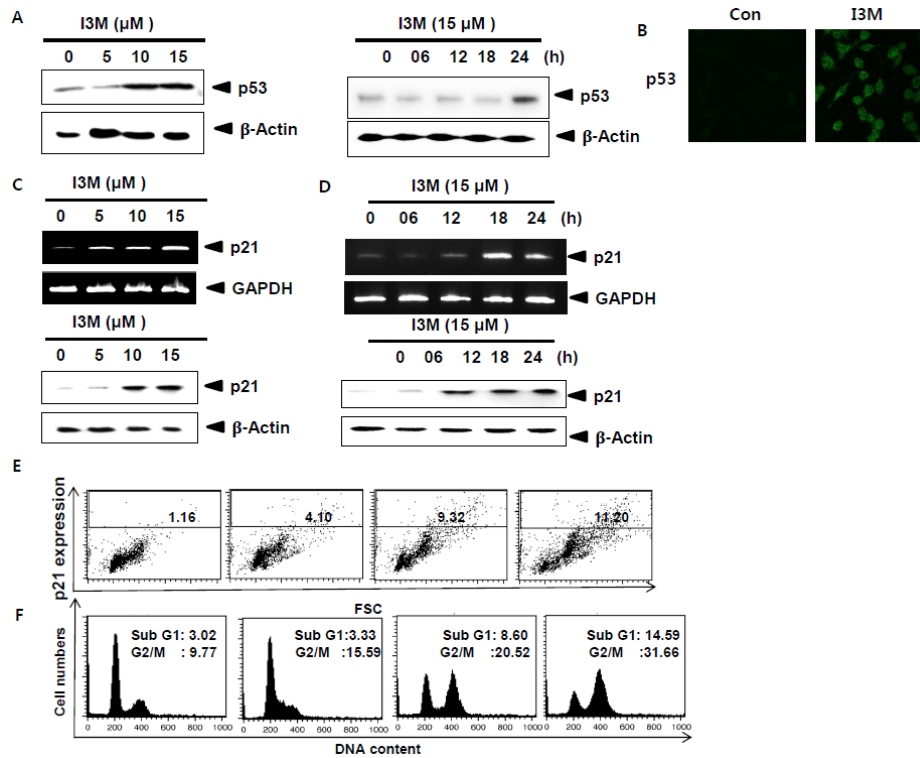
Fig. 11. I3M induces p53 and p21 expression. (A) Cells were incubated with indicated concentrations of I3M (0-15 μM) for 24 h and/or 15 μM I3M for indicated time (0-24 h). Western blot analysis of p53 was performed. (B) Cells were fixed, permeabilized, and stained with the p53 monoclonal antibody. The monoclonal antibody was detected using an antimouse secondary antibody conjugated with Alexa Fluor® 488. Stained-p53 then observed under a fluorescent microscope (×400). (C and D) Cells were incubated with indicated concentrations of I3M (0-15 μM) and/or 15 μM I3M for indicated time (0-24 h). RT-PCR and western blot analysis of p21 was performed at 6h and 24h, respectively. GAPDH and β-Actin were used as internal controls for RT-PCR and western blot analysis, respectively. (E and F) Cells were incubated with indicated concentrations of I3M (0-15 μM) for 24h. The expression of p21 (top panel) and sub-G_1 cell distribution (bottom panel) was analyzed by flow cytometry.

3.3.3. I3M-induced p21 expression regulate via p53

Cumulative data supported that p53 tumor suppressor protein directly regulates the activation of its transcriptional target, p21. Therefore, we postulated the biochemical relationship between p53 and p21 in Hep3B cells with exposure to I3M at 24h. A specific sip53 and p21 were transfected into Hep3B cells and transfection efficiency was analyzed by western blot (Fig. 12A). Transient knockdown of p53 suppressed I3M-induced p21 expression at protein level in Hep3B cells at 24 h (Fig. 12B). In a parallel experiment, we also analyzed mRNA expression level of p21 with the treatment of I3M in sip53 transfected Hep3B cells. As shown in Fig. 3C, the p21 mRNA expression was remarkably attenuated in sip53 transfected cells treated with I3M, contrary to that observed for the I3M alone treated group (Fig. 12C). In order to analyze the effect of p53 in regulation of p21 expression, next specific sip53 was transfected into Hep3B cells for 24 h, followed by treatment with 15μM I3M for 24 h before examine the intensity of p21 by immunofluorescent confocal microscopy. I3M significantly increased fluorescence intensity of p21 in Hep3B cells. On the other hand, sip53 transfection markedly decreased I3M-induced p21 fluorescence intensity in Hep3B cells (Fig. 12D). In particular, sip21 transfection slightly decreased the I3M-induced cell death; however, this downregulation did not reach the level observed for untreated control (Fig. 12E). These results demonstrate that I3M mediate p21 expression through p53 in Hep3B cells.

55
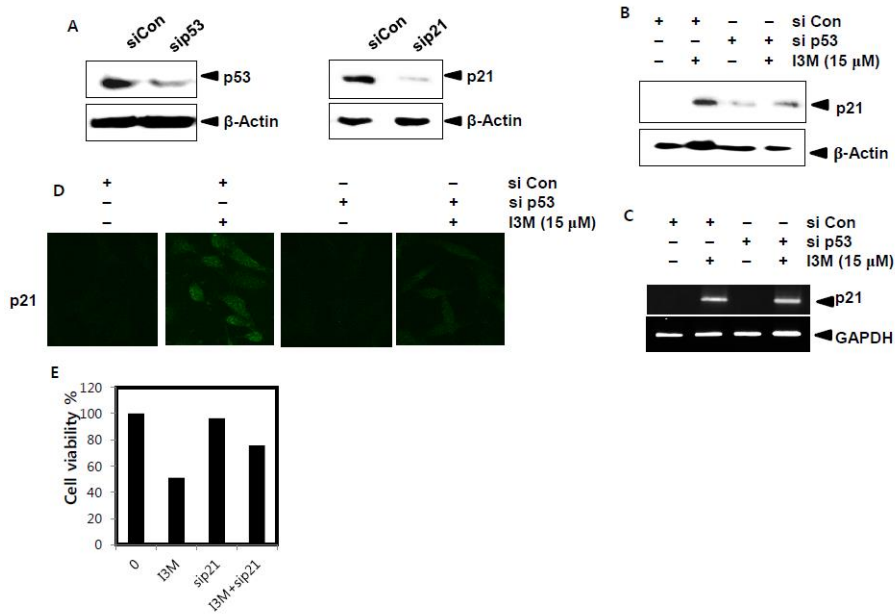
Fig. 12. I3M induces p21 expression via p53. (A) Cells were transiently transfected with *p53* and *p21* for 24 h and then to determine the transfection efficacy, western blot analysis was carried out. (B, C, and D) Cells were transiently transfected with *p53* siRNA for 24 h and then treated with or without before treatment with 15 μM I3M. Western blot analyses (B) and RT-PCR (C) of p21 was performed at 24 h and 6 h, respectively. GAPDH and β-Actin were used as internal controls for RT-PCR and western blot analyses, respectively. The expression of p21 level was detected by confocal microscopy (D). (E) Cells were transiently transfected with *p21* siRNA for 24 h and then treated with or without before treatment with 15 μM I3M for 24 h. Cell viability was measured by an MTT assay following 24 h.

3.3.4. I3M-induced ROS production via p21 reduces apoptosis

ROS generation play an important role in the stimulation of many cellular signaling pathways related to apoptosis. We thus investigated the effect of I3M-induced intracellular ROS generation and regulation of apoptosis in Hep3B cells. Moreover, researches have been

shown that upregulation of p21 expression can induce the ROS accumulation. Therefore, we were interest in elucidate the effect of p21 in ROS generation in I3M-treated Hep3B cells. First, we showed that ROS production was increased in Hep3B cells in response to I3M (Fig. 13A). Moreover, fluorometric data confirmed that treatment with antioxidants such as NAC and GSH significantly attenuates the I3M-induced ROS generation (Fig. 13B). Next to determine the effect of ROS generation on apoptosis in Hep3B cells were treated with 15 μM I3M for 2h followed by the treatment with ROS inhibitors, NAC and GSH and cytotoxicity was determined by the metabolic reduction of a tetrazolium salt to a formazan dye (MTT assay). We found that treatment with NAC and GSH further decreased I3M-reduced cell viability of Hep3B cells (Fig. 13B). In particular, morphological analysis was shown that I3M-induced formation of apoptotic bodies and cell shrinkage, which were significantly attenuated by the pretreatment of NAC (Fig. 13C). To investigate whether p21 is associated with ROS generation in Hep3B cells, we induced transient knockdown of p21 in Hep3B cells using siRNA of p21 (sip21). HE-based flow cytometric analysis showed that approximately 320 of the mean fluorescence intensity (MIF) of HE was increased in response to 15 μM I3M (Fig. 13D). In particularly, I3M-treated sip21-transfected group showed significant deduction of MFI as 278 in Hep3B cells. Accordingly, flow cytometry analysis fluorometric analysis also confirmed that I3M-induced ROS generation remarkably attenuated by transfection of p21 (Fig. 13E). Taken together, these results suggest that induce the expression of p21 mediate the ROS accumulation in I3M-treated Hep3B cells.
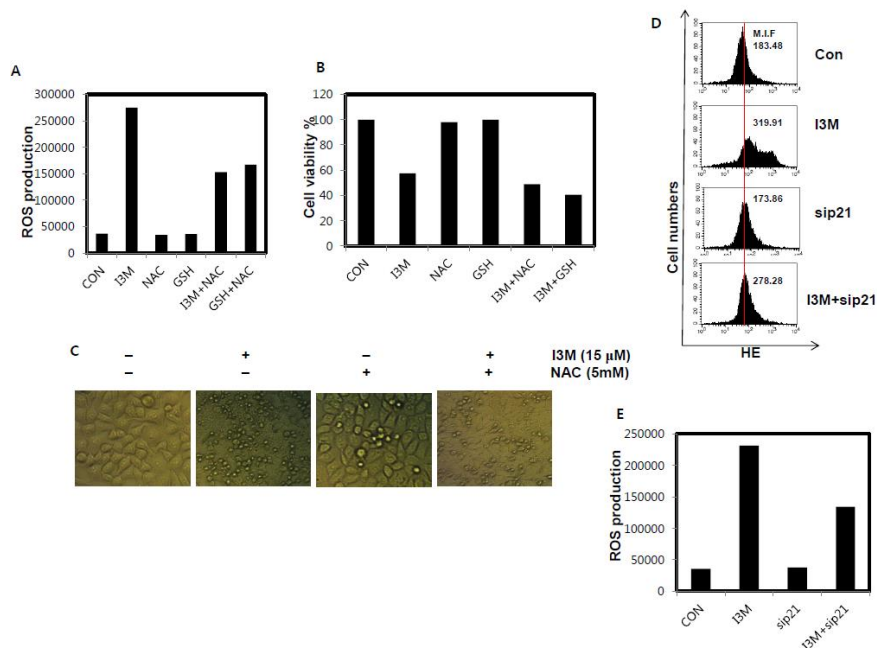
Fig. 13. The p21-mediated ROS decrease cell death. (A and B) Hep3B cells were pretreated with 20 μM DCFDA for 1h and then incubated with 5 mM of NAC and GSH for 1h and further treated with 15 μM I3M for 24h. ROS generation was analyzed by a fluorometer (A). Cell viability was measured by an MTT assay (B). (C) Cells were pretreated with 5mM of NAC for 1 h and further treated with 15 μM I3M for 24h. The morphology of cells treated with or without I3M was examined under light microscopy (×400). (D and E) Cells were transiently transfected with *p21* for 24 h and then treated with 15 μM I3M for 24 h and next stained with HE. Redox status was measured using flow cytometry (D). ROS generation was analyzed by a fluorometer (E).

3.3.5. I3M-induced NFκB activity via ROS

While NFκB transcription factor play a major role in regulating the amount of ROS in the cell next we determine the relationship between NFκB activity and ROS in I3M-treated Hep3B

cells, resulting in I3M-mediated apoptosis. Therefore, luciferase activity of NFκB was performed using transient transfection with reporter vectors that included NFκB promoters. Treatment with 10μM I3M significantly induced NFκB luciferase activity, whereas treatment of 5 mM NAC-downregulated I3M-induced NFκB luciferase reporter activity in Hep3B cells (Fig. 14A). Consistence with the above results, treatment with 10μM I3M substantially induced DNA-binding activity of NFκB in Hep3B cells (Fig. 14B). We also examined that I3M-induced DNA-binding activity of NFκB remarkably attenuated by pretreatment of NAC in Hep3B cells at 24 h (Fig. 14B). Further, it is revealed by examine the p50 and p65 protein expression level in cytosolic compartment in I3M and NAC treated Hep3B cells. Treatment of Hep3B cells with I3M for 24h significantly increased the protein expression level of p50 and p65 while pretreatment of 5mM NAC attenuated the I3M-induced p50 and p65 protein expression level (Fig. 14C). Moreover, next we investigate the effect of ROS in apoptosis using NFκB inhibitors PDTC and PS1145. Pretreatment with 20 μM PDTC and 10 μM PS1145 significantly attenuated I3M-reduced viability of Hep3B cells (Fig. 14D). Finally, MTT assay showed that pretreatment with PDTC remarkably enhanced I3M-induced cell death at 24 h in Hep3B cells (Fig. 14E). The data indicate that ROS play an important role in activation of NFκB transcription factor thereby reduced apoptosis in Hep3B cells.
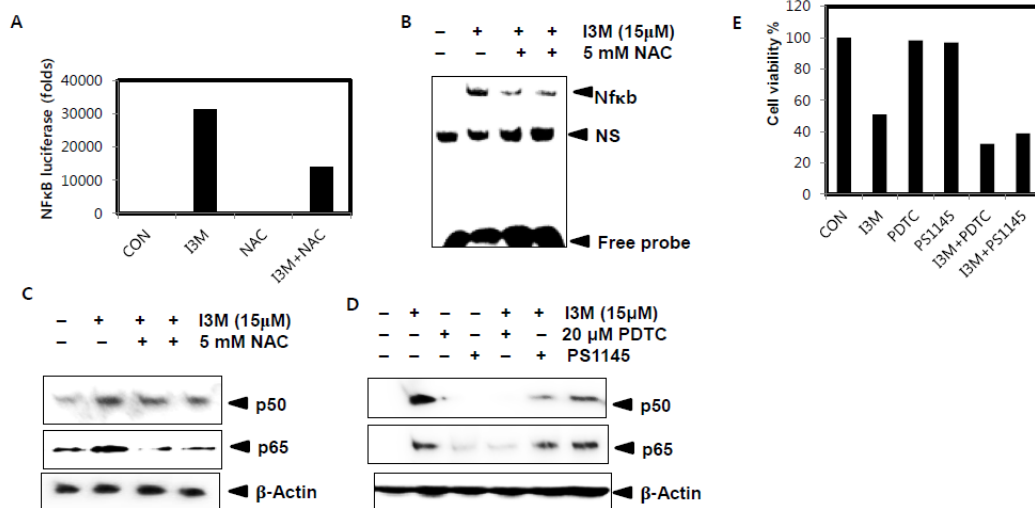
Fig. 14. I3M induces NFκB activity via ROS. (A) The cells were transfected with a NFκB promoter-containing reporter vector for 24 h and then 5 mM of NAC for 1 h and further treated with 15 μM I3M for 24 h. The luciferase activity was measured using luminometer. (B and C) Cells were pretreated with 5mM of NAC for 1h and further treated with 15 μM I3M for 24 h. Nuclear extracts were assayed for DNA-binding activity of NFκB using EMSA (B). Equal amount of cell lysates was resolved on SDS–polyacrylamide gels, transferred to nitrocellulose membranes, and probed with antibodies against p50 and p65 (C). β-Actin was used as a loading control. (D and E) The cells were preincubated with 20 μM PDTC and 10 μM PS1145 for 1 h before treatment with 5 μM I3M for 24 h. Cells were harvested and the indicated proteins were detected by Western blot analysis (D). β-Actin was used as a loading control. Cell viability was measured by an MTT assay (E).

3.3.6. I3M-induced p53 enhances apoptosis and paraptosis

In order to examine the role of p53 in apoptosis and paraptosis first specific sip53 was transfected into Hep3B cells according to the lipofectamine method. MTT data showed that

60

I3M-reduced cell viability was slightly altered in I3M-treated sip53 transfected cells (Fig. 15A). Treatment of 15 μM I3M decreased cell viability approximately 50% while I3M-reduced cell death altered approximately 20% in I3M-treated sip53 transfected cells. We next analyzed in detail the effect of p53 in apoptosis and paraptosis. Western blot analysis was conducted to determine the apoptotic effect of p53 induced by I3M in Hep3B cells at 24 h. As shown in Fig. 6B, I3M-induced protein expression level of Bid significantly attenuated by I3M-treated sip53 transfected cells (Fig. 15B). Furthermore, I3M-decreased Pro-Caspase-8 and Bcl-2 protein expression level remarkably upregulated by transfection of p53 into Hep3B cells (Fig. 15B). In order to examine the activity of p53 in paraptosis process, sip53 transfected Hep3B cells subjected to the flow cytometry analysis. For functional confirmation of p53 in paraptosis, we tested the Ca^{2+} uptake by mitochondria after exposure to mitochondrial Ca^{2+} indicator dye, Rhod-2. I3M-treated sip53 transfected Hep3B cells significantly reduced I3M-increased mitochondrial Ca^{2+} levels at 24 h (Fig. 15C). Additionally, we investigated mitochondrial Ca^{2+} uptake after exposure to Rhod-2 by immunofluorescent confocal microscopy. I3M sharply increased fluorescence intensity of Rhod-2 (Fig. 15D). On the other hand, I3M-induced Rhod-2 fluorescence intensity slightly decreased by I3M-treated sip53 transfected Hep3B cells. These results demonstrate that I3M mediate p53 regulate both apoptosis and paraptosis processes in Hep3B cells.
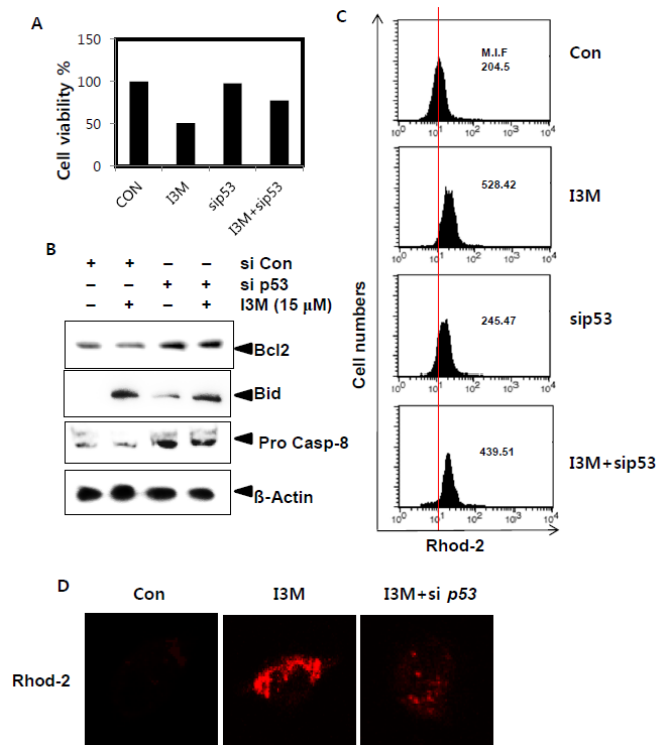
Fig. 15. I3M-induces p53 enhanced paraptosis and apoptosis. (A and B) Cells were transiently transfected with *p53* siRNA for 24 h and then treated with or without before treatment with 15 μM I3M for 24 h. Cell viability was measured by an MTT assay (A). Cells were harvested and the indicated proteins were detected by Western blot analysis (B). β-Actin was used as an internal control. (C and D) Rhod-2 fluorescence intensity was measured using flow cytometry and fluorescent microscope (×400), respectively.

3.4. Discussion

We reported previously that the I3M-induced cell death in MDA-MB-231 breast cancer cells via paraptosis by accumulation of Ca^{2+} into mitochondria by opening mitochondrial channel uniporters through ER stress and involving proteasome dysfunction. Moreover, in this study

62

we indicated that I3M-induced cell death regulated partially through paraptosis in Hep3B hepatocarcinoma cells. The current report investigated the molecular mechanism of cell death pathways, paraptosis and apoptosis enhanced by I3M in human hepatocarcinoma cell line, Hep3B, while assessing the involvement of paraptosis and apoptosis in I3M-induced cell death. In this study, we showed that I3M-enhanced cell death in Hep3B cells was mediated partially by caspase-dependent apoptosis and caspase-independent paraptosis. Nevertheless, here we describe the involvement of p53 in regulation of both process of apoptosis and paraptosis in Hep3B cells. Moreover, importance of p21-mediated ROS accumulation regulates NFκB transcription factor on apoptosis also investigated.

Apoptosis or programmed cell death and paraptosis are different types of cell death mechanisms characterized by specific morphological features and energy-dependent biochemical process (Elmore., 2007). Aside from the induction of apoptosis, I3M was found to induce paraptosis in Hep3B cells by triggering different signaling pathways. In addition to morphological variations, a main difference between the apoptosis and paraptosis is that apoptosis is predominantly caspase-dependent while paraptosis is caspase-independent. In particularly, pretreatment of pan caspase inhibitor z-VAD-fmk partially blocked I3M-enhanced cell death while further increasing the concentration of z-VAD-fmk could not completely blocked that I3M-induced cell death suggesting that there is another type of cell death being occurred in Hep3B cells. However; exposure to I3M gradually induced the protein expression level of pro-apoptotic family members Bid and Bax while decreasing anti-apoptotic Bcl-2 protein expression and also I3M treatment slightly formed the fragmented nuclei indicating I3M-partially involved in induction of apoptosis in Hep3B cells. As expanding body of evidence suggest as a distinct feature of paraptosis vacuoles are formed by subsequent fusion

of excessive swelled ER and mitochondria (Maltese and Overmeyer., 2014 and Wei et al., 2015). Accordance to that, vacuolation was examined after treatment with I3M in Hep3B cells. More importantly researches have been shown, Ca^{2+} influx from the extracellular space via the plasma membrane or by release of Ca^{2+} from endoplasmic (ER), sarcoplasmic (SR) like intracellular Ca^{2+} stores affect to the elevation in intracellular Ca^{2+} concentration (Patergnani et al., 2011). Hence, Rhod-2 staining of Hep3B cells shown that I3M treatment significantly increased the Rhod-2 staining intensity by suggesting I3M treatment increased the intracellular mitochondrial Ca^{2+} levels. Therefore, collectively above results indicate, aside induction of apoptosis by I3M, I3M was found to induced paraptosis in Hep3B cells.

P21 belongs to the Cip/Kip family of cdk inhibitors and is a key regulator of p53-dependent cell cycle arrest after DNA damage (Abbas and Dutta., 2009). The regulation of p21 mainly regulate through the tumor suppressor p53 (Thakur et al., 2010). p53 induces the constitutive expression of p21 in stressed cells, by binding to two highly conserved response elements located in p21 promoter region (Piccolo and Crispi., 2012). In this regards, our results also indicated that regulation of p21 via p53 by decreasing the p21 expression level in sip53 transfected Hep3B cells. To date, numerous researches have examined the tumor suppression role of p21. However, the mechanisms of apoptosis mediate by p21 is not well define and it may depend on cell type and environment (Piccolo and Crispi., 2012). Cumulative data supported that p21 is essentials for the upregulation of ROS level as well (Masgras et al., 2012). Recent study has shown transient overexpression of Myc-tagged p21 in HN31 cells significantly enhanced the ROS production level by indicating strong correlation between p21 and ROS in senescence of head and neck cancer cells (Fitzgerald et al., 2015). Consistence with these studies, I3M shown to be enhanced intracellular ROS production and this ROS level

mainly regulated through p21 as indicated by luminometer and flow cytometry data. The siRNA transfection of p21 significantly reduced I3M-induced ROS production in Hep3B cells. However, this induction of ROS via p21 resulted in enhanced the NFκB activity thereby it decreased the apoptosis in Hep3B cells. Since it is known the NFκB pathway promote apoptosis in cancers; there has been few reports regarding the antiapoptotic effect of NFκB in various cancer cell lines. The NFκB inhibitor DHMEQ, induced apoptosis in chronic lymphocytic leukemia cells by induction of antiapoptotic genes (Horie et al., 2006). Another study has indicated that NF-κB activity is necessary for survival of KSHV-infected lymphoma cells, while treatment of an irreversible inhibitor of IκBα phosphorylation, completely and specifically abrogated the NF-κB thereby induced apoptosis in primary effusion lymphoma cells (Keller et al., 2000). In the present study, we have shown, I3M-induced NFκB transcription was inhibit the apoptosis process in Hep3B cells. Treatment of inhibitors of NFκB, PDTC and PS1145 could not reduce the I3M-decreased cell viability in Hep3B cells as shown in MTT assay. Nevertheless, tumor suppressor p53 also act as a regulator of NFκB (Murphy et al., 2011), the importance of p53 in NFκB transcription should be investigated in I3M-induced cell death. Since p53 is a redox activate transcription factor, the evaluation of the indirect regulation of NFκB via ROS production is much importance in study of the molecular mechanism of apoptosis regulate by I3M.

In this study, we have shown that I3M potential to enhance p53 expression directly in Hep3B cells. According to our results, cell death in Hep3B cells by I3M mainly regulated by p53 which can enhance both apoptosis and paraptosis process directly while involving block of the apoptosis indirectly via p21-ROS-NFκB axis in Hep3B cells. p53 stimulates a wide network of signals in both intrinsic and extrinsic apoptotic pathways, while triggering

제주대학교 중앙도서관
JEJU NATIONAL UNIVERSITY LIBRARY

apoptosome formation, maintaining balance in pro-apoptotic Bcl-2 family members and inducing activation of caspases through death receptor pathway respectively (Haupt et al., 2003). On the other hand, p53 enhance paraptosis process also by inducing formation of cytoplasmic vacuoles (Rojpibulstit et al., 2014). Given the results presented here sip53 treatment significantly blocked I3M-induced apoptosis by decreasing Bid, increasing Bcl-2, pro-caspase 8 and paraptosis through decreasing Rhod-2 staining intensity. Because of NFκB represses the transactivation of p53, the investigation of these facts are needed as future studies (Webster and Perkins., 1999).

Taken together, we showed that I3M induced p53 expression, which contributes to trigger both apoptosis and paraptosis cell death. Nevertheless, our results also demonstrated, treatment of I3M enhance p21 via p53 and p21-mediated expression of ROS/NFκB axis block the apoptosis while simultaneously induces activation of two different pathways of cell death. In this regards, by targeting different cell death pathways for develop an anticancer agent using I3M may be a promising strategy for future anticancer therapy.

3.5. Conclusion

I3M enhance p21 via p53 and p21-regulated expression of ROS/NFκB axis inhibits the apoptosis while simultaneously induces activation of two different pathways of cell death in Hep3B hepatoma cancer cells. Therefore, I3M may be a good therapeutic option for treatment of hepatoma cancers.

Chapter 4

Indirubin-3′-monoxime induces apoptosis via nitric oxide (NO) in human prostate cancer cells: Involvement of ER stress, ROS, NF-κB, and Nrf2

Abstract

Indirubin is the active ingredient of the traditional Chinese medicine *Dang Gui Long Hui Wan*, a mixture of plants, acts a potent inducer of apoptosis in a variety of cell types. In the present study, we have shown the anticancer effect of indirubin-3'-monoxime (I3M), a derivative of indirubin, by targeting nitric oxide (NO). Our data showed that I3M treatment triggers the apoptotic signaling pathways in prostate cancer cells. Considering the NO-targeted apoptosis, transcriptional and translational regulation of NO regulate by various factors such as nuclear factor-κB (NF-κB), reactive oxygen species (ROS), Nuclear factor erythroid 2-related factor 2 (Nrf2) and endoplasmic reticulum (ER) stress etc: through alterations in iNOS activity. I3M induces NF-κB activity by enhancing the nuclear translocation of p65/p50 and degradation of IκBα, and consequently, induces the expression of *iNOS* in LNCaP cells. Except NF-κB, Nrf2 also involve in regulation of NO-mediated apoptosis by I3M. Treatment of I3M induced ROS generation and ROS act as key regulators of Nrf2 activity in the I3M-mediated apoptosis. Nevertheless, Nrf2 is an important factor that regulate ROS level thereby regulate the NO expression. On the other hand, NO importantly involve in nuclear translocation of Nrf2. Our data showed that I3M induces NF-κB activity in LNCaP cells via the ROS and consequently, regulates the expression of NO production by regulating iNOS expression. Moreover, through NF-κB and NO production potently regulate ROS level by I3M treatment in the LNCaP prostate cancer cells. The concentration dependent manner treatment of I3M remarkably induced ER stress which potently regulate by ROS in LNCaP cells. The current study indicated that the ER stress, NFκB and ROS are important factors that regulate NO expression by I3M. Further, the induction of NO regulates apoptosis via intrinsic and extrinsic pathways in LNCaP prostate cancer cells. Hence, NO-mediated cell death could be explored

as a crucial mode for apoptosis process; I3M may offer a 'NO targeting' approach as a potential chemotherapeutic agent.

Key words; Indirubin-3'-monoxime, Nuclear factor-κB, Reactive oxygen species, Nuclear factor erythroid 2-related factor 2, Endoplasmic reticulum

4.1. Introduction

Indirubin has been identified as the active ingredient of the traditional Chinese medicine *Dang Gui Long Hui Wan*, which has been used to treat chronic myelocytic leukemia along the centuries (Blažević et al., 2015). It has been reported that the indirubin derivatives acts a potent inducer of apoptosis in a variety of cell types, including lung cancers (Ahn et al., 2015), brain tumors (Zhang et al., 2015), chronic myeloid leukemia (Kim et al., 2013), thyroid (Preuss et al., 2015), cervical, hepatoma and colon cancers (Blažević et al., 2015). The commercially available analogue of indirubin, indirubin-3′-oxime (I3M), one of the indirubin derivative strongly induce apoptosis in cancer cells via multiple signaling pathways (Lo and Chang., 2013). However, the regulatory mechanisms underline the I3M-mediated apoptosis in human prostate cancer cells have yet to be investigated.

Over the past decades, it has become evident that nitric oxide (NO) plays a crucial role in the regulation of the homeostasis in immune, neurological and vascular systems but implicated in many physiological and pathological processes (Kolluru et al., 2013). NO is synthesized from the terminal guanido nitrogen of L-arginine to form three distinct isoforms, product of various genes with different regulation, localization, inhibitor sensitivity, and catalytic properties (González et al., 2015). It's relatively simple, however traditionally useful

categorization distinguishes inducible and constitutively expressed isoforms of NO, which estimates moderate versus elevated generation rates of endogenously expressed NO. NO involves in carcinogenesis via stimulation of cell proliferation, regulation of angiogenesis and cancer cell migration mainly in the progression and promotion stages of carcinogenesis (Kapral et al., 2015). On the other hand, NO exhibit its cytotoxic effect by peroxidation of lipid membrane, destruction of DNA, induction of membrane permeability and reduction of DNA repair enzymes, however, the mechanism of the cell death has not been fully clarified (Kapral et al., 2015).

It is controversial whether the release of NO by different cell types accounts for different factors such as NFκB (Dilshara et al., 2015), Nrf2 like transcription factors (Um et al., 2011), ROS generation (Hsieh et al., 2014), and via ER stress (Meares et al., 2011). The NO releases by variety of cells depend upon the transcription of the *iNOS* gene (Vanini et al., 2015). The *iNOS* promoters consist of binding sites for different transcription factors such as NFκB, IRF-1, IRF-2, STAT family which activated by IFN-γ and several C/EBP-, and CREB family members (Saldarriaga et al., 2012). Among these transcription factors, transactivate the iNOS promoter of NFκB is poorly understood. It is elucidated that number of NF-κB binding sites in human iNOS promoter can be effect the response intensity to NFκB determined by the concentration of particular transcription factor in certain cell type. In many in vitro and in vivo studies have been indicated that NO plays a crucial role as a proinflammatory mediator and that this effect may be mediated by NFκB. Nevertheless, transcription factors NF-E2-related factor 2 (Nrf2) attenuates NFκB-induced NO production via binding of Nrf2 directly to antioxidant response elements (AREs) of HO-1 (Dilshara et al., 2014). Nrf2 localize in the cytoplasm with an Nrf2-inhibitory protein known as Kelch-like ECH-associated protein 1

70

(Keap1) (Abed et al., 2015). In response to oxidative stress, Nrf2 releases from Keap 1 and subsequently enhances nuclear translocation for binding the AREs of HO-1 thereby regulates the NO production (Dilshara et al., 2014).

Accumulating evidence suggests that production of ROS and ER stress are closely linked events; however, the relationship is not well exposed yet. Consequently, accumulation of misfolded proteins in the ER lumen evokes leakage of Ca^{2+} into cytosol thereby increasing ROS production in the mitochondria (Ferreiro et al., 2012 and Görlach et al., 2015). Although, ROS have emerged as key regulators of ER stress and UPR activation however; ROS mediate ER stress during apoptosis process has not been fully clarified (Brown and Griendling., 2015). Notwithstanding, unfolded protein response arise due to ER stress and excessive ROS triggers the activation of NFκB (Chaudhari et al., 2014), thus ER stress and ROS are indirectly involves to regulation of NO level in the cell. As well as Nrf2 is an emerging regulator of ROS production via stimulating transcription of antioxidant proteins (Ma., 2013). Recent studies have shown that activation of Nrf2 modulate via ROS as well (Paul et al., 2014). The interaction between ROS and Nrf2 involves indirectly to regulate NO production via regulating NF-κB while that NO production is directly modulated by Nrf2. Taken together several mechanisms seem to involves to regulate NO production thereby induced cell death.

Eventhough cell death occurred via NO by regulating several processes such as apoptosis (Snyder et al., 2009), autophagy (He et al., 2014) and necrosis (Bal-Price and Brown., 2000), in this study we focused on apoptosis since apoptosis concern as main pathway that leading to cell death. NO is implicated in a wide range of regulating factors despite play crucial role in cell death either by stimulating extrinsic or intrinsic apoptosis pathway. Hence, NO mediated

71

cell death could be explored as a key mode for apoptosis process; I3M may offer a 'NO targeting' approach as a potential chemotherapeutic agent.

4.2. Materials and method

4.2.1. Antibodies and reagents

Antibodies against JNK, phospho (p)-JNK, PARP, LC3, eIF2α, p-eIF2α, 3-(4,5-dimethyl-2-thiazolyl)-2,5-diphenyl-2H-tetrazolium bromide (MTT), N-acetylcysteine (NAC), γ-L-glutamyl-L-cysteinylglycine (Glutathione), propidium iodine (PI), and annexin V were from Sigma Chemical Co. (St. Louis, MO). Rabbit anti-human antibodies against Bid, Bax, caspase-3, PARP, Bcl2, cytochrome c, and β-Actin were from Santa Cruz Biotechnology (Santa Cruz, CA). Peroxidase-labeled goat anti-rabbit immunoglobulin was from KOMA Biotechnology (Seoul, Republic of Korea). ER-Tracker-FITC was purchased from Molecular Probes (Eugene, OR). Roswell Park Memorial Institute (RPMI)-1640 medium and fetal bovine serum (FBS) were from WelGENE Inc. (Daegu, Republic of Korea).

4.2.2. Cell line and cell viability assay

LNCaP and DU145 prostate cancer cell lines were maintained using RPMI medium with 10% heat-inactivated FBS and 1% penicillin–streptomycin in 5% CO_2 at 37°C. For cell viability assay, cells were seeded in 24 well plates at 37°C. The 3-(4,5-dimethyl-2-thiazolyl)-2,5-diphenyl-2H-tetrazolium bromide (MTT) was used under different experimental conditions. I3M was treated according to the indicated concentrations 24 h after incubation time. 24 h after 0.5 mg/ml MTT solution was treated for 45 min at 37°C. Then removed the

culture media and 700 µl of dimethyl sulfoxide was added to each well. The absorbance was carried out at 540 nm using the microplate reader. Three independent experiments were done by triplicate.

4.2.3. NO assay

NO$^{\bullet-}$ was measured as stable nitrite, the end product of NO$^{\bullet-}$ generation by spectrophotometric assay based on the Griess reagent (1% sulfanilamide in 5% phosphoric acid and 0.1% naphthylethylenediamine dihydrochloride). The absorbance at 540 nm was taken in a microplate spectrophotometer (Thermo Electron Copporation, Marietta, OH). The concentration of nitrite was determined by interpolation in a sodium nitrite standard curve. Three independent experiments were carried out.

4.2.4. Western blot analsysis

Cell pellet was taken after 24 h treatment of specified chemical concentrations. The total extraction of cells was prepared using an ice-cold PROPREP protein extraction kit (iNtRON Biotechnology) in 100 µl of volume. Supernatant was taken after centrifugation at 16,000 rpm at 4°C for 30 min. By using the Bio-Rad protein assay kit (Bio-Rad, Hercules, CA) protein concentrations of the supernatant was measured.   For electrophoresis process proteins were loaded on 5% SDS-PAGE and transferred to the nitrocellulose membranes (Schleicher and Schull, Keene, NH). Chemiluminescence detection system was used to detection of proteins (Amersham, Arlington Heights, IL).

4.2.5. Isolation of total RNA and RT-PCR

Easy-blue reagent (iNtRON Biotechnology, Sungnam, Republic of Korea) was used to extraction of total RNA from the cells. Interest genes were amplified from cDNA and 1 μg total RNA reverse-transcribed using the One-Step RT-PCR Premix (iNtRON Biotechnology). The specific primers for *iNOS* (forward 5′-CCT CCT CCA CCC TAG CAA GT-3′ and reverse 5′-CAC CCA AAG TGC TTC AGT CA-3′), *HO-1* (forward 5′-TGA AGG AGG CCA CCA AGG AGG-3′ and reverse 5′-AGA GGT CAC CAG GTA GCG GG-3′), *glyceraldehydes-3-phosphate dehydrogenase* (*GAPDH*) reverse 5′-CCA CCC ATG GCA AAT TCC ATG GCA-3′); and *GAPDH* forward 5′-TCT AGA CGG CAG GTC AGG TCC ACC-3′). PCR reaction was initiated at 94°C for 2 min followed by 31 cycles of 94°C for 30 min, 30-min annealing temperature, 72°C for 30 min followed by final extension at 72°C for 5 min. Annealing temperatures for *HO-1*, and *GAPDH* was and 62°C. For *iNOS*, 25 cycles of denaturation at 94°C for 30 s, annealing at 59°C for 30 s and extended at 72°C for 30 s.

4.2.6. Electrophoretic mobility shift assay (EMSA)

Nuclear extracts were prepared using NE-PER nuclear extraction reagents (Pierce, Rockford, IL). Using the biotin 3′-end DNA labeling kit (Pierce) synthetic complementary NF-κB (5′-AGT TGA GGG GAC TTT CCC AGG C-3′) binding oligonucleotides (Santa Cruz Biotechnology) were 3′-biotinylated following the manufacturer's instructions. After the annealed for 2 4h at room temperature, assays were loaded onto native 4% polyacrylamide gels pre-electrophoresed for 60 min in 0.5× Tris borate/EDTA before being transferred onto a positively charged nylon membrane (Hybond™-N⁺) in 0.5× Tris borate/EDTA at 100 V for 30 min. Transferred DNAs were cross-linked to the membrane at 120 mJ/cm^2 and detected using horseradish peroxidase-conjugated streptavidin according to the manufacturer's

instructions.

4.2.7. Flow cytometric analysis

After the treatment with indicated concentrations of chemicals cells were incubated for 24 h, then cells were harvested and incubated in dark with PI and RNase A for 30 min at 37°C. Flow cytometric analysis was performed with a FACSCalibur flow cytometer (Becton Dickinson, San Jose, CA).

4.2.8. Luciferase assay

Cells were seeded onto plates with 5×10^5 cells/ well density and allowed to grow overnight. Nuclear transcription factor-κB reporter construct was purchased from Clontech (Palo Alto, CA, USA). Lipofectamine method was used to transfection of cells. Transfection was carried out 2 μg each plasmid construct for 6 h and cells were cultured in 10% Dulbecco modified Eagle medium containing I3M and fetal bovine serum for 24 h. Using lysis buffer (1% Triton X-100, 20 mM Tris-HCl [pH 7.8], 150 mM NaCl, and 2 mM DTT) cells were lysed. Five μl cell lysates were mixed with 25 μl luciferase activity assay reagent and after the produce luminescence was measured using a GLOMAX luminometer (Promega, Madison, WI).

4.2.9. Transient knockdown of Nrf2

LNCaP cells were plated on a 24-well plate at a density of 1×10^5 cells/ml. Then, cells were transfected with *Nrf2*-specific silencing RNA (siRNA, Santa Cruz Biotechnology) for 24 h. 450 μl of cell growth medium and 20 nM siRNA duplex was added with transfection reagent G-Fectin (Genolution Pharmaceuticals Inc., Seoul, Republic of Korea) in each transfection.

4.2.10. DNA fragmentation assay

After treatment of indicated chemical concentrations for 24 h cells were lysed on ice using DNA lysis buffer containing 10 mM Tris–HCl (pH 7.4), 150 mM NaCl, 5 mM EDTA, and 0.5% Triton X-100 for 30 min. Lysates were vortexed and centrifugation at $16,000 \times g$ for 20 min. Equal volume of neutral phenol:chloroform:isoamylalcohol (25:24:1, v/v/v) was used to extract fragmented DNA from the supernatant. Fragmented DNA was electrophoretically analyzed on 1.5% agarose gel containing ethidium bromide.

4.2.11. Statistical analysis

Chemi-Smart 2000 (Vilber Lourmat, Marine, Cedex, France) was used to visualize images. Chemi-Capt (Vilber Lourmat) was used to capture images and transported into Photoshop. Using SigmaPlot software (version 12.0) statistical analysis was performed. All data were derived from 3 independent experiments for in vitro assays. All values were indicated as means ± SE.

4.3. Results

4.3.1. I3M effects on viability of prostate cancer cells

In order to investigate whether or not I3M induces cell death, we treated LNCaP and DU145 prostate cancer cells for 24 h with I3M at concentrations ranging from 0 to 40 μM. Treatment with I3M at concentrations up to 10 μM did not significantly reduce the cell viability; however, a concentration of 20 μM I3M resulted in approximately 40% cytotoxicity (Fig. 16A). Furthermore, the effect of I3M on cell viability was determined by the annexin-V positive cell

populations using flow cytometry analysis. Treatment with I3M ranging from 0 to 30 μM, significantly enhanced annexin-V positive cell population from 5% to 23% respectively (Fig. 16B). Next, western blot analyses of proapoptotic and antiapoptotic factors were performed to monitor changes in the activation of caspases and the expression of the other apoptosis-related proteins. Dose dependent manner treatment with I3M minimally decreased the expression of procaspase-3, and increased the expression of Bax and cleaved BID level in LNCaP and DU145 prostate cancer cells (Fig. 16C). We found that dose dependent manner treatment with I3M influence on DNA fragmentation in LNCaP cells (Fig. 16D). Under the light microscope, I3M-treated cells exhibited a rounded and granulated morphology, and eventually degraded after treatment of I3M up to 20 μM in both LNCaP and DU145 prostate cancer cells (Fig. 16E). The results indicate that I3M treatment triggers the apoptotic signaling pathways in prostate cancer cells.
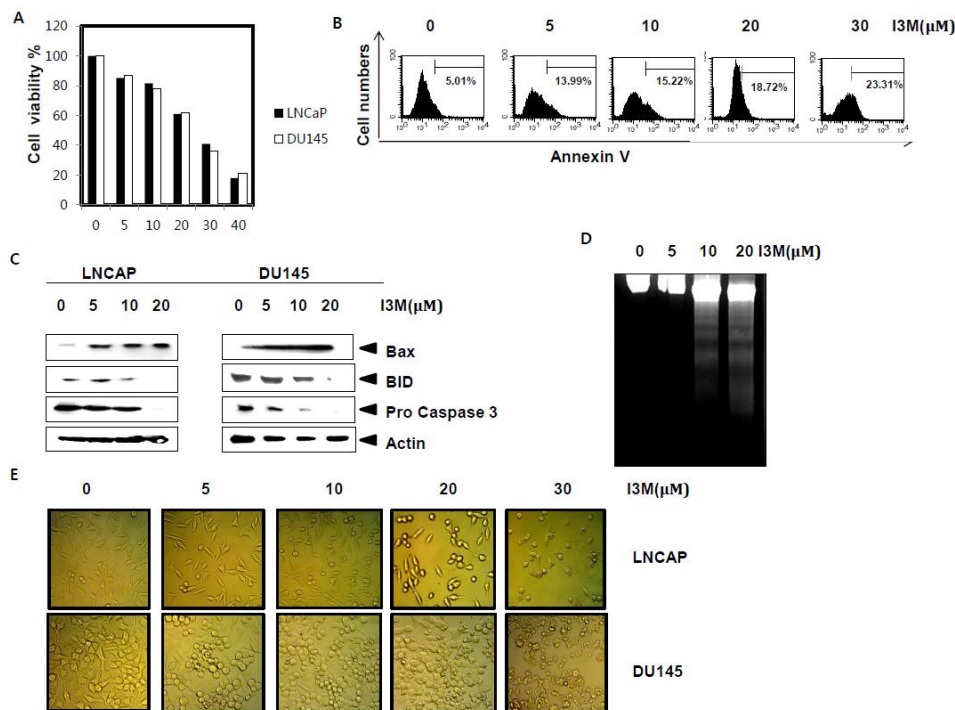
Fig. 16. Effects of I3M on the viability of LNCaP and DU145 cells. LNCaP and DU145 cells treated with the indicated concentrations of I3M for 24 h. (A) Cell viability was measured by an MTT assay following 24 h. (B) The cells were then stained with annexin-V and analyzed by flow cytometer. (C) Equal amount of cell lysates were resolved on SDS–polyacrylamide gels, transferred to nitrocellulose membranes, and probed with antibodies against Bax, BID, and caspase-3. (D) Total DNA was extracted from the cells and DNA fragmentation assay was performed using 1.5% agarose gel. (E) The morphology of cells treated with or without I3M was examined under light microscopy (×400).

4.3.2. I3M induces NO production via NFκB pathway in LNCaP prostate cancer cells

NO seems to play an important role in apoptosis in many cancer cells (Bonavida and Garban., 2015); therefore, to elucidate the molecular mechanism underlying the enhancement of apoptosis by I3M, we examined the production of NO in LNCaP prostate cancer cells. LNCaP cells were treated with different concentrations of I3M for 24 h, and 20 μM of I3M treated in different time points before determination of the levels of NO in the culture media by Griess assay. Concentration (Fig. 17A, left) and time (Fig. 17A, right) dependent manner treatment of I3M increased NO production in LNCaP cells. In particular, 10 μM and 20 μM I3M significantly induced NO production (10 ± 3 μM and 23 ± 5 μM at 10 μM and 20 μM I3M, respectively). Additionally, we investigated whether I3M regulates iNOS mRNA expression. Dose dependent manner exposure to I3M enhanced iNOS mRNA expression in LNCaP cells consistent with the NO production (Fig. 17B). Nevertheless, western blot analysis showed that treatment with I3M markedly increased iNOS protein expression at 24 h in a concentration-dependent manner (Fig. 17C). These results demonstrate that I3M possesses significant

78

enhance effects on the iNOS expression and NO production. In order to determine the activity of NF-κB against iNOS expression, we conducted an EMSA and western blot analysis. EMSA data confirmed that I3M treatment significantly increased the specific DNA-binding activity of NF-κB at 24 h (Fig. 17D). Additionally, we investigated whether I3M regulates nuclear translocation of NF-κB subunits, p50, p65, and IκBα in LNCaP cells. Western blot analysis showed that I3M significantly decreased the total amount of p50, p65, and IκBα in the cytosolic extracts indicating that I3M promotes NF-κB activity by inducing nuclear translocation of the NF-κB subunits (Fig. 17E). In addition, NF-κB luciferase activity significantly increased by approximately 4-fold in I3M treated LNCaP cells, compared with the untreated control group (Fig. 17F). These data indicate that I3M induces NF-κB activity by enhancing the nuclear translocation of p65/p50 and degradation of IκBα, and consequently, induces the expression of *iNOS* in LNCaP prostate cancer cells.
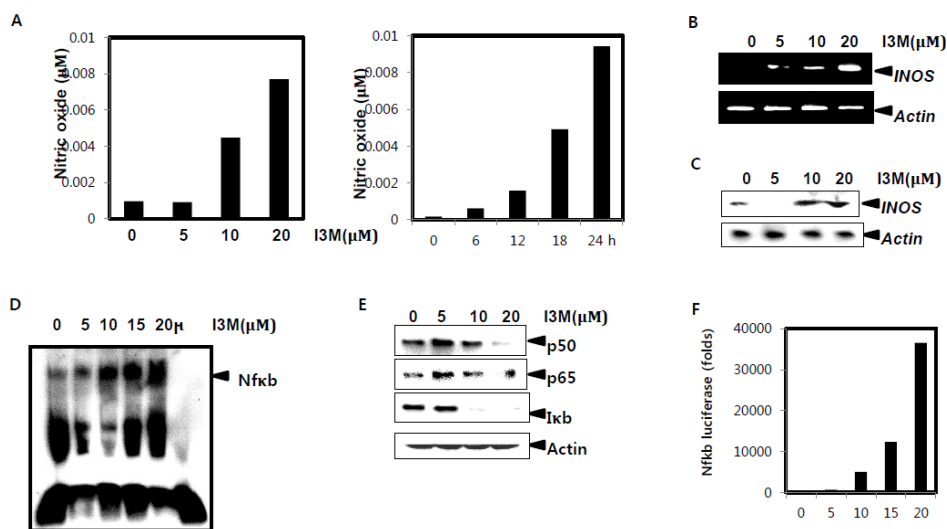
Fig. 17. Effect of I3M on NFκB mediated NO production. (A) Cells were seeded at 2×10^5 cells/ml and incubated with indicated concentrations of I3M (0-15 μM) for 24 h and 20 μM I3M for indicated time (0-24 h). NO production was determined by Griess reagent. (B)

제주대학교 중앙도서관
JEJU NATIONAL UNIVERSITY LIBRARY

Cells were incubated with indicated concentrations of I3M (0-20 μM) for 24 h. RT-PCR and (C) western blot analyses of iNOS was performed at 24 h, respectively. Nuclear extracts were assayed for DNA-binding activity of NFκB using EMSA. (E) Cells were incubated with indicated concentrations of I3M (0-20 μM) for 24 h. Western blot analyses was done for indicated proteins. (F) The cells were transfected with a NFκB promoter-containing reporter vector, and luciferase activity was measured 24 h after transfection. β-Actin and GAPDH were used as internal controls for western blot and RT-PCR analyses respectively.

4.3.3. I3M activates Nrf2 pathway regulate the NF-κB pathway

Next, we evaluate the relationship between Nrf2 and NF-κB and effect on I3M induced apoptosis through NO production in LNCaP cells. Essentially, we evaluated whether I3M potently enhance the activity of Nrf2 transcription factor via EMSA at 24 h treatment with indicated concentration of I3M. Obviously, according to EMSA data, Nrf2 activity significantly increased with I3M treatment in a dose-dependent manner (Fig. 18A). Moreover, Western blot analysis confirmed that I3M decreased Nrf2 levels in the cytoplasmic compartment and gradually increased Nrf2 levels in the nuclear extract (Fig. 18B). This indicates that I3M promotes the specific DNA-binding activity of Nrf2 by inducing translocation of Nrf2 to the nucleus. To investigate the relationship between Nrf2 and NF-κB next cells were treated with a specific NF-κB inhibitor PDTC, prior to exposure to 20 μM I3M. Interestingly, I3M induced NF-κB-DNA binding ability greatly enhanced by the presence of PDTC as indicated by EMSA results (Fig. 18C). For further tested the functional effects of Nrf2 on the NF-κB in LNCaP cells, cells were treated with NF-κB inhibitor PDTC prior to treatment with I3M. The PDTC significantly induced the expression of I3M-induced Nrf2 both

in m-RNA (Fig. 18D, top) and protein (Fig. 18D, bottom) level in nuclear compartment, suggesting that I3M-mediated NF-κB induction is an important factor contributing to the observed antagonistic effect on iNOS expression in LNCaP cells. Similarly, we investigated whether I3M-induced Nrf2 regulates the expression of NF-κB using Nrf2 siRNA (siNrf2). Therfore, we conduct the western blot analysis to determine the transient efficiency of Nrf2 in LNCaP cells. The siNrf2 treatment group remarkably depleted Nrf2 expression compared with the sicontrol treatment group (Fig. 18E). Transient knockdown of Nrf2 remarkably enhanced I3M-induced NF-κB DNA-binding activity (Fig. 18F). In addition, relative luciferase activity of NF-κB significantly induced when exposure to Nrf2 siRNA (Fig. 18G). Next, investigation focused on nuclear translocation of NF-κB with the treatment of si Nrf2 in LNCaP prostate cancer cells. As indicated by Western blot analysis our results showed that si Nrf2 treatment increased the p50 and IκBα in nuclear portion (Fig. 18H). Collectively, our results demonstrate NF-κB and Nrf2 involved in the regulation of NO-mediated apoptosis by I3M.
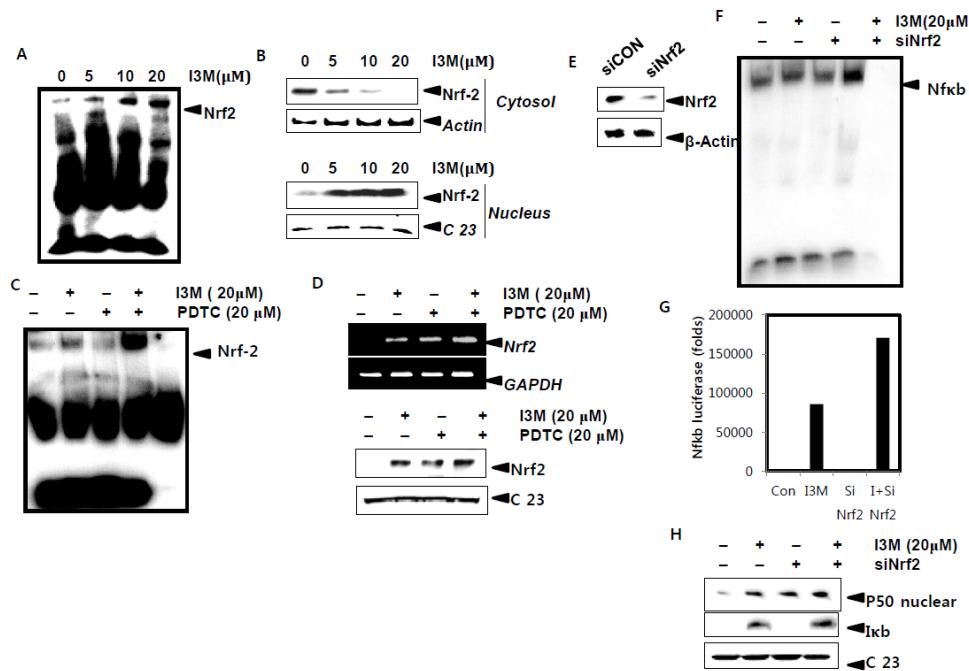
Fig. 18. Effect of I3M on NFκB and Nrf2 pathways. (A) Cells were incubated with indicated concentrations of I3M (0-20 μM) for 24 h. Nuclear extracts were assayed for DNA-binding activity of NFκB using EMSA. (B) Equal amount of cytosol and nuclear extracts were resolved on SDS–polyacrylamide gels, transferred to nitrocellulose membranes, and probed with antibodies against Nrf2. (C) Nuclear extracts were assayed for DNA-binding activity of Nrf2 using EMSA. (D) The cells were preincubated with 20 μM PDTC 1 h before treatment with 20μM I3M for 24h. RT-PCR and western blot analyses of Nrf2 was performed at 24 h, respectively. (E) Cells were transiently transfected with *Nrf2* siRNA for 24 h and then to determine the transfection efficacy, western blot analysis was carried out. (F) Cells were transiently transfected with *Nrf2* siRNA for 24 h and then treated with or without before treatment with 20 μM I3M for 24 h. Nuclear extracts were assayed for DNA-binding activity of NFκB using EMSA. (G) The cells were transfected with a NFκB promoter-containing reporter vector, and luciferase activity was measured 24 h after transfection. (H) Equal amount of nuclear extracts were resolved on SDS–polyacrylamide gels, transferred to nitrocellulose membranes, and probed with antibodies against p50 and Iκb.

4.3.4. I3M induces ROS generation activates Nrf2 pathway

Since Nrf2 is one of the key cellular defense mechanisms on oxidative stress (Lv et al., 2015), here we investigated the whether I3M has potential to enhance ROS production in LNCaP cells and thereby ability to regulate Nrf2 transcription. First, LNCaP cells were treated with indicated concentrations of I3M for 24 h and then H_2DCFDA and HE-based fluorescence analysis was done to detect the ROS production. As shown in Fig. 19A, concentration dependent manner treatment of I3M increased ROS generation by increasing intracellular

superoxide anion and hydrogen peroxide levels respectively. Furthermore, we evaluate the ROS production in the presence of the ROS inhibitors, NAC and GSH. Those inhibitors significantly decreased the I3M-induced expression of the ROS production at 24 h (Fig. 19B). To evaluate the cross-relation among oxidative stress and Nrf2, next we perform an EMSA to detect the specific DNA-binding activity of Nrf2 in the presence of ROS inhibitors in I3M stimulated LNCaP prostate cancer cells. I3M-induced DNA-binding ability of Nrf2 dramatically decreased in the presence of antioxidants NAC and GSH (Fig. 19C). NAC and GSH treatment resulted in a remarkable downregulation of I3M-enhanced Nrf2 expression (Fig. 19D). Flow cytometric data shown that reduced expression of ROS in the treatment of NAC and GSH corresponding reduction in cell death in LNCaP cells (Fig. 19E). Taken together, these data indicate that ROS act as key regulators of Nrf2 activity in the I3M-mediated apoptosis in LNCaP prostate cancer cells.
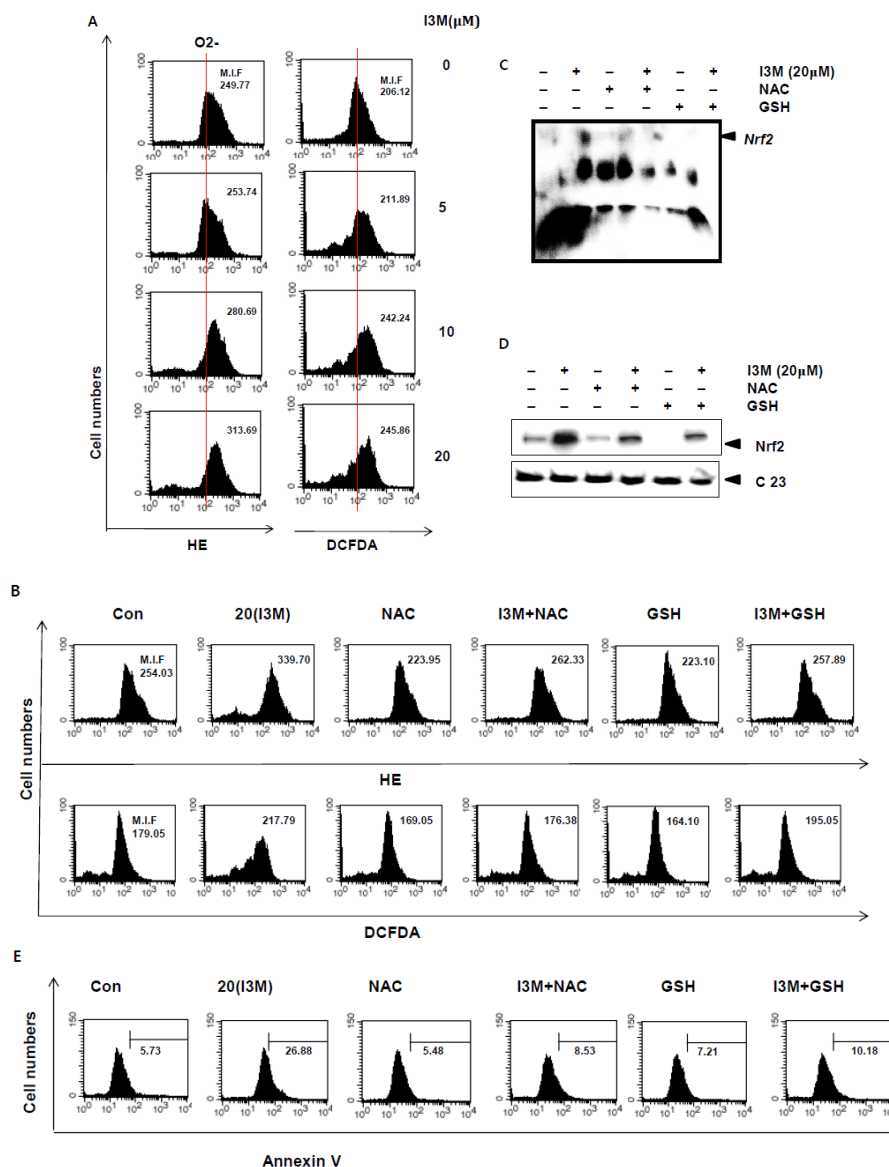
Fig. 19. Effect of I3M on ROS production via Nrf2 pathway. (A) Cells treated with indicated concentrations of I3M (0-15 μM) for 24 h and then stained with HE and DCFDA. Redox status was measured using flow cytometry. The cells were preincubated with NAC and GSH 1 h before treatment with 20 μM I3M for 24 h. (B) Redox status was measured using flow cytometry. (C) Nuclear extracts were assayed for DNA-binding activity of Nrf2 using EMSA.

(D) Western blot analyses was done for indicated proteins. (E) The cells were then stained with annexin-V and analyzed by flow cytometer.

4.3.5. I3M-induced Nrf2 regulates ROS production

It is previously detected how regulate Nrf2 activity via ROS generation, but still have to elucidate the inter-relationship between ROS and Nrf2 activity, whether generation of ROS could regulate by Nrf2. To investigate this mechanism, we first detected the ROS production with treatment of transient knockdown of Nrf2. Fluorometric data showed that administration of siNrf2 into the LNCaP cells remarkably induced I3M-enhanced ROS production at 24 h (Fig. 20A). Next, flow cytometry was carried out to evaluate the effect of Nrf2 inhibition on the ROS production. Flow cytometry data showed the treatment of the cells with siNrf2 resulted in a significantly increased ROS production as indicated by the induction of intracellular superoxide anion and hydrogen peroxide levels (Fig. 20B). HE and DCFDA based analysis shown this induction of superoxide anion and hydrogen peroxide expression remarkably higher than that induction by I3M (Fig. 20B). Nevertheless, then to determine the effect of knockdown of Nrf2 on the viability of LNCaP cells, we performed an MTT assay 24 h after treatment with 20 μM concentration of I3M in the absence of Nrf2. Treatment with I3M decreased the cell viability; however, administration with transient knockdown of Nrf2 resulted in approximately 60% cytotoxicity (Fig. 20C). To further confirm whether Nrf2 indeed has influence on cell viability, the percentage of apoptotic annexin-V$^+$ cells were detected by performing flow cytometry (Fig. 20D). As seen with flow cytometric data, siNrf2 treatment 2-fold time increased that I3M-induced annexin-V$^+$ cells population (Fig. 20D). Moreover, to confirm these results we performed western blot analyses at 24 h after treatment of I3M in LNCaP cells.

85

We found that knockdown of Nrf2 significantly decreases the Pro-caspase 3 and Bid expression level (Fig. 5E). Therefore, these results indicate that Nrf2 is an important factor that regulate ROS level, thereby effect to the viability of LNCaP prostate cancer cells.
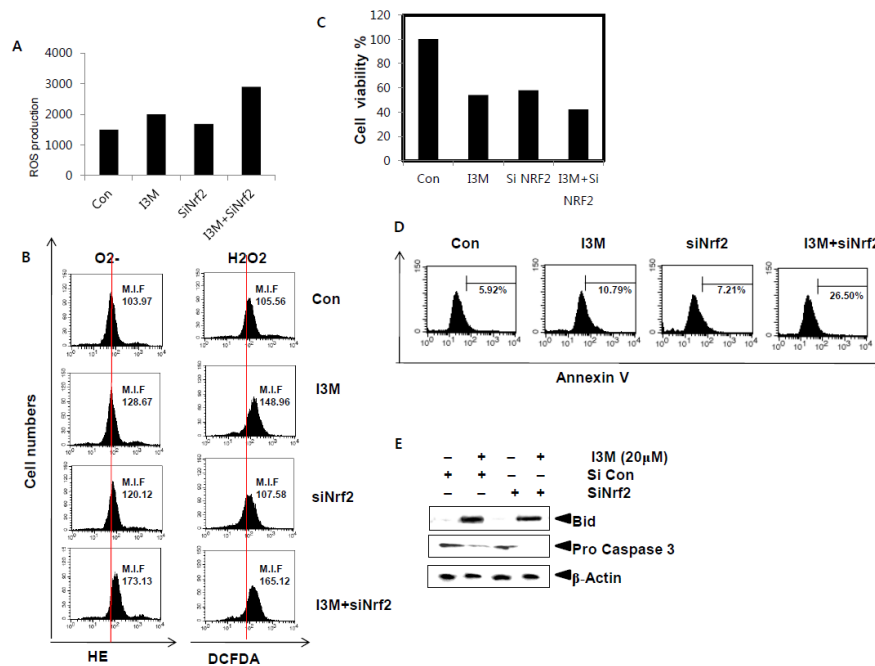
Fig. 20. Effect of I3M on ROS generation regulate via NRF2. Cells were transiently transfected with *Nrf2* siRNA for 24 h and then treated with or without before treatment with 20 μM I3M for 24 h. (A) ROS production was assessed by fluorometer. (B) Redox status was measured using flow cytometry. (C) Cell viability was determined by MTT assay. (D) The cells were then stained with annexin-V and analyzed by flow cytometer. (E) Western blot analyses was carried out for indicated proteins.

4.3.6. Crosstalk between NO and Nrf2, induces by I3M

86

Lack of researches focused on the functional role in between NO production and Nrf2, next we focused on this matter whether regulation of NO and Nrf2 by each other thereby how effect to the I3M-induced apoptosis. To evaluate the effect of Nrf2 on regulation of NO production and its related gene iNOS expression first we investigated the levels of nitrite released into the culture medium treatment with siNrf2 with the help of the Griess reagent. The untreated control group released low levels of NO (3 ± 1 μM); however, treatment of 20 μM I3M significantly enhanced the levels of NO production (23 ± 4 μM). The knockdown of Nrf2 increased the I3M-induced NO elevation in the medium (Fig. 21A). Western blot analysis also showed a significant increase in the expression of iNOS 24 h after I3M treatment; however, pretreatment with siNrf2 for 24 h further induced the protein expression level of iNOS (Fig. 21B). Further, siNrf2 treatment enhanced the I3M-induced cytochrome c level in the cytosol (Fig. 21B). To assess whether the upregulation of iNOS is regulated at the transcriptional level, we performed RT-PCR at 6 h. RT-PCR analysis showed that the inducing pattern of iNOS mRNA expression was similar to that seen with the protein expression after the administration of siNrf2 (Fig. 21C). Therefore, these data indicate that functional regulation of NO via Nrf2. Next to evaluate the regulatory effect of NO on activity of Nrf2, LNCaP cells were pretreated with L-NMMA, a NO synthesis inhibitor prior to I3M treatment for 24 h. As shown in Fig. 21D, nuclear translocation of Nrf2 significantly increased after treatment with 20 μM I3M; however, the nucleus Nrf2 levels gradually decreased in response to L-NMMA, which indicates that NO regulates nuclear translocation of Nrf2. Therefore, we further examined the decreases in Nrf2 level in the nucleus in the presence of NO inhibitor at transcription level by RT-PCR. Consistence with the above results the I3M-induced m-RNA transcription of Nrf2 remarkably inhibited by treatment with L-NMMA (Fig. 21E). EMSA also confirmed that I3M

significantly augmented the specific DNA-binding activity of Nrf2 at 24 h after I3M treatment, and that the Nrf2 activity decreased in the exposure to L-LMMA (Fig. 21F). Thus, our data suggested NO importantly involved in nuclear translocation of Nrf2. Taken together these results shown that cross-relation between NO and Nrf2 which is mediated by I3M in LNCaP cells.
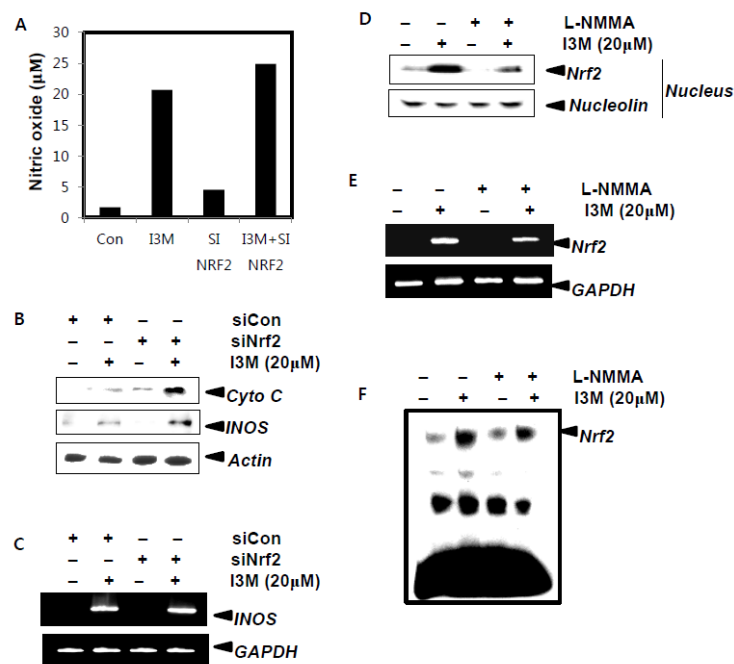
Fig. 21. Effect of I3M on Nrf2 regulate NO production. Cells were transiently transfected with *Nrf2* siRNA for 24 h and then treated with or without before treatment with 20 μM I3M for 24 h. (A) NO production was assessed by Griess reagent. (B) Western blot analyses and (C) RT-PCR was carriedout for iNOS. The cells were preincubated with L-NMMA 1 h before treatment with 20 μM I3M for 24 h. (D) Western blot analyses and (E) RT-PCR was done for Nrf2. (F) Nuclear extracts were assayed for DNA-binding activity of Nrf2 using EMSA.

4.3.7. I3M regulates NF-κB *via ROS production*

In 3.2 section we have shown that as one of key factor which regulate the NO production induced by I3M via activation of NF-κB pathway. On the other hand, our data indicate that I3M-induced ROS production after exposure to I3M at 24 h in LNCaP cells. Thus, we interest to elucidate the regulation of I3M-induced NO production by NF-κB activation through the ROS. Western blot analysis indicated that I3M alone significantly induces the levels of p50 and p65 in the nucleus (Fig. 22A). However, pretreatment with ROS inhibitor, NAC sustained the levels of p50 and p65 compared with the I3M-treated group. In addition, NF-κB luciferase activity significantly increased by approximately 2.5-fold in I3M-treated LNCaP cells, compared with the untreated control group. However, I3M-induced luciferase activity was significantly reduced in the presence of NAC in concentration dependent manner (Fig. 22B). DNA-binding activity of NF-κB also gradually decreased in the presence of NAC (Fig. 22C). Because, activated NF-κB induces the iNOS gene expression, our next examine focused on expression of iNOS and NO production by ROS. To evaluate the effects of ROS on NO production, LNCaP cells were treated with I3M after pretreatment with the indicated concentrations of NAC for 1 h. Nitric oxide production was low in the untreated control group $(2 \pm 2 \ \mu M)$. Exposure to I3M resulted in a significant increase of NO production $(15 \pm 4 \ \mu M)$; however, pretreatment with NAC decreased I3M-induced NO production, in a dose-dependent manner (Fig. 22D). In addition, RT-PCR data indicated that treatment with I3M significantly increased the expression of *iNOS* at 6 h; however, pretreatment with NAC resulted in a significant decrease of the expression of *iNOS*, in a dose-dependent manner (Fig. 22E). Consistent with the results of RT-PCR, western blot analysis showed that treatment with I3M significantly increased the protein synthesis of iNOS at 24 hours; however, the expression of

iNOS was significantly down-regulated in the presence of NAC according to the concentration dependent manner (Fig. 22F). Thus, above data indicate that I3M induces NF-κB activity in LNCaP cells via the ROS and consequently, regulates the expression of NO production by regulating iNOS expression.
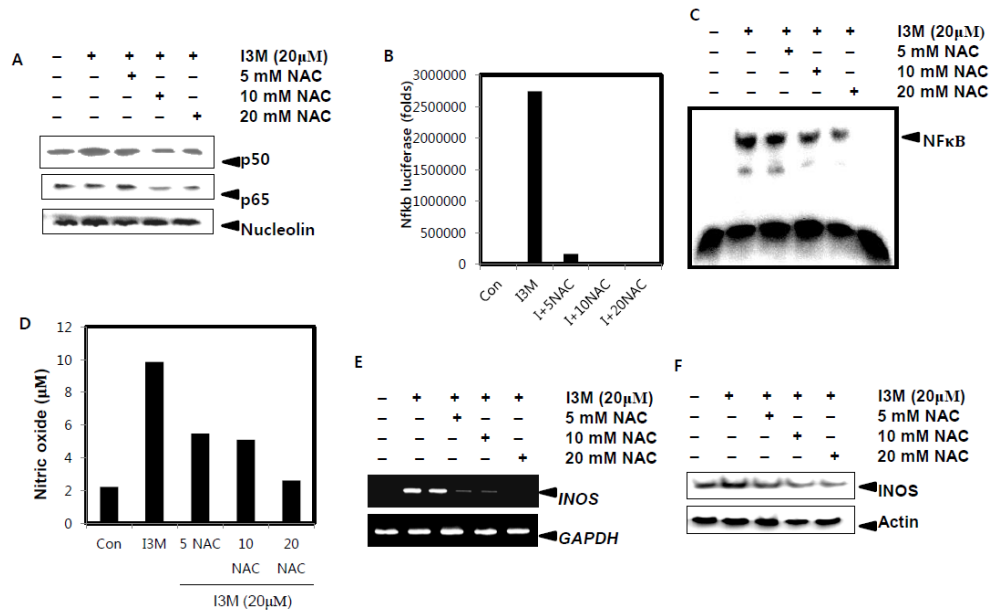
Fig. 22. Effect of I3M on NO production and NFκB pathway regulate via ROS. The cells were preincubated with various concentrations of NAC 1 h before treatment with 20 μM I3M for 24 h. (A) Western blot analyses was performed for indicated proteins. (B) The cells were transfected with a NFκB promoter-containing reporter vector, and luciferase activity was measured 24 h after transfection. (C) Nuclear extracts were assayed for DNA-binding activity of Nrf2 using EMSA. (D) NO production was determined by Griess reagent. (E) RT-PCR and western blot analyses was performed for iNOS.

4.3.8. I3M-induced ROS production regulate via NF-κB and NO expression

90

In order to examine the interaction of ROS production and NO expression via NF-κB activity next we evaluate the I3M mediate production of ROS in the presence of inhibitor of NF-κB, PDTC. As expected, PDTC significantly decreased I3M-induced ROS production in LNCaP cells after 24 h (Fig. 23A). To further confirmation of above results, next, LNCaP cells were treated with PDTC for 1h prior to axposure to I3M for 24 h and then HE-based fluorescence analysis was done to detect the ROS production. As shown in Fig. 23B, treatment of PDTC significantly decreased I3M-induced ROS generation by increasing intracellular superoxide anion levels. Furthermore, to evaluate the direct interaction between NO and ROS production cells were pretreated with L-NMMA for 1 h, then treated with I3M for 24 h. Flurometric data confirmed as PDTC treatment, L-NMMA also down-regulated the I3M-induced ROS production (Fig. 23C). Nevertheless, HE-based fluorescence analysis was shown that I3M-induced intracellular superoxide anion levels significantly decreased by L-NMMA treatment (Fig. 23D). Collectively, these data were shown through NF-κB and NO production potently regulate ROS level by I3M treatment in the LNCaP prostate cancer cells.
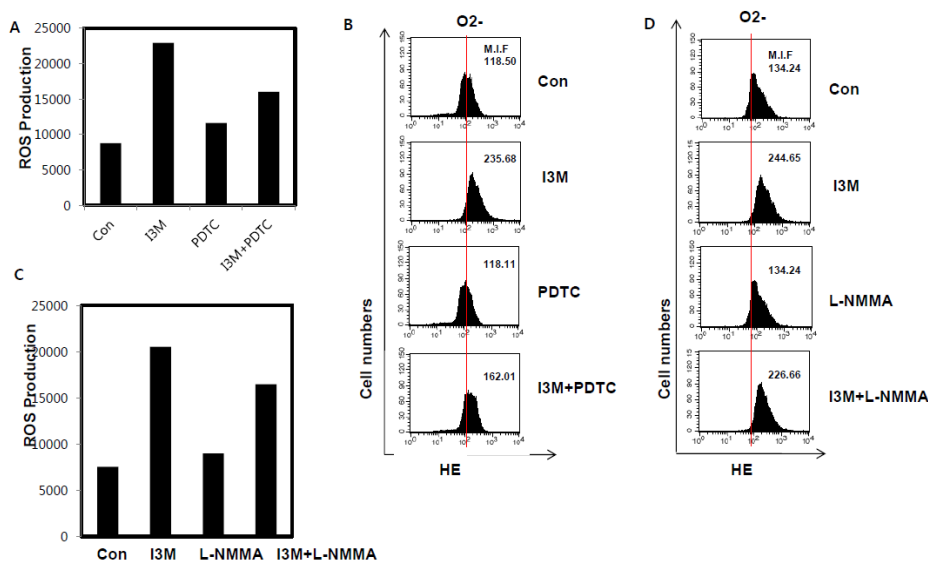
Fig. 23. Effect of I3M on ROS mediated NFκB and NO production. The cells were preincubated with 20 μM PDTC 1 h before treatment with 20 μM I3M for 24 h. (A) ROS production was assessed by fluorometer. (B) Redox status was measured using flow cytometry. The cells were preincubated with L-NMMA 1 h before treatment with 20 μM I3M for 24 h. (C) ROS production was assessed by fluorometer. (D) Redox status was measured using flow cytometry.

4.3.9. I3M induces ER stress in LNCaP cells

ER stress pathway induced by the accumulation of unfolded protiens in ER to preserve ER functions and ER stress-mediated apoptosis pathway described in previuos studies (Sano and Reed., 2013). Therefore, first we examined whether I3M enhance the ER stress in LNCaP cells. Treatment with I3M increased the intensity of ER-tracker-FITC dye in LNCaP cells in a dose-dependent manner (Fig. 24A). This dye specifically stains the ER in live cells, and this data showed that I3M-treated LNCaP cells exhibited rearkably increased staining intensity compared to the control, suggesting that I3M induced ER stress. Next, we investigated the levels of several ER stress marker proteins such as JNK, eIF2α which usually induce during ER stress. Time- and concentration dependent manner treatment with I3M significantly enhanced the ER stress proteins JNK and eIF2α expression level which indicates ER stress induced by I3M (Fig. 24B). To determine how I3M induces the ER stress, we examined the role of ROS in untreated or I3M-treated LNCaP cells treated with ROS inhibitors. Treatment with ROS inhibitors NAC and glutathione (GSH), decreased I3M-induced expression of ER stress marker proteins level by suggesting ROS generation subsequently induced ER stress in

LNCaP cells (Fig. 24C). These finding suggest that I3M induces ER stress which potentiate to regulate by ROS in LNCaP cells.
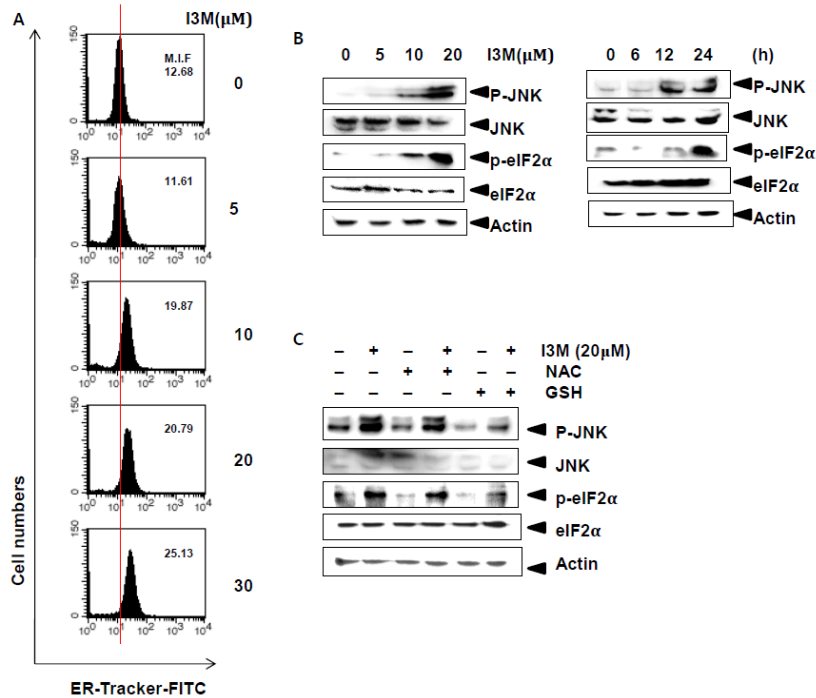
Fig. 24. Effect of I3M on ER stress in prostate cancer cells. The cells were incubated with various concentrations of I3M for 24h. (A) Cells were incubated with ER-tracker-FITC and mean fluorescence intensity (MIF) was measured using flow cytometry. (B) Western blot analyses was performed for indicated proteins. The cells were preincubated with 5mM NAC and GSH1 h before treatment with 20 μM I3M for 24 h. (C) Western blot analyses was performed for indicated proteins.

4.3.10. Crosstalk between NO and ER stress, induces by I3M

Lack of past reports have shown the NO activates the ER stress pathway we interest on elucidate the relationship among NO and ER stress which is mediated by I3M. ER stress

induced by I3M was accompanied by Ca^{2+} release, which was detected using Fluo-4AM calcium indicators where as treatment with L-NMMA reduced the I3M-induced Ca^{2+} release at 24 h (Fig. 25A). It is indicated by MIF, that of I3M alone treated group given 306.32 and combined treatment of I3M and L-NMMA shown 253.99 in LNCaP cells. Next to evaluate the NO regulate ER stress we carried out western blot analysis to detect the ER stress protein markers with the treatment of I3M and L-NMMA. We examined the I3M-induced the protein expression levels of JNK and eIF2α, however, the treatment of I3M plus L-NMMA significantly decreased the I3M-induced that protein levels (Fig. 25B). Next we interest to find out whether ER stress regulates the NO production which regulate by I3M. First, we conduct the western blot analysis to determine the transient efficiency of sieIF2α in LNCaP cells. The sieIF2α treatment group remarkably depleted eIF2α expression compared with the sicontrol treatment group (Fig. 25C). The amount of NO production was higher in I3M-treated cells than cells transfected with sieIF2α followed by I3M treatment (Fig. 25D). As shown in Fig. 10E, treatment with I3M for 24 h significantly increased the protein expression of iNOS however; exposure to sieIF2α gradually down regulated the I3M-induced Inos protein expression (Fig. 25E). Moreover, luciferase activity of NF-κB was examined using transient transfection with reporter vectors that included NF-κB promoters. Treatment with sieIF2α reduced the I3M-induced NF-κB luciferase activity (Fig. 25F). Therefore, these data demonstrated that interaction between NO and ER stress which regulate by I3M in LNCaP prostate cancer cells.
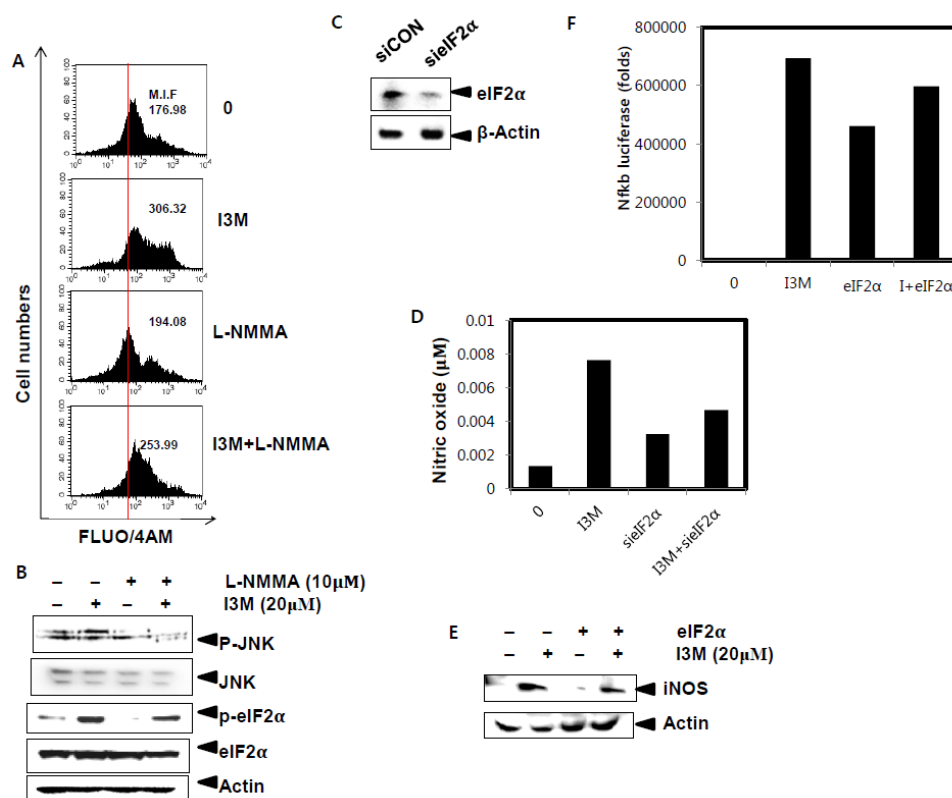
Fig. 25. Effect of I3M on NO and ER stress. The cells were preincubated with L-NMMA 1 h before treatment with 20 μM I3M for 2 4h. (A) Redox status was measured using flow cytometry. (B) Western blot analyses was performed for indicated proteins. (C) Cells were transiently transfected with *eIF2α* siRNA for 24 h and then to determine the transfection efficacy, western blot analysis was carried out. (D) NO production was measured by Griess assay. (E) Western blot analyses was performed for iNOS. (F) The cells were transfected with a NFκB promoter-containing reporter vector, and luciferase activity was measured 24 h after transfection. (A) RT-PCR and (B) western blot analyses of iNOS was performed.

4.3.11. NO induces I3M, involved ER stress and NFκB via ROS

Heretofore, indicated that involvement of I3M regulate apoptosis through NO via various factors that mediate NO such as NF-κB, ER stress, ROS, and Nrf2. Finally, we clarify the critical factor which mediates NO among the above factors. For that first we carried out RT-PCR analysis to detect the mRNA expression level of iNOS, with the treatment of siNrf2, sieIF2α for 24 h and NAC, PDTC for 1h prior to treatment with I3M for 24 h in LNCaP cells. Consistence with I3M treatment group, exposure to siNrf2 did not change the iNOS the mRNA expression level in LNCaP cells however; pretreatment with sieIF2α, NAC and PDTC resulted in inhibition of mRNA expression level of iNOS (Fig. 26A). Similar to the RT-PCR analysis, the protein expression level of iNOS inhibited by pretreatment with sieIF2α, NAC, and PDTC while did not effect by siNrf2 treatment (Fig. 26B). Next, apoptotic events in the mitochondria were evaluated by measuring the mitochondrial membrane potential using DiOC$_6$. Marked reduction in the mitochondrial membrane potential had occurred in cells treated with I3M (Fig. 26C). In addition, this process was accompanied by the release of cytochrome *c* from the mitochondria into the cytosol (Fig. 26D). However, pretreatment with 10 μM NO inhibitor L-NMMA normalized mitochondrial membrane potential and blocked the release of cytochrome *c* into cytosol (Fig. 26D). Furthermore, these caspases activity was remarkably increased by the I3M treatment (Fig. 26E). In contrast, the level of pro-caspase-3 expression was upregulated by the L-NMMA treatment. The L-NMMA treatment also increased the expression of Bax and Bid level (Fig. 26E). Taken together these results indicate ER stress, NFκB and ROS are important factors that regulate NO expression by I3M. Further, the induction of NO regulates apoptosis via intrinsic and extrinsic pathways in LNCaP prostate cancer cells.
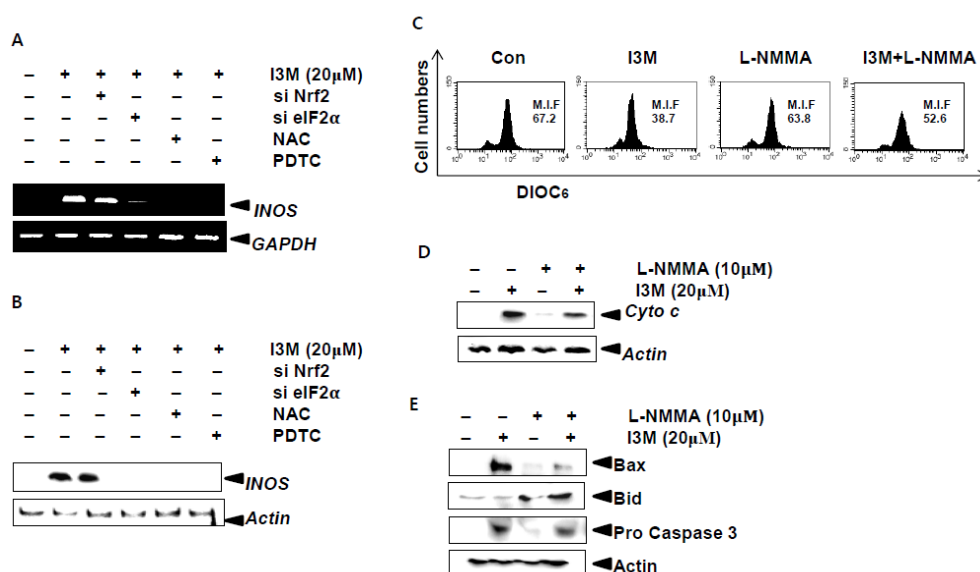
Fig. 26. Involvement of ER stress and NFκB via ROS for regulation of iNOS by I3M. Cells were transiently transfected with *eIF2α* siRNA and Nrf2 siRNA for 24 h and preincubated with NAC and PDTC 1 h before treatment with 20 μM I3M for 24h. The cells were preincubated with L-NMMA 1 h before treatment with 20 μM I3M for 24 h. (C) Mitochondrial membrane potential was measured using flow cytometry. (D and E) Western blot analyses was performed for indicated proteins.

4.4. Discussion

Since, nitric oxide discovery as a biological active molecule, has been investigated to play a crucial role as a signal molecule in different parts of the organism and also as regulatory or cytotixic molecule of the innate immune response (Nahrevanian et al., 2009). Numerous studies have been delineated the beneficial or detrimental importance of iNOS in humans, specially in various types of diseases. More importantly, researchers have elucidated, nitric oxide is

97

important in control in cancers, specially, despite beneficial effect of iNOS have been reported very rarely. Despite in this study we have focus on beneficial effect of iNOS which is induce by I3M in LNCaP and DU145 prostate cancer cells by induction of apoptosis via nitric oxide mediation.

NO can be determined the cell survival or apoptosis by regulating shutting off the apoptosis signaling pathways or switch them on respectively. However, this dichotomy of NO signaling mechanisms still remains to be investigated. Considering the transcriptional and translational regulation, various factors regulate NO production through alterations in NOS activity such as NF-κB (Dilshara et al., 2015), ROS (Hsieh et al., 2014), Nrf2 (Um et al., 2011) etc: As a beneficial effect of NO promoted apoptosis in cancer cells, therefore in this study we focused on induction of apoptosis by I3M via NO in LNCaP prostate cancer cells by regulating multiple factors and either interactions of these factors to regulate NO production. It is well known that NF-κB activation induces expression of gene encoding the inducible form of nitric oxide synthase (iNOS) (Dilshara et al., 2015). In the present study have shown that I3M induce NO and its gene expression by inducing NF-κB signaling pathway. Since NF-κB activity modulate through multiple factors for instance; ER stress, Nrf2, reactive oxygen species (ROS) production, thereby effect to the NO and its gene expression in the present study, we indicated the effect of those factors on NO expression and link between to modulate either one.

NF-E2-related factor 2 (Nrf2), a bZIP transcription factor, plays an important role in the basal and or inducible expression regulation of phase 2 genes by binding to the "antioxidant response element" in their promoters. However, inter-relationship underlying the NO and transcription factor Nrf2 still poorly understood. Nrf2, which is which is sequestered in the cytoplasm as an inactive complex with the repressor Klech-like ECH-associated protein

98

1. According to the past researches, that dissociation of Nrf2 from Keap1 in cytosol and translocate to the nucleus induced by various stimuli. Um *et al* reported NO-mediated thiol modification in Keap1 is a plausible process of activation of Nrf2 in rat pheochromocytoma PC12 cells (Um et al., 2011). Nevertheless, NO mediated by Nrf2, play a crucial role to inhibition of detrimental effects of NO. Our previous publication shown that TIA-induced NO downregulation is mediated through Nrf2 in BV2 microglial cells by reducing NO-contributed deleterious effects (Dilshara et al., 2014). In this study, we found that pretreatment with NO inhibitor L-NMMA resulted in the downregulation of I3M-induced Nrf2 expression in LNCaP cells. Furthermore, transiently knockdown of Nrf2 comparatively induced I3M-enhanced NO expression, indicating that I3M-induced the expression of NO through Nrf2 activation. Previous studies indicated, the effect of various factors that regulate Nrf2 activity, thus, the influence of these factors on regulation of Nrf2 and thereby NO mediation should investigate for a better understanding of apoptosis mechanism regulate by NO. Therefore, we were interested to reveal the connection between Nrf2 and NFκB both are the two key transcription factors that regulate the NO expression. Our data indicated that absence of Nrf2, exacerbate the NF-κB activity and inhibition of NF-κB activity resulted in induced the Nrf2 activity. Hence, Nrf2 and NFκB possess both positive and negative effects on the NO production by modulating its target gene expression.

Notwithstanding, ROS play a significant role regulate the NO expression. According to our data indicated that I3M treatment enhanced the ROS generation in LNCaP cells. Our recent publication was shown that pretreatment of ROS inhibitors reduced the LPS-induced iNOS transcription and translation level in BV2 microglial cells in response to RG3I (Dilshara et al., 2014). In current study also we observed that pretreatment of I3M induced ROS generation in

99

LNCaP cells however; further we have observed this up-regulation of ROS induce Nrf2 activity also in I3M-treated LNCaP cells. Consequently, in addition to the NF-κB pathway, ROS also play a main role in regulating Nrf2 transcription. To date few studies have examined the inter-connection among ROS and Nrf2 thus current study focused to elucidate the link between ROS and Nrf2. Kovac *et al*., were reported mitochondrial ROS generation is modulated through Keap1–Nrf2 pathway in Nrf2-KO cells and tissues (Kovac et al., 2015). Moreover, this study indicated that in Nrf2 deficiency condition dramatically enhanced the NOX2 level. Another study was suggested the loss of Nrf2 leads to enhanced ROS production in hematopoiesis and stem cells (Merchant et al., 2011). According to the fluorometric and flow cytometry analysis, transient knockdown of Nrf2 further enhanced I3M induced ROS production. Investigation of link in between these two factors, Nrf2 and ROS is important as both are directly or indirectly regulate the NO expression thereby involve in apoptosis process. Nrf2 and ROS potently regulate the NO though NFκB pathway that inter-connection of these factors with NO also reported.

Cumulative data supported the correlation between NFκB and ROS and thereby regulate the various cellular process. Pretreatment with I3M remarkably upregulate the NFκB DNA binding ability and its related protein expression p50 and p65 in the nucleus however; pretreatment with NAC comparatively decreased that I3M-induced NFκB DNA binding ability and nucleus expression of p50 and p65 by suggesting ROS play a key role in regulating NFκB activation. Aside from the regulating of NFκB, ROS was found to regulate NO production directly in I3M-treated LNCaP cells. Moreover, pretreatment with NFκB and NO inhibitors significantly reduced the I3M-induced ROS and NO production respectively. However, the

ROS and NFκB modulate via multiple factors such as ER stress and Nrf2, involvement of these factors in I3M-induced apoptosis via NO have to be investigated.

Endoplasmic reticulum (ER) stress identified as a stress response triggered by the accumulation of unfolded proteins in ER to preserve ER activities (Zhou et al., 2016). To date, few reports have shown the correlation between ER stress and NO thus, involvement of ER stress in I3M-mediated apoptosis via NO have indicated. It is reported that NO disturb ER functions by disturbing Ca^{2+} homeostasis, because of that NO-induced ER signaling activation (Gotoh and Mori., 2006). In present data indicated the pretreatment of NO inhibitor L-NMMA and sieIF2α result in down regulation of I3M-induced ER stress and NO expression in LNCaP cells respectively. Therefore, ER stress also plays a crucial role regulating the NO-mediated apoptosis.

Our study explained the inter-relationship among various factors and also regulation of NO expression and apoptosis via these factors. Finally, we investigated the most critical factor or factors involve for the regulation of NO-mediated apoptosis in LNCaP prostate cancer cells. The RT-PCR and western blot analysis clearly shown that I3M-induced iNOS expression declined by pretreatment of sieIF2α, NAC and PDTC. Therefore, I3M mediate NO and iNOS gene expression mainly via involvement of NFκB, ER stress, and ROS generation. However, transcription factor Nrf2 also involved in regulation of NO and its gene transcription, negligible effect was shown may be the regulation of Nrf2 by other factors. Eventhough I3M-induced ER stress, ROS and NF-κB positively regulate NO expression, and that NO production also effects to regulate of these factors it has negligible effect since apoptosis mediate by NO through above factors.

101

Taken together, we showed that I3M potently enhances NO-mediated apoptosis by enhancing ER stress, ROS and NFκB pathway. Further, we have demonstrated that involvement of transcription factor Nrf2 in expression of NO and regulation of apoptosis process. Therefore, I3M used as a potent anticancer agent by targeting NO-mediated apoptosis in LNCaP prostate cancer cells.

4.5. Conclusion

I3M enhances apoptosis via nitric oxide production in LNCaP prostate cancer cells. The I3M-mediated apoptosis via NO regulate by ER stress, ROS and NFκB pathway. Further, Nrf2 critically involve for the regulates the NO production by mediating ER stress, ROS, and NFκB pathway.

Chapter 5

Indirubin-3′-monoxime suppresses matrix metalloproteinase-9 and invasiveness of LNCaP and DU145 prostate cancer cells by suppressing the AP-1 activity by Nrf2 mediated HO-1 pathway

Abstract

Indirubin-3′-monoxime (I3M), is a synthetic derivative of indirubin, was originally accepted as potent anticancer agent. Recent reports have suggested I3M exhibits anticancer properties by modulating cell cycle arrest, apoptosis, cell invasion and metastasis, very lack of data about the mode of action. Despite, in the current study, we have shown that I3M suppresses cellular invasiveness of LNCaP prostate carcinoma cells and to further investigate the underlying mechanisms of the I3M-inhibited invasiveness of cancer cells via down regulating Matrix Metalloproteinase-9 (MMP-9) activity. I3M does not affect the viability of LNCaP prostate cancer cells upto 5µM of concentration. According to the western blot and RT-PCR analysis, concentration dependent manner treatment of I3M reduced PMA-stimulated protein and mRNA expression level of MMP-9 in LNCaP and DU145 cells. Further, Matrigel invasion assay showed that I3M substantially reduced the PMA-induced cell invasion. Nevertheless, I3M significantly enhanced the protein and m-RNA expression level of HO-1 in LNCaP cells. Accordance to the induction of HO-1 expression, I3M resulted in remarkably induction of Nrf2 expression in LNCaP cells at 24 h. Moreover, I3M treatment notably enhanced PI3K and Akt phosphorylation, suggesting that the I3M-induced Nrf2 expression associated with the PI3K/Akt signaling pathway. Treatment with I3M reduced PMA-induced AP-1 activity by providing evidence that AP-1 may critically require to induce the MMP-9 transcription in prostate cancer cells. We also investigated that I3M-decreased c-Jun and c-Fos activation by blocking their respective phosphorylation. Considering above facts our results indicated that I3M attenuates PMA-induced expression of MMP-9 at mRNA and protein level by suppressing AP-1 activity via Nrf2 signaling pathway in LNCaP prostate carcinoma cells.

Keywords: Indirubin-3'-monoxime; Matrix metalloproteinase-9; Nrf2; AP-1; HO-1

5.1. Introduction

Traditional medicines and in particularly traditional Chinese medicine, represent an extremely useful source of potential new anticancer drugs. Indirubin, a red isomer of indigo, is the active ingredient of the traditional Chinese medicinal formulation *Danggui Longhui Wan*, which comprises 11 plant ingredients was reported to be active for the treatment of chronic myelocytic leukemia (Berger et al., 2011). Indirubin is one of the major components in a series of indigo-producing Chinese medicinal herbs including *Strobilanthes cusia, Isatis indigotica* and *Polygonum tinctorium* that are commonly used for treatment of inflammatory-based diseases (Zhu et al., 2012). Several indirubin analogues, such as N-methyl isoindigo, 5-chloro-indirubin and indirubin-3'-monoxime (I3M), have been synthesized by various molecular substitution of the parental indirubin with improved selectivity, solubility, and bioavailability (Damiens et al., 2001 and Blažević et al., 2015). Furthermore, different indirubin derivatives showed anticancer activity in various human cancer cells. Among them indirubin-3'-monoxime (I3M) exhibits anticancer properties by modulating cell cycle arrest, apoptosis, cell invasion and metastasis, yet mode of action of these chemotherapeutic agent has remained largely unclear until lately (Lo et al., 2013).

Proteinases play pivotal roles in altering local microenvironments during embryonic growth development as well as in physiologic and pathologic tissue remodeling processes (Bonnans et al., 2014). In particular, matrix metalloproteinases (MMPs) such as MMP-9 have emerged as regulators of tumor cell invasion and metastasis because of its unique ability to degrade type IV collagen which is a major component of the basement membrane and other essential extracellular matrix components (Bonnans et al., 2014). The extensive expression of MMP-9 has been reported in various types of carcinoma cells, including the bladder, prostate,

breast (Jayasooriya et al., 2014), brain (Aroui et al., 2015), and pancreatic carcinoma (Zhang et al., 2011). Virtually, prostate cancer can metastasize to distant organs such as the liver, thorax, digestive system, bone and brain (de Oliveira Barros et al., 2014 and Gandaglia et al., 2014). According to the recent population based study most common matastases sites in patients with prostate cancer were indicated as 84.4% of bone, 10.6% of lymph nodes, 10.2% of liver, 9.1% of thorax, 3.1% of brain and 2.7% of digestive system (Gandaglia et al., 2014). Despite, targeting MMP-9 inhibition for treating prostate cancers is a good strategy in noval cancer therapeutics.

The transcription factor AP-1 (activator protein 1) is one of the crucial effectors activated by oncogenic factors and by the hepatocyte growth factor (HGF) receptor tyrosine kinase (Ding et al., 2013). AP-1 comprises heterodimers of FOS and JUN family proteins that has an ability to bind to a consensus DNA sequence, (5'-TGAG/CTCA-3') usually in the promoter region of genes or bind to 12-O-tetradecanoylphorbol-13-acetate response elements (Ding et al., 2013). The FOS family consists of proteins such as FOS, FOSL1, FOSL1 and JUNB and JUN family of proteins comprises JUN, JUND, JUNB and ATF family members (Shaulian and Karin., 2001). AP-1 can be activated by multiple extracellular stimuli such as FOS and JUN or phosphorylation of FOS and JUN (Shaulian and Karin., 2001). FOSL1 and JUN positively regulate its own expression via AP-1 sites on their promoters, thereby amplifying AP-1 activation (Evellin et al., 2013). Thus, AP-1 family members play a critical role in the metastasis and invasion of cancers (Parker et al., 2013). Although substantial progress has been made in understanding the molecular control of prostate cancer metastatis and invasion, lack of data about the molecular mechanisms regulate the tumor metastatis and invasion. Emerging evidence suggests that inhibition of the expression of AP-1 component proteins and AP-1

activity reduces the invasiveness of cancer cells. Therefore, understanding the AP-1 signaling pathway may help to develop therapeutic strategies to prevent invasiveness of prostate cancers.

Considering the critical involvement, NF-E2-related factor 2 (Nrf2) plays a crucial role in the cellular defense against the carcinogenesis (Jaramillo and Zhang., 2013). Nrf2 is a basic-region leucine zipper (bZIP) transcription factor that along with small Maf proteins, regulate induction of genes encoding antioxidant proteins and phase II detoxifying enzymes including heme-oxygenase-1 (HO-1) (Biswas et al., 2014). It has been shown that activation of Nrf2 in response to oxidative stress protects cells and tissues from oxidative stress. In normal conditions, Nrf2 localized in the cytoplasm where its bind with the Keap 1, which functions as an adaptor for Clu3-based E3 ligase to control the proteasomal degradation of Nrf2. In fact, the interaction of Nrf2-keap 1 leads to the rapid degradation of Nrf2 through Clu3-based E3 ligase polyubiquitination (Jung et al., 2013). Notwithstanding, after direct attack by reactive oxygen species (ROS) or resulting phosphorylation like indirect mechanism, Nrf2 dissociates from Keap 1 and thereby translocates into the nucleus for transactivates its target genes via ARE (Espinosa-Diez et al., 2015). Additionally, a number of reports have addressed the possible role involved by phosphoinositide 3- kinase (PI3K) in Nrf2 activation (Zou et al., 2015). Multiple studies have demonstrated induced expression of Nrf2 associate with reduction of cancer progression.   It has been reported that Nrf2 knockout mice have shown an invaluable tool for studying the functions of Nrf2-mediated pathways in vivo. *Satoh et al* reported that Nrf2-deficient (Nrf2$^{-/-}$) mice tend to form a large number of tumors than wild-type (Nrf2$^{+/+}$) mice on chemically induced lung carcinogenisis (Satoh et al., 2013). Moreover, the efficacies of different chemopreventive agents were found to be remarkably attenuated in Nrf2 deficient animals (Shin et al., 2011). For instance, inducibility of heme-oxygenase-1 was examined to

be blunted in Nrf2 deficient animals compared to wild-type (Shin et al., 2011). Another report was shown; epigenetically restore the expression of Nrf2 and Nrf2 downstream detoxification and antioxidant related genes during the initiation and development of prostate cancer by sulforaphane in TRAMP mice (Zhang et al., 2013). Nevertheless, it has been well established that Nrf2 is ubiquitously expressed in wide range of tissues. For this reason, the involvements of Nrf2 activation in invasion of prostate cancers and its possible applications, as a therapeutic target to prevent and treatment for prostate cancers have been extensively investigated.

5.2. Materials and method

5.2.1. Reagent and antibodies

Antibodies against MMP-9, Nrf2, HO-1, p-PI3K, PI3K, p-Akt, Akt, p-c-Jun, c-Jun, p-c-Fos, c-Fos, and β-actin were purchased from Santa Cruz Biotechnology (Santa Cruz, CA). 3-(4,5-dimethyl-2-thiazolyl)-2,5-diphnyl-2H-tetrazolium bromide (MTT) were purchased from Sigma (St. Louis, MO) and Roswell Park Memorial Institute Medium (RPMI), antibiotics mixture, and fetal bovine serum (FBS) were obtained from WelGENE Inc. (Daegu, Republic of Korea). Peroxidase-labeled goat anti-rabbit immunoglobulin was purchased from KOMA Biotechnology (Seoul, Republic of Korea). Other chemicals were purchased as Sigma grades.

5.2.2. Cell culture

LNCaP and DU145 prostate cancer cells obtained from the American Type Culture Collection, Manassas, VA, were cultured in RPMI medium supplemented with 10% fetal bovine serum and antibiotics (Sigma) in a humidified 5% CO_2 incubator at 37°C. Then cells

were harvested by trypsinization and plated 24h before treatment with the test compounds.

5.2.3. MTT assay for cytotoxicity

The effects of I3M on the cytotoxic effects against PMA were determined by the MTT uptake method as following. Briefly, 1×10^5 cells were incubated with I3M in triplicate on a 24-well plate and then treated with the indicated concentrations of I3M, with or without treatment of PMA for 24 h at 37°C. Cells were incubated with MTT solution (final concentration 0.5 mg/ml) for 15 min at 37°C allowing viable cells to reduce the yellow tetrazolium salt into dark blue formazan crystals. The formazan crystals were dissolved using dimethyl sulfoxide (DMSO). Then the absorbance was measured at 540 nm using the microplate reader (Thermo Electron Corporation, Marietta, OH).

5.2.4. Western blot analysis

To determine the levels of protein expression in the nucleus and the cytoplasm, we prepared extracts and fractionated them by SDS-PAGE. After electrophoresis, the proteins were electrotransfered onto nitrocellulose membranes. The membranes were blocked with a rabbit primary polyclonal antibody at 4°C overnight. Then, the membranes were treated with horseradish-peroxidase-conjugated goat anti-rabbit secondary antibody. Antibody binding was visualized with a chemiluminescence system.

5.2.5. Real-time polymerase chain reaction (RT-PCR)

Total RNA was isolated from cells using Trizol reagent according to the manufacture's protocol. First, strand complementary DNA (cDNA) was synthesized. RT-PCR was performed

with PCR Master Mix according to the protocols. The following primers were used to amplify *HO-1* cDNA: sense, 5′-TGA AGG AGG CCA CCA AGG AGG-3′ and antisense, 5′-AGA GGT CAC CAG GTA GCG GG-3′, *MMP-9* cDNA: sense, 5′- CCTGGA GAC CTG AGA ACC AAT CT-3′ and antisense, 5′- CCA CCC GAG TGT AAC CAT AGC *-3′ glyceraldehydes-3-phosphate dehydrogenase* (*GAPDH*) cDNA: sense, 5′-CCA CCC ATG GCA AAT TCC ATG GCA-3′ and antisense, 5′-TCT AGA CGG CAG GTC AGG TCC ACC-3′. The following PCR conditions were applied: For HO-1, 30 cycles of denaturation at 94°C for 30 s, annealing at 59°C for 30 s and extended at 72°C for 30 s; and for MMP-9, 30 cycles of denaturation at 94°C for 30 s, annealing at 63°C for 30 s and extended at 72°C for 30 s; and for GAPDH, 28 cycles of denaturation at 94°C for 30 s, annealing at 62°C for 30 s and extended at 72°C for 30 s. Relative *HO-1* and *MMP-9* mRNA levels were normalized to *GAPDH* expression.

5.2.6. Invasion assay

Since invasion through the extracellular metrix is a crucial step in tumour metastasis, a membrane invasion culture system was used to assess cell invasion. Using modified Boyden chambers with polycarbonate nuclear pore membrane (Corning, NY) with 8 μm pore size and is coated with a Matrigel 100 μg/cm^2. A total 5×10^4 LNCaP cells were suspended in serum-free RPMI medium and seeded into the upper wells. After incubation overnight, cells were treated with I3M and then stimulated with PMA. Following 24 h, lower surface of the filter was fixed and stained with 0.125% Commassie Blue in a mixture of methanol: acetic acid: water as 45:10:45 (v/v/v) ration and then stained cells were counted.

5.2.7. Luciferase assay

제주대학교 중앙도서관
JEJU NATIONAL UNIVERSITY LIBRARY

Briefly, LNCaP cells were seeded at a density of 1×10^4 cells/well. After 24 h, cells were transfected with 2 μg each plasmid construct according to the Lipofectamine method. Then cells were treated with I3M next stimulated with PMA and then harvested. Luciferase activity was measured by according to the manufacture's protocol and detected by GLOMAX luminometer (Promega, Madison, WI, USA).

5.2.8. Electrophoretic mobidity shift assay (EMSA)

Using NE-PER nuclear and cytoplasmic extraction reagents (Pierce, Rockford, IL, USA), cytoplasmic and nuclear extracts was prepared. Using nuclear extract DNA-protein binding assays were carried out. Synthetic complementary AP-1-binding oligonucleotides (Santa Cruz Biotechnology) were biotinylated using the biotin 30-end DNA labeling kit (Pierce) according to the manufacturer's instructions and annealed for 1 h at room temperature. In the presence of 50 ng/ml poly (dI-dC), 0.05 % Nonidet P-40, 5 mM MgCl$_2$, 10 mM EDTA, and 2.5% glycerol in 1× binding buffer (LightShiftTM chemiluminescent EMSA kit) with 20 fmol of biotin-end-labeled target DNA and 10 μg nuclear extract, binding reactions were carried out for 20 min at room temperature. Assays were loaded onto native 4% polyacrylamide gels before being transferred onto a positively charged nylon membrane. Transferred DNAs were cross-linked to the membrane at 120 mJ/cm^2 and detected using horseradish peroxidase-conjugated streptavidin according to the manufacturer's instructions.

5.2.9. Flow cytometry

LNCaP cells were seeded at a density of 5×10^4 cells/well, pretreated with I3M, stimulated with PMA for 24 h at 37°C and then subjected to annexin-V staining. The cells were washed

in PBS, resuspended in annexin-V FITC (R&D Systems, Minneapolis, MN). Cells were analyzed by flow cytometry (Becton Dickinson, San Jose, CA).

5.2.10. Statistical analysis

All data were derived from at least three independent experiments. The images were visualized with Chemi-Smart 2000 (Vilber Lourmat, Cedex, France). Images were captured using Chemi-Capt (Vilber Lourmat) and transported into Adobe Photoshop (version 8.0). All data are presented as mean ± SE. Significant differences between the groups were determined using one-way ANOVA test. $P < 0.05$ was considered to indicate a statistically significant difference.

5.3. Results

5.3.1. I3M does not affect the viability of LNCaP prostate cancer cells

To determine the effect of I3M on cell viability, LNCaP prostate cancer cells were treated with various concentrations of I3M (1, 2, 3, 4, and 5 μM) for 24 h, then inhibitory effect of I3M was examined by MTT assay. MTT data showed that I3M had no influence on cell viability up to dose of 5 μM regardless of the presence of PMA (Fig. 27A). Furthermore, the effect of I3M on viability of cells was determined by the annexin-V positive cell populations using flow cytometry analysis. Considering the annexin-V positive cells, no apoptotic cell death was examined in each panel compared with the positive H_2O_2- treated group (Fig. 27B). Moreover, the morphology changes of LNCaP cells were observed in Fig.1C. The cellular morphology was not changed according to the increasing concentrations of I3M. The most important morphological change was that formation of apoptotic bodies were appeared in H_2O_2 positive

112

control treatment indicating up to 5μMof I3M there was no apoptotic effect on LNCaP cells (Fig. 27C). Taken together these results indicate upto 5 μM I3M have no influence on the cell viability of LNCaP prostate cancer cells, regardless of the presence of PMA.
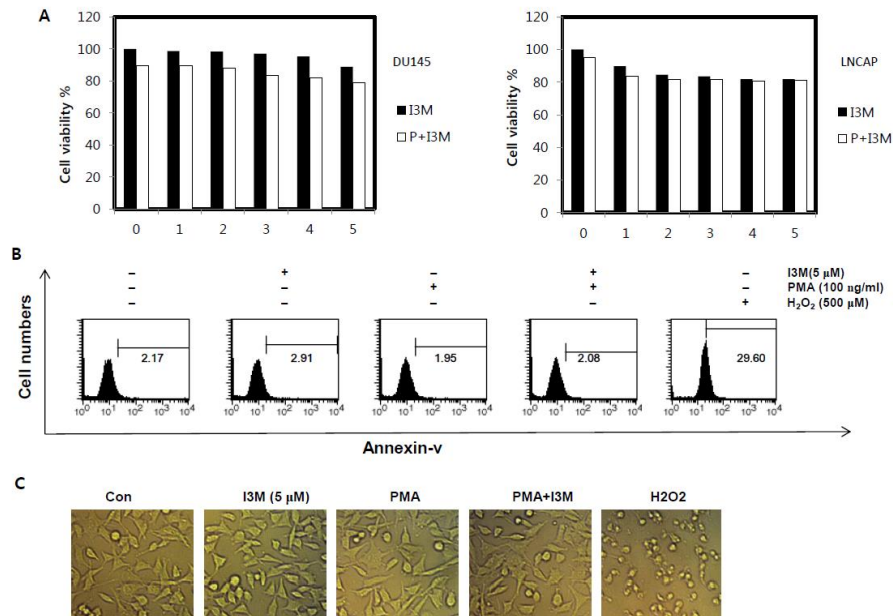
Fig. 27. Effects of I3M on the viability of LNCaP and DU145 cells. LNCaP and DU145 cells treated with the indicated concentrations of I3M and/or 100 ng/ml PMA for 24 h. (A) Cell viability was measured by an MTT assay following 24 h. (B) The cells were then stained with annexin-V and analyzed by flow cytometer. (C) The morphology of cells treated with or without I3M was examined under light microscopy (×400).

5.3.2. I3M inhibits PMA-induced invasion of LNCaP prostate cancer cells by suppressing MMP-9 activation

To verify the effect of I3M on MMP-9 expression, we pretreated cells with I3M and then stimulated with PMA for 24 h. The expression levels of MMP-9 mRNA and protein were

determined by semi-quantitative RT-PCR and western blot analysis at 6 h and 24 h, respectively. According to the western blot analysis, I3M reduced PMA-induced MMP-9 expression in concentration dependent manner at 24 h in LNCaP and DU145 cells (Fig. 28A). Similar to the expression of MMP-9 protein, remarkably *MMP-9* mRNA expression was observed with I3M at 6 h (Fig. 28B). Moreover, luciferase activity of MMP-9 was examined using transient transfection with reporter vectors that included MMP-9 promoters. Treatment with PMA significantly induced MMP-9 luciferase activity, whereas I3M downregulated PMA-induced MMP-9 luciferase reporter activity in LNCaP cells (Fig. 28C). Since it is known MMP-9 is a crucial factor involved in the tumor invasion (Bonnans et al., 2014), the regulatory effect of I3M on the invasion of LNCaP cells were observed by invasion assay. According to the Fig. 1D, the treatment with PMA remarkably increase invasion of cells as 3-fold time when compared with the untreated control group. However, the addition of I3M resulted in as ~40% decrease in penetration of LNCaP cells through the matrigel-coated membrane when compared with the PMA-stimulated group (Fig. 28D). These results confirm that I3M downregulated the PMA-enhanced MMP-9 activity at the transcription level, thereby inhibited PMA-induced invasion of LNCaP carcinoma cells.
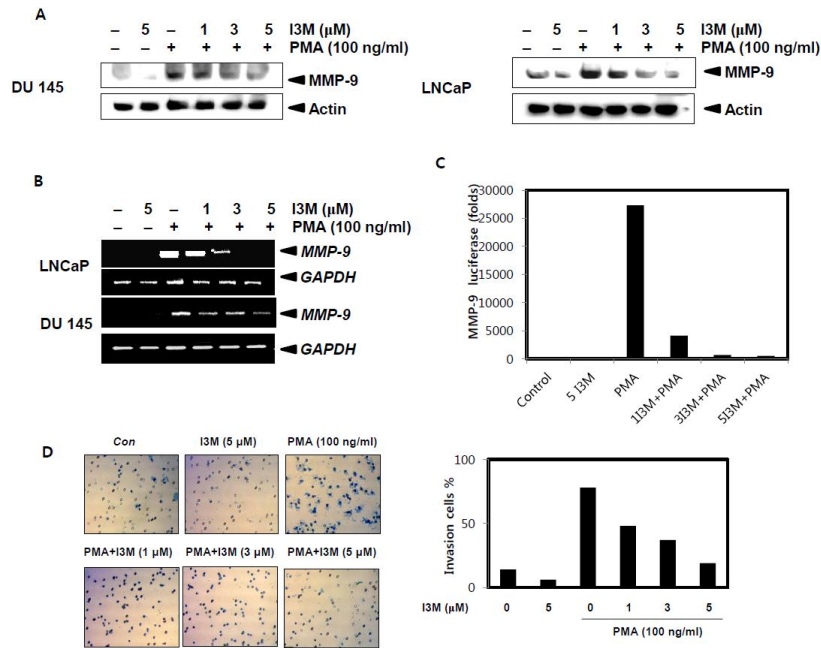
Fig. 28. Effects of I3M on MMP-9 activity and invasion. LNCaP and DU145 cells were treated with various concentrations of I3M in the presence of PMA (100 ng/ml). (A) Equal amount of cell lysates were resolved on SDS–polyacrylamide gels, transferred to nitrocellulose membranes, and probed with antibodies against MMP-9. (B) In a parallel experiment, total RNA was isolated at 6 h and RT-PCR analysis of *MMP-9* was performed. (C) Cells were transfected with an MMP-9 promoter-containing reporter vector and luciferase activity was measured 24 h following transfection. (D) For the invasion assay, the lower and upper parts of the Transwells were coated with Matrigel. LNCaP cells were cultured with I3M in the presence or absence of PMA. Invasiveness of the cells was determined by measuring their ability to pass through a layer of a Matrigel-coated filter. Following 24 h, cells on the bottom side of the filter were fixed, stained and counted as described in Materials and methods. β-Actin and GAPDH were used as an internal control for western blot and RT-PCR analyses respectively. Data from 3 independent experiments are expressed as overall mean ± SE. Statistical significance was determined by one-way ANOVA test ($^{*}P<0.05$ vs. TNF-α-treated group).

115

5.3.3. I3M inhibits PMA-induced expression of MMP-9 activity by induction of HO-1expression

Growing evidence suggest that increase in HO-1 protein expression in accordance with a decrease in MMP-9 activity (Park et al., 2014). Therefore, to test this concept we first evaluated whether treatment of I3M potential to induce HO-1 protein expression in LNCaP carcinoma cells. Interestingly, as shown in Fig. 3A, treatment of I3M enhanced the expression of HO-1 protein and m-RNA level in concentration dependent manner (Fig. 29A). Nevertheless, exposure to I3M on LNCaP cells, increased the expression of HO-1 protein and m-RNA level in time dependent manner and the peak expression level of HO-1 was seen at 24 h (Fig. 29B). Consequently, we used a HO-1 inducer, CoPP, for further functional confirmation of the above mentioned results. According to the western blot analysis, CoPP treatment remarkably reduced PMA-induced MMP-9 expression in LNCaP cells (Fig. 29C). In contrast, an HO-1 inhibitor, ZnPP, reversed the inhibition of MMP-9 activity in the presence of I3M in PMA-stimulated LNCaP cells (Fig. 29D). Therefore, these results indicate that HO-1 expression is the main effector in PMA-induced MMP-9 inhibition in LNCaP cells.
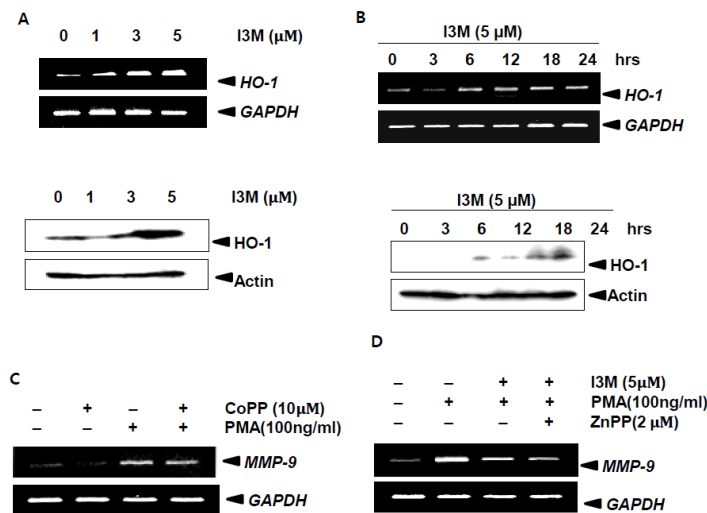
Fig. 29. Effect of I3M on HO-1 expression in LNCaP prostate carcinoma cells. Cells were treated with indicated concentrations of I3M (0–5 μM) for 6 h and 24 h. (A) RT-PCR and western blot analyses of HO-1 was performed at 6 h and 24 h, respectively. (B) Cells were treated with 5 μM I3M for the indicated times (0–24 h) for 24h. RT-PCR and western blot analyses of HO-1 were performed. (C) Cells were pretreated with CoPP for 1 h and then stimulated with PMA (100 ng/ml) for 24 h to examine the MMP-9 mRNA expression. (E) Cells were pretreated with 5 μM I3M in the presence or absence of 2 μM ZnPP for 1 h and then incubated with PMA (100 ng/ml) for 24 h. Total cellular RNA was isolated and RT-PCR analysis for the *MMP-9* gene was performed. β-Actin and GAPDH were used as internal controls for western blot and RT-PCR analyses, respectively.

5.3.4. Effects of Nrf2 as HO-1 regulator in PMA-induced MMP-9 inhibition

Nrf2 regulate the coordinated expression of HO-1 (Biswas et al., 2014); therefore, we next correlated the activity of Nrf2 to the expression of HO-1 in LNCaP cells. As shown in Fig. 4A, western blot data showed that pretreatment with I3M resulted in significant induction of Nrf2

117

expression in nuclear compartment while decreased its expression in cytosolic compartment (Fig. 30A). We further examined HO-1 and MMP-9 expression in the transient knockdown of *Nrf2*. According to the western blot data and RT-PCR analysis, *Nrf2* siRNA treatment reversed I3M-inhibited MMP-9 expression while reducing I3M-induced HO-1 expression both protein and m-RNA levels respectively in LNCaP cells (Fig. 30B and 30C). To determine the involvement of Nrf2 in invasiveness of LNCaP cells, we tested invasion ability in *Nrf2*-knockdown LNCaP cells. Compared to untreated control group *Nrf2* siRNA treatment group remarkably enhanced invasion of LNCaP cells by 5-times (Fig. 30D). Taken together, these results indicate that I3M-induced HO-1 expression via Nrf2 activity thereby Nrf2 is crucially involved to reduction of invasion of LNCaP prostate cancer cells.
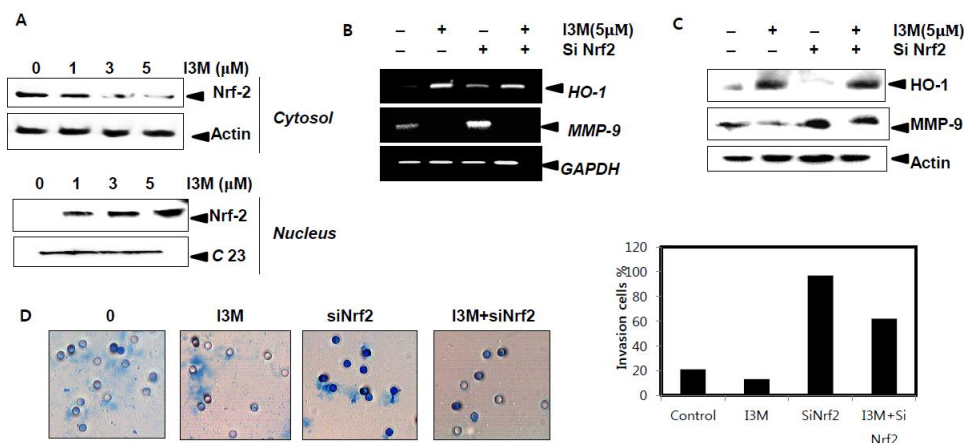
Fig. 30. I3M-induced Nrf2 activity in LNCaP prostate carcinoma cells. LNCaP cells were treated with various concentrations of I3M (0–5 μM) for 24 h. (A) Expression of Nrf-2 was measured by Western blot analysis in cytosol and nuclear compartments. (B) The cells were transiently transfected with *Nrf2* siRNA for 24 h and then treated with or without 5 μM I3M for 2 h. RT-PCR analysis of *HO-1*, and *MMP-9* was performed at 12 h. (C) Equal amount of cell lysates were resolved on SDS–polyacrylamide gels, transferred to nitrocellulose

membranes, and probed with antibodies against HO-1 and MMP-9. β-Actin and GAPDH were used as an internal control for western blot and RT-PCR analyses respectively. (D) Invasion assay was performed as shown in Section 2.

5.3.5. I3M activates the PI3K/Akt pathway as an upstream molecule of Nrf2

Past researches have been shown convincing data that suppressed phosphorylation of PI3K/Akt could significantly inhibited the activation of Nrf2/HO-1 expression (Park et al., 2014). Thus, next we examined the role of PI3K/Akt pathway in Nrf2/HO-1 expression as it is an upstream molecule of Nrf2. As shown in Fig. 5A, that I3M treatment notably enhanced PI3K and Akt phosphorylation after treatment in dose-dependent manner, suggesting that the I3M-induced Nrf2 expression associated with the PI3K/Akt signaling pathway (Fig. 31A). To further investigate the particular mechanism, we used LY294002, a specific PI3K/Akt inhibitor. The EMSA assay showed that treatment of I3M significantly increased Nrf2 expression; however, LY294002 significantly attenuated the I3M-induced Nrf2 activation (Fig. 31B). Similar to that, LY294002 obviously induced the MMP-9 activity while decreasing the activity of HO-1 m-RNA and protein level in LNCaP cells (Fig. 31C). Nevertheless, luciferase activity of MMP-9 was examined using transient transfection with reporter vectors that included MMP-9 promoters. Treatment with LY294002 significantly enhanced the PMA-stimulated induction of MMP-9 luciferase activity (Fig. 31D). As expected, these data demonstrated that the PI3K/Akt pathway regulates the Nrf2 expression accordance with its effect on HO-1 expression in LNCaP prostate cancer cells.
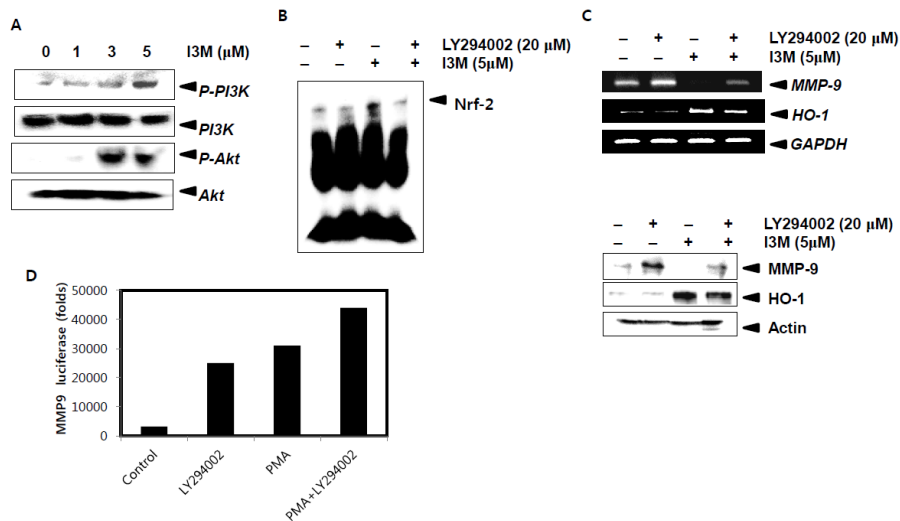
Fig. 31. Effect of I3M on phosphorylation of PI3K/Akt in DU145 cells. (A) LNCaP cells (2 × 10^5 cells/ml) were treated with various concentrations of I3M for 24 h. Western blot analysis was performed for PI3K/Akt phosphorylation. (B) The cells were preincubated with 20 μM LY294002 2 h before treatment with 5 μM I3M for 24 h. The DNA promoter region binding activity of Nrf-2 in the nuclear protein extract was analyzed using EMSA. (C) After treatment with 5 μM I3M for 12 h in the presence or absence of 20 μM LY294002 for 2 h, total RNA was isolated and RT-PCR analysis of *HO-1* and *MMP9* was performed. Cells were treated with indicated concentrations of I3M (0–5 μM) in the absence or presence of 20 μM LY294002. (C) RT-PCR and western blot analyses of HO-1 was performed at 12 h and 24 h, respectively. β-Actin and GAPDH were used as an internal control for western blot and RT-PCR analyses respectively. (D) I3M (5 μM) was applied and MMP-9 luciferase activity was measured 24 h after treatment of 20 μM LY294002.

5.3.6. I3M downregulates AP-1 activity

Since AP-1 is an important transcriptional factor for invasion and metastasis (Liuet al.,

2014), next we assessed whether I3M regulates the specific DNA-binding activity of AP-1 in LNCaP prostate cancer cells. Treatment with I3M substantially reduced PMA-induced DNA-binding activity of AP-1 in LNCaP cells (Fig. 32A). We also conducted a promoter assay in LNCaP cells transiently transfected with a luciferase reporter vector that included the AP-1 binding sites. Consistence with the above results, treatment with I3M reduced the luciferase activity of AP-1 in LNCaP cells (Fig. 32B). Several studies indicated that the binding of c-Fos/c-Jun heterodimer at the AP-1 site elicits MMP-9 expression (Xia et al., 2015). Therefore, next we examined the expression level of c-Fos and c-Jun which regulate AP-1-mediated MMP-9 expression in LNCaP cells, with exposure to I3M. Interestingly, 5μM of I3M-treated LNCaP cells reduced PMA-induced c-Fos and c-Jun protein expression level (Fig. 32C). Nevertheless, past studies revealed that activity of AP-1 regulates through JNK pathway (Li et al., 2015). Because of this reason, we examined the involvement of JNK pathway regulation of MMP-9 expression in LNCaP cells. Treatment of 20 μM of SP-1, specific JNK inhibitor, remarkably reduced PMA-induced DNA-binding activity of AP-1 in LNCaP cells by suggesting JNK pathway play an important role in regulation of AP-1 (Fig. 32D). Further, it is revealed the PMA-induced m-RNA level of MMP-9 was reduced by SP-1 indicating that AP-1 regulate MMP-9 activity via JNK pathway in LNCaP cells (Fig. 32E). Taken together these results indicate AP-1 plays a crucial role in activating MMP-9 gene via activating of c-Fos and c-Jun protein in LNCaP prostate cancer cells.
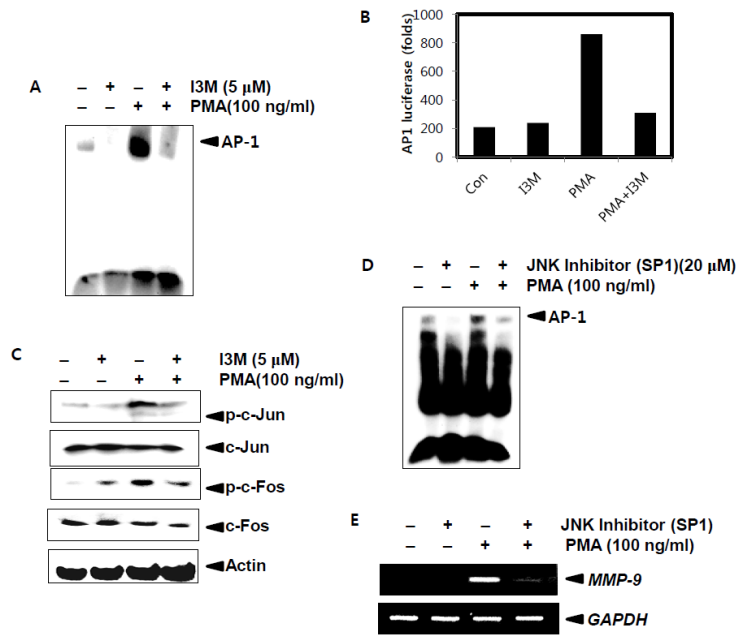
Fig. 32. Effect of I3M on the AP-1-DNA binding activity. (A) The cells were preincubated with 5 μM I3M 2 h before treatment with 100 ng/ml PMA for 30 min. Nuclear extracts were assayed for DNA-binding activity of AP-1 using EMSA. (B) The cells were transfected with a WT-AP-1 promoter-containing reporter vector, and luciferase activity was measured 24 h after transfection. (C) In a parallel experiment, cytosolic protein lysates were prepared at 24 h, subjected to SDS-PAGE, and immunoblotted using specific antibodies against p-c-Jun, c-Jun, p-c-Fos, and c-Fos. (D) The cells were preincubated with 20 μM SP1 2 h before treatment with 100 ng/ml PMA for 30 min. Nuclear extracts were assayed for DNA-binding activity of AP-1 using EMSA. (E) In a parallel experiment, total RNA was isolated and RT-PCR analysis of *MMP9* was performed. β-Actin and GAPDH were used as internal controls for western blot and RT-PCR analyses respectively.

5.3.7. I3M downregulates AP-1 activity regulate by Nrf2

122

Furthermore, to investigate the correlation of AP-1 activity with Nrf2 underlines and examined in LNCaP cells. To determine the DNA binding ability of AP-1 we performed EMSA assay with the treatment of transient knockdown of Nrf2. According to the Fig. 7A, the use of transient knockdown of Nrf2, increased 100 ng/ml of PMA induced DNA binding ability of AP-1 in LNCaP cells (Fig. 33A). For further clarification of above matter, we treated 100 ng/ml of PMA as an inducer of AP-1 activation thus; regulate expression of c-Fos and c-Jun protein levels. As shown in Fig. 33B, siNrf2 treatment induced PMA-induced expression of c-Fos and c-Jun protein levels in LNCaP cells (Fig. 33B). Moreover, the expression of HO-1 was regulated by Nrf2, we next examined the effect of HO-1 for the regulation of AP-1 activity. Similar to above results, treatment of ZnPP, HO-1 inhibitor enhanced the expression of c-Fos and c-Jun protein level in LNCaP cells (Fig. 33C). Taken together these results indicate, AP-1 activity regulate directly or indirectly by Nrf2.
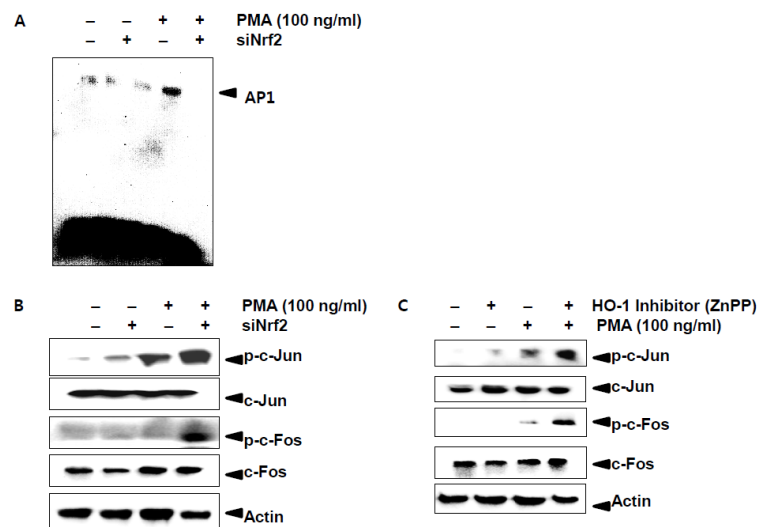
Fig. 33. Effect of I3M on downregulation of AP-1 activity via Nrf-2 in LNCaP cells. (A) The LNCaP cells were transiently transfected with *Nrf2* siRNA for 24 h and then treated with or without before treatment with 100 ng/ml PMA for 24 h. Nuclear extracts were prepared and

analyzed for AP-1-binding activity using EMSA. (B) In a parallel experiment, cytosolic protein lysates were prepared at 24 h, subjected to SDS-PAGE, and immunoblotted using specific antibodies against p-c-Jun, c-Jun, p-c-Fos, and c-Fos. (C) The cells were pretreated with 2 μM ZnPP for 2 h and then incubated with 100 nM PMA for 24 h. The expression of p-c-Jun, c-Jun, p-c-Fos, and c-Fos proteins were detected by Western blot assay.

5.4. Discussion

I3M has been exhibited to possess of anti-inflammatory, anticarcinogenic activities (Kim and Park., 2012 and Lo and Chang., 2013). Recently much interest has been focused on analyzing these pharmaceutical properties, as I3M seems to response on cell-cycle regulation, reduction of cellular invasiveness, induction of apoptosis and antioxidant metabolism. In consideration of AP-1 and Nrf2 play a crucial role in the cell survival and proliferation as well as cell invasiveness and metastasis these transcription factors were examined as I3M targets. We have reported that 5 μM I3M decreased PMA-stimulated MMP-9 expression thereby reduced the cellular invasiveness. Nevertheless, the present study has shown that I3M activates the Nrf2 signaling via PI3K/Akt pathways and reduces AP-1-binding activity by down regulation of c-Jun and c-Fos in LNCaP prostate cancer cells.

The PI3K/Akt signaling pathway is involved in regulating Nrf2 expression (Huang et al., 2014). Therefore, in this study we examined the possibility that PI3K/Akt mediates I3M-induced Nrf2 expression. According to our data, I3M treatment notably enhanced the phosphorylation level of Akt and PI3K proteins, while no significant changes were found in the total Akt and PI3K protein level, suggesting that enhancement of Akt and PI3K protein

124

phosphorylation may contribute to the I3M-induced Nrf2 expression. To further clarify the role of PI3K/Akt pathway, LY294002, a specific PI3K/Akt inhibitor, was used to treat LNCaP cells. The results showed that inhibition of the PI3K/Akt signaling pathway remarkably blocked Nrf2 expression in the presence of I3M. Nevertheless, we observed whether PI3K/Akt plays an important role in expression of HO-1, accordance with its regulation of Nrf2 expression. According to the western blot analysis and RT-PCR data, blocking of PI3K/Akt signaling by LY294002 attenuated the I3M-induced expression of HO-1 protein and m-RNA level respectively. Therefore, we determined that the PI3K/Akt signaling pathway played a central role in I3M-induced HO-1 expression by regulating Nrf2.

Researchers have been shown convincing data that HO-1 exhibit anti-invasive activity by reducing the expression of pro-metastatic genes, thus suggesting a potential therapeutic strategy for treating prostate cancer metastasis (Ferrando et al., 2011). Similar to that our results also indicated role for HO-1 expression as a negative regulator of pro-metastatic gene MMP-9. In agreement with these past studies, the results of the present study demonstrated that I3M induces the expression of HO-1, providing a potential explanation for its anti-invasive properties. We observed whether HO-1 expression correlates with the inhibition of PMA-induced MMP-9 activity. Treatment with HO-1 inhibitor ZnPP (2 µM), markedly reversed the inhibitory effects of I3M on MMP-9 activity in LNCaP cells. Therefore, the present study provide evidence that, treatment with I3M, the upregulation of HO-1 appears to be one of the mechanisms by which I3M protects against cellular invasiveness occurred via MMP-9 in LNCaP prostate cancer cells.

Moreover, to investigate the mechanism by which I3M down-regulated PMA-induced MMP-9 expression, we tried to discover the essential transcription factor in the PMA-induced

MMP-9 expression pathway. Growing evidence suggests that AP-1 is the positive regulator of MMPs: plays a key role in the regulation of transcription of MMP-1 gene expression, and mutations of this element dramatically reduce the basal activity and responsiveness of the MMP-1 promoter to external stimuli (Qin et al., 2014). In the MMP-9 promoter upstream regulation sequence, there are two AP-1 binding site at 98 bp which play essential roles in MMP-9 expression in human oral squamous cell carcinoma (Bedal et al., 2014). In our study, treatment of I3M reduced PMA-induced AP-1 activity by providing evidence that AP-1 may critically required to increase MMP-9 transcription in prostate cancer cells. Since AP-1 consists of either homodimers of Jun family members or heterodimers between members of the c-Fos and c-Jun families we examined the effect of these proteins for the regulation of MMP-9 mediated cellular invasiveness (Krämer et al., 2015). We discovered that I3M-decreased c-Jun and c-Fos activation by blocking their respective phosphorylation.

We were further interested in I3M inhibitory mechanism on c-Jun and c-Fos. JNK or c-Jun N-terminal kinase, a member of the MAPK (mitogen-activated protein kinase) family that regulates a range of biological processes implicated in tumor invasiveness, is considered to be the essential kinase of AP-1 activation (Koul et al., 2013 and Benbernou et al., 2013). Accordance with that, to investigate whether I3M mediate AP-1 activation via MAPK pathway, we pretreated specific JNK inhibitor SP-1 on LNCaP prostate cancer cells. Interestingly, SP-1 inhibited PMA-induced AP-1 DNA binding activity. Further, as shown in RT-PCR data with the presence of SP-1 reduced the PMA-induced expression of MMP-9 mRNA level in LNCaP cells. Thus, we find direct evidence in prostate cancer cells that JNK is critically required for AP-1 activation.

In summary, this study describes LNCaP prostate cancer cells anti invasive activity of I3M,

synthesized by various molecular substitution of the parental indirubin. I3M blocked PMA-induced MMP-9 activity by suppressing AP-1 trascription via Nrf2 signaling pathway in LNCaP prostate carcinoma cells. This study would provide a new clue for exploiting I3M as a potent anticancer agent for the treatment of prostate cancer.

5.5. Conclusion

I3M blocked PMA-induced MMP-9 activity by suppressing AP-1 trascription via Nrf2 signaling pathway in LNCaP prostate carcinoma cells. The hemeoxigenase-1 (HO-1) regulate by Nrf2 is critically involve for the regulation of invasion of prostate cancer cells by inhibiting MMP-9 expression in LNCaP prostate cancer cells.

Chapter 6

Indirubin-3'-monoxime induces CHOP expression in wild type p53 HCT116 colon cancer cells to oxidative stress increases apoptosis through TRAIL sensitization

Abstract

We investigated the molecular mechanism that Indirubin 3-monoxime (I3M) induce apoptosis via CHOP, DR5 upregulation in p53$^{+/+}$ HCT-116 cells sensitize to tumor necrosis factor-related apoptosis inducing ligand (TRAIL). We have shown that treatment of I3M induce apoptosis in HCT-116 cells depends on the p53 status. I3M significantly induced Ras levels in p53$^{-/-}$ HCT-116 cells whereas reduced the expression of Ras in p53$^{+/+}$ HCT-116 cells. These results suggested that the effect of I3M on regulation of Ras expression in colon cancer cells independent on the status of p53. Further, I3M remarkably enhanced m-RNA and protein level of DR5. We found that p53 controls the sensitivity to TRAIL-induced apoptosis through enhancing the expression of DR5 in p53$^{+/+}$ HCT-116 cells. Our results showed that I3M-induced the expression of CHOP, with optimum induction occurring at around 24 h. The p53$^{+/+}$ HCT-116 cells transfection with CHOP siRNA significantly abrogated the up-regulation of DR5 protein and m-RNA level by confirming that I3M-induced up-regulation of DR5 is mediated via the induction of CHOP. The H$_2$DCFDA and HE-based fluorescence analysis showed that concentration dependent manner treatment of I3M increased ROS generation by increasing intracellular superoxide anion and hydrogen peroxide levels respectively. Moreover, fluorometric data indicated that silencing of p53 had more dramatic effect on I3M-induced ROS production. Pretreatment of NAC remarkably blocked I3M-induced ROS production. Nevertheless, I3M treatment induced the TRAIL expression in time dependent manner in p53$^{+/+}$ HCT-116 cells. Treatment of TRAIL synergistically enhanced I3M-induced DR5 expression thereby induced the TRAIL-induced apoptosis. Concentration dependent manner addition of a DR5 specific blocking antibody significantly blocked I3M/TRAIL-induced apoptosis. Taken together, our data have shown that I3M potently enhances TRAIL-induced

apoptosis by upregulating DR5 expression via activating p53. We suggest that relationship between p53 and oxidative stress indirectly regulate I3M/TRAIL induced apoptosis in p53$^{+/+}$ HCT-116 cells.

Key words: I3M; TRAIL; Ras; ROS; CHOP

6.1. Introduction

In spite of notable advances over the last decades in understanding of the genesis of colon cancer and the application of targeted drug therapy, colon cancers remain the second most common cause of cancer-related death. Because of the resistance of colon cancers to current treatment regimens, possible chemopreventative and new chemotherapeutic approaches should be investigated (Temraz et al., 2014). It is essential to develop novel drugs which are potent in inhibiting the proliferation of cancer cells while exhibiting minimal cytotoxicity towards the normal cells. The use of novel promising therapeutic compounds derived from natural products or Chinese herbs has attracted much interest as an alternative in cancer treatment.

Indirubin, a 3,2-bisindole is the active ingredient of Dang Gui Long Hui Wan, from a mixture of herbal medicines customarily used in traditional Chinese medicine to treat chronic myelocytic leukemia (CML) (Kim et al., 2011). The anti-leukemic activity of this ingredient has been attributed to the red-colored indigo isomer indirubin (Perabo et al., 2006). Over the last half century, a number of indirubin analogs have been synthesized to optimize this promising drug scaffold. The commercially available analogue of indirubin, indirubin-3-oxime, one of the indirubin analogue strongly inhibit the growth of various human cancer cells, mainly via the apoptosis. In the attempt to reveal the mechanism of action of I3M, various biological

제주대학교 중앙도서관
JEJU NATIONAL UNIVERSITY LIBRARY

activities of I3M have been discovered. It has been reported to induce apoptosis in human cervical cancer HeLa cells, hepatoma HepG2 cells, colon cancer HCT116 cells (Shi and Shen, 2008), human laryngeal carcinoma Hep-2 cells (Kameswaran et al., 2009 and Paulkumar et al., 2010) and renal cell cancer cell lines in a time- and dose-dependent manner (Perabo et al., 2011). *In vivo* study carried out in rat tumor model provides further evidence for the anti-cancer activity of I3M. Ravichandran *et al* was shown I3M exhibited anticancer effect against [B(α)P] induced lung cancer by its apoptotic action in A/J mice (Ravichandran et al., 2010). However, the modulatory effects and the detailed molecular action mechanisms of I3M on human HCT 116 colon cancer cells have yet to be studied.

Apoptosis is generally characterized by distinct morphological characteristics and energy-dependent biochemical mechanisms and evolutionarily conserved cell death mechanism that is activated by various stimuli (Orrenius et al., 2011). Apoptosis induced by p53 is strongly established as a central mechanism of tumor suppression (Loughery and Meek., 2013). Primarily, p53 is located in the cytoplasm in normal cells and, upon genotoxic stresses, it translocates into the nucleus in a tightly regulated manner (Loughery and Meek., 2013). However, this subcellular localization and subsequent function of p53 in nuclear and cytoplasmic compartments of a cancerous cell is compromised by p53's cytoplasmic sequestration (Comel et al., 2014). Oxidative stress is also known to induce apoptosis that depends on the p53 expression level (Hussain et al., 2004). Following stabilization as a result of apoptotic stimuli, activation of p53 leads to enhance expression of various genes that are involved in apoptosis and growth arrest (Liebermann et al., 2007). This status is based on the fact that p53 is functionally mutated in a high percentage of human cancers (Essmann and Schulze-Osthoff., 2012). Indeed, the activation of p53 in cancers has been recognized as a

131

promising strategy for treatment of cancers, and several drugs targeting p53 are currently being evaluated in preclinical and clinical trials (Essmann and Schulze-Osthoff., 2012). Studies with mouse cells, for example, have provided obvious evidence of drug resistance after p53 inactivation. The systematic screening of panels of human tumor-derived cell lines for sensitivity to therapeutic agents has revealed associations between p53 status and drug sensitivity (Brown and Wouters., 1999). In consequence, a precise understanding of the diverse activities of p53 has been an important research objective with significant clinical impact.

It has been reported that p53 directly modulates expression of death receptors DR4 and DR5, thus enhance the sensitivity to TRAIL-induced apoptosis (Carter et al., 2008). Surget *et al* was shown that silencing of p53 strongly decreased the expression of DR5 in human myeloma cells (Surget et al., 2012). Therefore, both p53 and DR5 is believed to be significant factors regulating TRAIL-induced apoptosis. Although the mechanism of p53 regulates expression of DR5 is not fully understood, several mechanisms have been suggested so far. At transcriptional level, expression of DR5 can be regulated by binding of CHOP to promoter region of the DR5 gene (Liu et al., 2012). CHOP is primarily regulated at the transcriptional level and is one of most induced gene during ER stress (Liu et al., 2012). Numerous recent studies have been indicated that CHOP regulates apoptosis via induction of DR5 expression (Yamaguchi et al., 2004). Consequently, TRAIL potently induces apoptosis in cancer cells by binding to the DR5 (Liu et al., 2012). Therefore, death receptors are attractive therapeutic approaches through TRAIL as well as p53 status for the induction of the apoptosis of the target cancer cells.

Although the efficacy and potential use of TRAIL in treatment of cancers has been suggested, little is known about the factors that determine the sensitivity of cancer cells to killing by

TRAIL. Recently, there were some reports on the determinants of TRAIL sensitivity in breast cancer cells, melanoma, and brain tumors (Kim et al., 2000). Since TRAIL signaling pathway somewhat controversial we were interested to investigate the I3M/TRAIL-mediated apoptosis in HCT colon cancer cells through the expression of DR5 depend on the p53 status. In addition, we also reported the correlation between DR5, p53 and Ras to enhance TRAIL-sensitization via increasing oxidative stress. Our results provide essential preclinical information that may be useful in the design of clinical trials using I3M/TRAIL in the therapy of human colon cancers.

2.6. Materials and method

2.6.1. Materials and reagents

3-(4,5-dimethyl-2-thiazolyl)-2,5-diphenyl-2H-tetrazolium bromide (MTT), N-acetylcysteine (NAC), propidium iodine (PI), and annexin V were purchased from Sigma Chemical Co. (St. Louis, MO). Rabbit anti-human antibodies against Bid, Bax, caspase-3, RAS, p53, CHOP, DR5, TRAIL, caspase-8, PARP, Bcl2, cytochrome c, and β-actin were purchased from Santa Cruz Biotechnology (Santa Cruz, CA). Peroxidase-labeled goat anti-rabbit immunoglobulin was purchased from KOMA Biotechnology (Seoul, Republic of Korea). Dulbecco's Modified Eagle's Medium (DMEM), antibiotic mixture, pan-caspase inhibitor, z-VAD-fmk, Roswell Park Memorial Institute (RPMI)-1640 medium, and fetal bovine serum (FBS) were obtained from WelGENE Inc. (Daegu, Republic of Korea).

2.6.2. Cell culture

P53-Null (p53$^{-/-}$) and wild-type (p53$^{+/+}$) human HCT-116 colon carcinoma cells were obtained from the American Type Culture Collection (Manassas, VA) and maintained in a RPMI medium supplemented with 10% heat-inactivated FBS and 1% penicillin–streptomycin in 5% CO_2 at 37°C. Periodically, cells were tested and resulted negative for mycoplasma contamination using the MycoAlert Mycoplasma Detection Kit (Lonza, Rockland, ME).

2.6.3. Cell viability assay with MTT reduction

Cell viability was measured using the MTT assay, which is based on the conversion of MTT to formazan crystals by mitochondrial dehydrogenases. p53-Null (p53$^{-/-}$) and wild-type (p53$^{+/+}$) human HCT-116 colon carcinoma cells (1×10^5 cells/ml) were cultured in medium with or without serum in 24 well plates at 37ºC. 24 h after incubation cells were pretreated with various concentrations of I3M and 1 h after followed by TRAIL treatment. The medium (500 µl) was then incubated with 0.5 mg/ml MTT solution for 45 min at 37°C. The culture medium was removed, and 700 µl dimethyl sulfoxide was added to each well to dissolve the formazan. The absorbance was measured at 540 nm using a microplate reader.

2.6.4. Western blotting

Briefly, 24 h after the treatment of indicated chemical concentrations cells were harvested by scraping from the wells and washed twice with cold phosphate buffered saline (PBS). Total cell extracts were prepared using a 100 µl ice-cold PROPREP protein extraction kit (iNtRON Biotechnology). Lysates were centrifuged at 16,000 rpm at 4°C for 30 min to obtain the supernatants. Protein concentrations of the supernatants were determined with a Bio-Rad

제주대학교 중앙도서관
JEJU NATIONAL UNIVERSITY LIBRARY

protein assay kit (Bio-Rad, Hercules, CA). Proteins were loaded on 5% SDS-PAGE for electrophoresis. Then proteins were electrophoretically transferred to a polyvinylidene difluoride membrane. The membrane was incubated with primary antibodies overnight at 4°C, rinsed the blot 3 times for 10 min with TBST (20 mM Tris pH 7.5, 150 mM NaCl, and 0.1% Tween 20). Membranes were incubated with peroxidase-labeled goat anti-rabbit secondary antibody solution (KOMA Biotechnology, Seoul, Republic of Korea) for 2hrs at room temperature. Using TBST, membranes were rinsed 3 times for 10 min and detection of specific proteins was carried out with a Chemiluminescence (ECL) western blotting kit (Amersham) according to the recommended procedure.

2.6.5. Flow cytometry analysis

The p53-null (p53$^{-/-}$) and wild-type (p53$^{+/+}$) human HCT-116 colon carcinoma cells were treated with different concentrations of I3M for the indicated time, then trypsinized and washed in cold 1× PBS. The cells were then resuspended in 1× annexin-V binding buffer for 15 min at room temperature. The stained samples were measured using a fluorescence-activated cell sorting caliber bench-top flow cytometer (Becton Dickinson San Jose, CA).

2.6.6. Reverse transcription-polymerase chain reaction (RT-PCR)

Total RNA was extracted using Easy-blue reagent (iNtRON Biotechnology, Sungnam, Republic of Korea) according to the manufacturer's protocol. A total of 2 μg RNA was reverse transcribed to cDNA using the One-Step RT-PCR Premix (iNtRON Biotechnology). Synthesized single stand cDNA was amplified by RT-PCR with the following primer pairs: *DR5* forward, 5′-AAG ACC CTT GTG CTC GTT GTC-3′, DR5 reverse 5′-GAC ACA TTC

GAT GTC ACT CCA-3′, CHOP forward 5′-CAA CTG CAG AGA TGG CAG CTG A-3′ and

CHOP reverse 5′-CTG ATG CTC CCA ATT GTT CAT-3′, *glyceraldehyde-3-phosphate*

dehydrogenase (*GAPDH*) forward 5′-GTC TTC ACC ACC ATG GAG-3′ and GAPDH reverse

5′-CCA CCC TGT TGC TGT AGC-3′. The reaction sequence consisted of 50°C for 30 min,

94°C for 2 min, and 94°C for 29 cycles of 15 s each; 60°C for 30 s; and 72°C for 45 s with an

extension at 72°C for 10 min. PCR products were analyzed by electrophoresis on 1% agarose

gel and expression levels of each molecule were normalized to *GAPDH* levels within the same

sample.

2.6.7. DNA fragmentation assay

I3M-treated or untreated cells were fixed in ice-cold buffer containing 10 mM Tris–HCl

(pH 7.4), 150 mM NaCl, 5 mM EDTA, and 0.5% Triton X-100 for 30 min. Lysates were

vortexed and purified by centrifugation at 10,000 *g* for 20 min. Using the equal volume of

neutral phenol:chloroform:isoamylalcohol (25:24:1,v/v/v) fragmented DNA in the supernatant

was extracted and analyzed electrophoretically on 1.5% agarose gels. DNA was visualized by

ethidium bromide staining.

2.6.8. Transient knockdown of CHOP

Cells were transfected CHOP-specific silencing RNA (siRNA, Santa Cruz Biotechnology)

for 24 h. For each transfection, 450 μl growth medium was added to 20 nM siRNA duplex with

the transfection reagent G-Fectin (Genolution Pharmaceuticals, Inc., Seoul, Republic of Korea)

and the entire mixture was added gently to the cells.

2.6.9. Confocal microscopy

Cells were stained with phycoerythrin-conjugated rabbit monoclonal anti-human DR5 for 45 min at 4°C according to the manufactures protocol and analyzed by flow cytometry with FITC-conjugated IgG.

2.6.10. Statistical analysis

All values are expressed as means ± SEM. The data were derived from at least three independent experiments. Multiple group comparison was performed by one-way ANOVA test. The images were visualized with Chemi-Smart 2000 (Vilber Lourmat, Cedex, France). Images were captured using Chemi-Capt (Vilber Lourmat) and transported into Adobe Photoshop (version 8.0). Values of $P < 0.05$ were considered to be statistically significant.

6.3. Results

6.3.1. I3M influence the viability of HCT-116 colon cancer cells depends on the p53 expression

It has been reported that I3M is known to be a potent anticancer agent, while the molecular mechanism underlying I3M-induced apoptosis has not been fully elucidated. Therefore, we first investigated the effects of I3M on the viability of HCT-116 colon cancer cells by MTT assay and annexinV staining. To establish the optimal conditions for apoptosis of human colon carcinoma cells by I3M, $p53^{+/+}$ HCT-116 or $p53^{-/-}$ HCT-116 colon cancer cell lines were

cultured in the absence or presence of I3M for 24 h. Cell viability was then measured by MTT assay. Fig. 34A demonstrates dose-dependent I3M-induced cytotoxicity in $p53^{+/+}$ HCT-116 colon cancer cells while did not affect cell viability of $p53^{-/-}$ HCT-116 colon cancer cells (Fig. 1A). Maximum I3M-induced cytotoxicity was evident after 24 h exposure to 20 μM I3M on $p53^{+/+}$ HCT-116 colon cancer cells (Fig. 34A). Therefore, the sub-toxic concentrations ($\leq$ 20 μM) were used in subsequent experiments. Next, flow cytometric analysis performed to evaluate I3M cytotoxicity in more detail. Data obtained using annexinV staining showed that of the 15 μM I3M-treated $p53^{+/+}$ HCT-116 cells, 59.64% were annexin V+ or apoptotic; however, a negligible population of I3M-treated $p53^{-/-}$ HCT-116 cells were found to be annexin V+, thereby suggesting that I3M influence on viability of HCT-116 colon cancer cells regards to the p53 expression (Fig. 34B). Parallel, we also analyzed expression of proteins level of Bid, Bax, and pro-caspase-3 in cell lysates of $p53^{+/+}$ HCT-116 cells. Treatment of 15 μM of I3M caused significant expression levels of apoptotic proteins Bid and Bax while decreasing pro-caspase-3 expression level (Fig. 34C). Elevated Bid and Bax were not observed in I3M-treated $p53^{-/-}$ HCT116 cells, although notable accumulation of pro-caspase-3 was noted (data was not shown). Moreover, concentration dependent manner treatment of I3M produced comparable levels of DNA fragmentations that are characteristic of apoptosis in $p53^{+/+}$ HCT-116 cells (Fig. 34D). Taken together, these data indicate that p53 status influence the ability of I3M to induce apoptosis in HCT-116 cells.
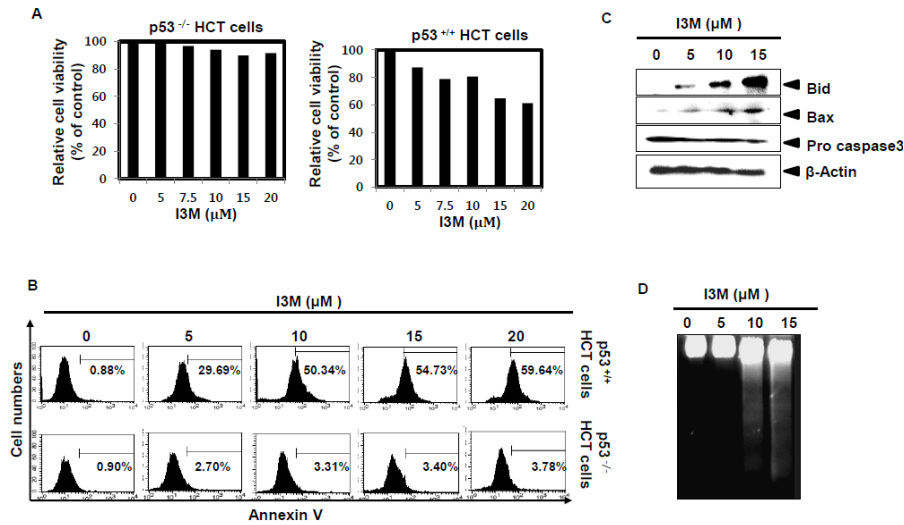
Fig. 34. Effect of I3M on the viability of p53-null (p53$^{-/-}$) and wild-type (p53$^{+/+}$) human HCT-116 colon carcinoma cells. The p53-null (p53$^{-/-}$) and wild-type (p53$^{+/+}$) HCT-116 cells were treated with various concentrations of I3M (0-20 μM). (A) Cell viability was measured by an MTT assay following 24 h. (B) In a parallel experiment, apoptotic (p53$^{-/-}$) and (p53$^{+/+}$) HCT-116 cells were measured by flow cytometric analysis. The percentages of gates (apoptosis) are represented in each panel. (C) The cytosolic protein lysates were prepared at 24 h, subjected to SDS-PAGE, and immunoblotted using specific antibodies against Bid, Bax, and caspase-3. β-Actin was used as an internal control for western blotting analysis. (D) Total DNA was extracted from the cells and DNA fragmentation assay was performed using 1.5% agarose gel.

6.3.2. I3M enhances Ras expression in HCT-116 colon cancer cells dependent of p53 expression

Previous reports have been shown that expression of p53-induced apoptosis accompanied by accumulation of oncogenic *Ras*. Therefore, we were interest in elucidate the apoptotic

effect of I3M via TRAIL sentizisation in p53$^{+/+}$ and p53$^{-/-}$ HCT-116 cells regards the Ras expression. Recent evidence suggests a link between Ras activity and the death receptor mediated apoptosis through TRAIL sentizisation. For example, transformation by oncogenic Ras sensitizes TRAIL-induced apoptosis by up-regulating DR4 and DR5 in human colon cancer cell lines (Zhang et al., 2005 and Nesterov et al., 2004). Nevertheless, to extend our finding beyond the association between Ras activity and TRAIL sensitivity, we addressed the issue of whether p53 regulates the expression of Ras in colon cancer cells. Evidence supported that biochemical interaction between Ras and p53 to promote apoptosis (Lowe et al., 2004). To explore this possibility, we performed a western blot analysis to examine the Ras and p53 protein expression level which correlated with the TRAIL sentizisation. Concentration dependent treatment of I3M down-regulated the Ras expression level while increasing p53 expression level in p53$^{+/+}$ HCT-116 cells (Fig. 35A). Moreover, I3M significantly reduced Ras proteins levels whereas inducing protein level of p53 in p53$^{+/+}$ HCT-116 cells, with the starting point at 18h and clearly at 24 h after treatment (Fig. 35B). To confirm the critical role of p53 in upregulation of Ras by I3M, p53$^{-/-}$ HCT-116 cells were used to assed the role of p53 status. As shown in Fig. 2C and Fig. 2D, I3M significantly induced Ras levels in p53$^{-/-}$ HCT-116 cells both in time and concentration dependent manner respectively (Fig. 35C and 35D). Further, western blot results confirmed that p53 expression was knocked out successfully with no induction of p53 in p53$^{-/-}$ HCT-116 cancer cells, whereas increased p53 levels were observed in p53$^{+/+}$ HCT-116 cells. These results suggest that the effect of I3M on regulation of Ras expression in colon cancer cells independent on the status of p53.
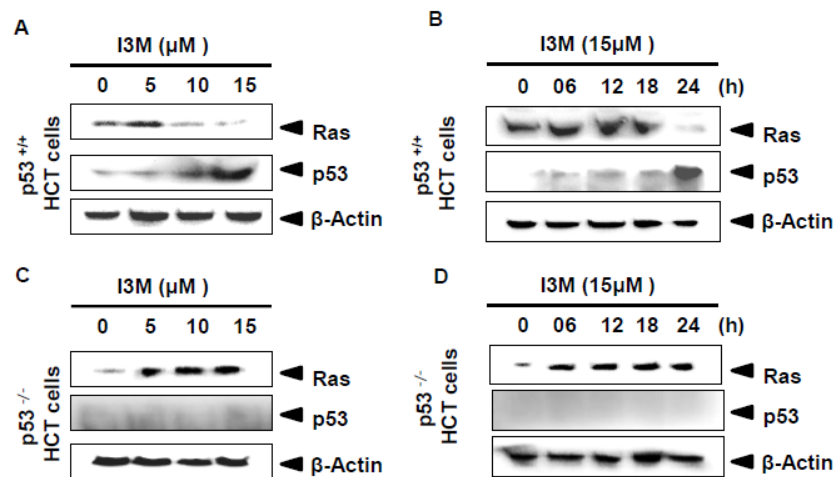
Fig. 35. Effect of I3M on the expression of p53 and Ras in (p53$^{-/-}$) and (p53$^{+/+}$) HCT-116 cells. (A) (p53$^{+/+}$) HCT-116 cells treated with indicated concentrations of I3M (0-15 μM) for 24 h and (B) the indicated times (0–24 h). The expression of p53 and Ras protein was detected by Western blot assay. (C) (p53$^{-/-}$) HCT-116 cells treated with indicated concentrations of I3M (0-15 μM) for 24 h and (D) the indicated times (0–24 h). Equal amounts of cell lysates were separated by SDS–PAGE and specific protein detection was performed using Western blotting as indicated. β-actin was used as a loading control.

6.3.3. I3M induced DR5 expression dependent of p53 expression

Researchers have been shown that the versatile relationship between p53 and DR5 thereby induced the sensitivity to TRAIL-induced apoptosis (Deguin-Chambon et al., 2000). More importantly, Surget *et al*. have reported that p53 affects the sensitivity of myeloma cells to the DR5 agonistic human antibody (Surget et al., 2012). In order to determine the relationship between the DR5 and p53, we analyzed the expression of DR5 and p53 at transcriptional level. We found that p53 controls the sensitivity to TRAIL-induced apoptosis through enhancing the

expression of DR5 in p53$^{+/+}$ HCT-116 cells. Pretreatment of p53$^{+/+}$ HCT-116 cells with time dependent manner significantly increased the expression of m-RNA and protein level of DR5 by I3M, however markedly increased DR5 expression was observed after 18 h after the treatment of I3M (Fig. 36A). To further show whether I3M could modulate the DR5 expression depends on the p53 status we analyzed the m-RNA and protein level of DR5 in concentration dependent manner treatment of I3M by RT-PCR and western blot analysis respectively. Confirming above data, concentration dependent manner treatment of I3M remarkably enhanced mRNA and protein level of DR5 (Fig. 36B). The confocal microscopic analysis with FITC-conjugated antibodies to DR5 receptor confirmed the upregulation of DR5 during the treatment of colon cancer cells in the presence of I3M (Fig. 36C). Moreover, to further verification of DR5 expression directly regulates via p53 expression, a specific sip53 was transfected into p53$^{+/+}$ HCT-116 cells. Then, we conduct the western blot analysis to determine the transient efficiency of p53 in p53$^{+/+}$ HCT-116 cells. The sip53 treatment group remarkably depleted p53 expression compared with the sicontrol treatment group (Fig. 36D). Transient knockdown of p53 alone suppressed the m-RNA expression level of DR5 (Fig. 36E). Further, western blot analysis has shown transfection of p53 into p53$^{+/+}$ colon cancer cells, comparatively reduced I3M-induced DR5 expression (Fig. 36F). We next examined whether the suppression of DR5 by specific DR5 blocking antibody could abrogate the effects of I3M-induced apoptosis using flow cytometry. As shown in Fig. 3G, the pretreatment with the DR5-specific blocking antibody significantly blocked sub-G$_1$ cell population induced by I3M alone treatment (Fig. 36G). Nevertheless, the DNA fragmentation assay showed typical DNA ladders in p53$^{+/+}$ HCT cells treated with I3M alone, whereas treatment with DR5-blocking antibody crucially inhibited fragmented DNA indicating that DR5 play a key role in apoptosis process

142

(Fig. 36H). Therefore, these results indicate that I3M enhances the apoptosis in colon cancer cells through intensifying interaction of p53 via DR5 overexpression.
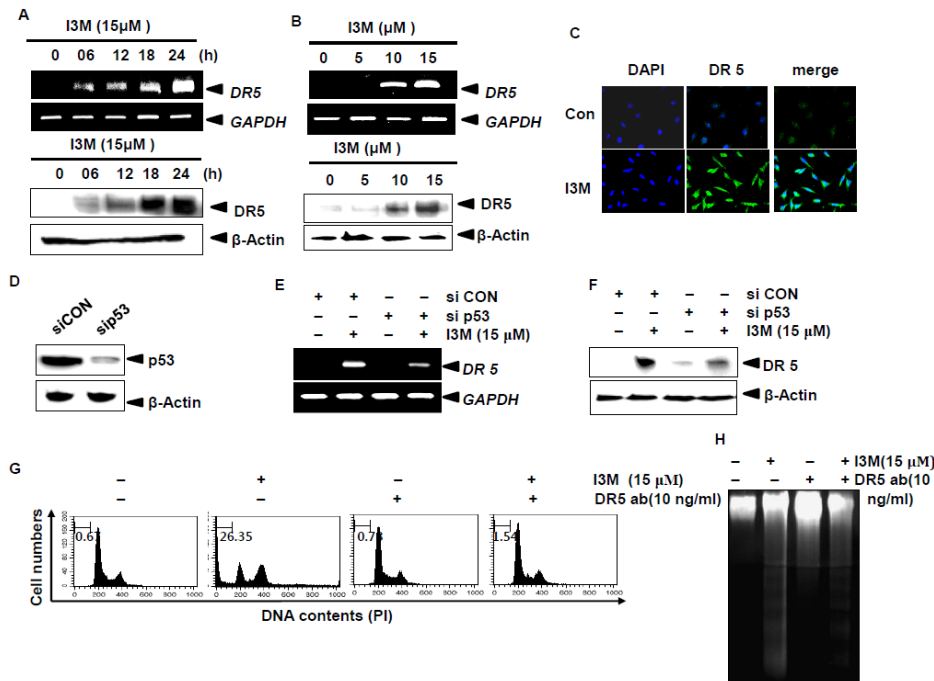
Fig. 36. I3M upregulates DR5 expression in (p53$^{+/+}$) HCT-116 cells. (A) Cells were seeded at 2×10^5 cells/ml and incubated with 15 μM I3M for the indicated time (0-24 h) and (B) cells were incubated with indicated concentrations of I3M (0-15 μM) for 24 h. RT-PCR and western blot analyses of DR5 was performed at 24 h, respectively. (C) DR5 immunofluorescence of (p53$^{+/+}$) HCT-116 cells treated for 24 h with I3M (15 μM). The cells were fixed, permeabilized, and stained with the DR5 monoclonal antibody. The monoclonal antibody was detected using an antimouse secondary antibody conjugated with Alexa Fluor$^®$ 488 and then stained with DAPI solution. Stained-DR5 and nuclei were then observed under a fluorescent microscope (×400). Cells were pretreated with 15 μM I3M for 24 h with or without DR5-specific chimeric antibody. (D) Cells were transiently transfected with *p53* siRNA for 24 h and then to determine the transfection efficacy, western blot analysis was carried out. Cells were transiently

transfected with *p53* siRNA for 24 h and then treated with or without before treatment with 15 μM I3M for 6 h and 24 h. (E) RT-PCR and (F) western blot analyses of DR5 was performed at 6 h and 24 h, respectively. (G) The percentage of apoptotic cells were analyzed by flow cytometry. Percentages of apoptotic cells are represented in each panel. Data in the figure represent percentages of each apoptotic cell populations in cell cycle distribution. (H) Fragmented DNAs were extracted from the treated cells and analyzed on 1.5% agarose gel.

6.3.4. I3M-induced DR5up-regulation is mediated through induction of CHOP

Because CHOP has been linked with the up-regulation of DR5 expression, we next examined the role of CHOP in I3M-induced DR5 up-regulation (Yamaguchi et al., 2004). Our results showed that I3M-induced the CHOP mRNA expression level with optimum induction occurring at around 24 h (Fig. 37A, upper panel). On the other hand, I3M markedly increased m-RNA levels of CHOP expression in concentration dependent manner (Fig. 37A, lower panel). In a parallel experiment, we further examined the I3M-induced CHOP expression at protein level by western blotting analysis. Treatment with I3M (15 μM) enhanced maximum protein expression level of CHOP at 24 h (Fig. 37B, upper panel). According to that concentration dependent manner treatment of I3M remarkably increased the CHOP protein expression level in p53$^{+/+}$ HCT cells at 24 h (Fig. 37B, lower panel). To date, no studies have examined the relationship between the expression of CHOP and p53 and the induction of apoptosis. Therefore, to examine the above relationship between CHOP and p53 knockdown was performed by siRNA transfection. The western blot analysis shown the transfection efficacy of both p53 and CHOP protein expressions with the depletion of both proteins in transfected group

compared to the control-transfected (CON siRNA) group (Fig. 4C). Compared to the control-transfected (CON siRNA) group, p53 siRNA transfected HCT cells reduced the I3M-induced p53 expression (Fig. 37D). Additionally, we investigated Ras expression in p53 transfected (p53 siRNA) and control-transfected (CON siRNA) cells. We found that I3M-down regulated the expression of Ras whereas p53 siRNA transfected group sharply increased the Ras expression in colon cancer cells (Fig. 37D). Nevertheless, to clarify the functional role of CHOP in I3M-induced up-regulation of DR5, CHOP siRNA was used. The DR5 expression was up-regulated by I3M in control-transfected (CON siRNA) cells transfection with CHOP siRNA significantly abrogated the up-regulation of DR5 protein and m-RNA level (Fig. 37E and 37F). Thus our results indicate that I3M-induced DR5up-regulation is mediated via the induction of CHOP in p53$^{+/+}$ HCT cells.
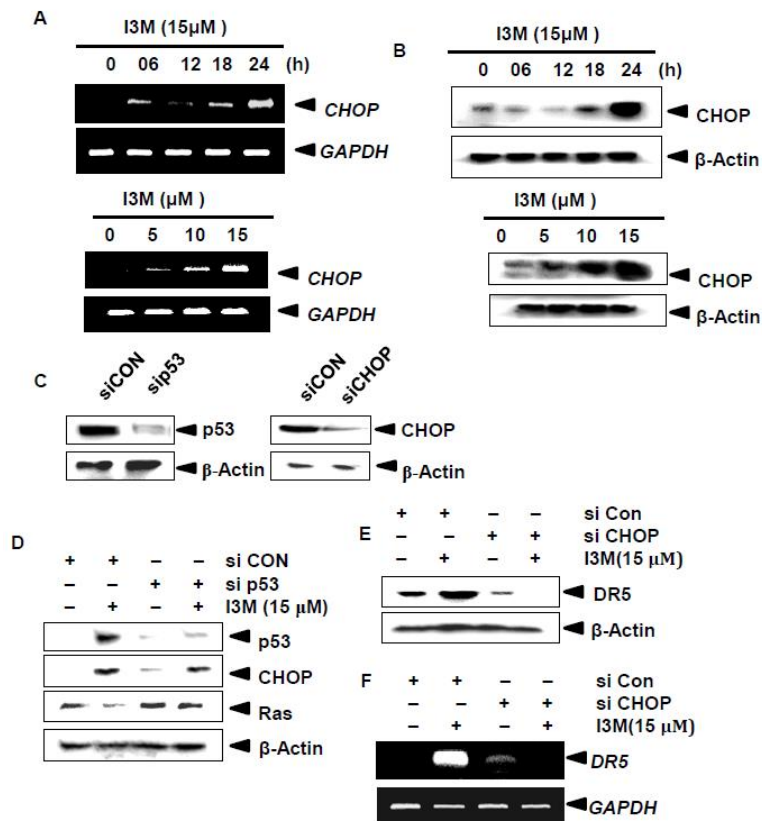
Fig. 37. I3M upregulates CHOP expression in (p53$^{+/+}$) HCT-116 cells. Cells were seeded at 2×10^5 cells/ml and incubated with 15 μM I3M for indicated time (0-24 h) and/or cells were incubated with indicated concentrations of I3M (0-15 μM) for 24 h. (A) Total RNA was isolated and RT-PCR analysis of CHOP was performed. (B) The cytosolic extracts were prepared to determine the level of CHOP by western blot analysis. (C) Cells were transiently transfected with *p53 and CHOP* siRNA for 24 h. The transfection efficiency was assayed by western blot analysis. (D) Cells were transiently transfected with *p53 and (E and F) CHOP* siRNA for 24 h and then treated with or without before treatment with 15 μM I3M for 24 h. The cytosolic protein lysates were prepared at 24 h, subjected to SDS-PAGE, and immunoblotted using specific antibodies against p53, CHOP, Ras and DR5 respectively. (F) Total RNA was isolated and RT-PCR analysis of DR5 was performed. β-Actin and GAPDH were used as an internal control for western blot and RT-PCR analyses respectively.

6.3.5. I3M-induced up-regulation of p53 increases apoptosis to I3M-enhanced oxidative stress.

Cumulative data have revealed that role of p53 in regulating cellular oxidative stress. Given that both ROS and p53 occupies a pivotal position in maintaining apoptosis processes, we were interested to investigate the interactions between p53 and oxidative stress in I3M-treated p53$^{+/+}$ HCT-116 cells. First, we examined whether I3M can induce oxidative stress via ROS production. H$_2$DCFDA and HE-based fluorescence analysis showed that treatment with I3M increased ROS generation by increasing intracellular superoxide anion and hydrogen peroxide levels respectively (Fig. 38A). Then, to understand the roles of p53 in regulating I3M-induced oxidative stress, cells were transfected with p53 siRNA. As shown in Fig. 38B, fluorometric data confirmed that silencing of p53 had more dramatic effect on I3M-induced

146

ROS production. Past studies have suggested that ROS are important for the induction of apoptosis. Therefore, we next investigated whether ROS generation was directly associated with I3M-induced apoptosis. NAC pretreatment markedly blocked I3M-induced ROS production thereby reduced the accumulation of annexin-V positive cells indicating the importance of ROS to enhance the apoptosis by I3M (Fig. 38C). Because of the co-relation between p53 and ROS, we next examined the effect of p53 regulating of apoptosis. As shown in Fig. 5D, western blot analysis indicated that I3M-induced expression of Bid and Bax level were markedly reduced by sip53 transfection proving that p53 play a key role in induction of apoptosis via regulating ROS level in colon cancer cells (Fig. 38D). Nevertheless, transfection of p53 si RNA enhanced the pro-caspase 3 expression level where as its reduced by I3M alone treatment. Furthermore, cell viability assay shown transfection of p53 si RNA comparatively increased I3M-attenuated viability of colon cancer cells (Fig. 38E). In particularly, morphological analysis also shown I3M-induced apoptotic body formation significantly attenuated by treatment of sip53 in p53$^{+/+}$ HCT-116 cells (Fig. 38F). Collectively, these results are consistent with p53 involved induction of oxidative stress in I3M-treated colon cancer cells.
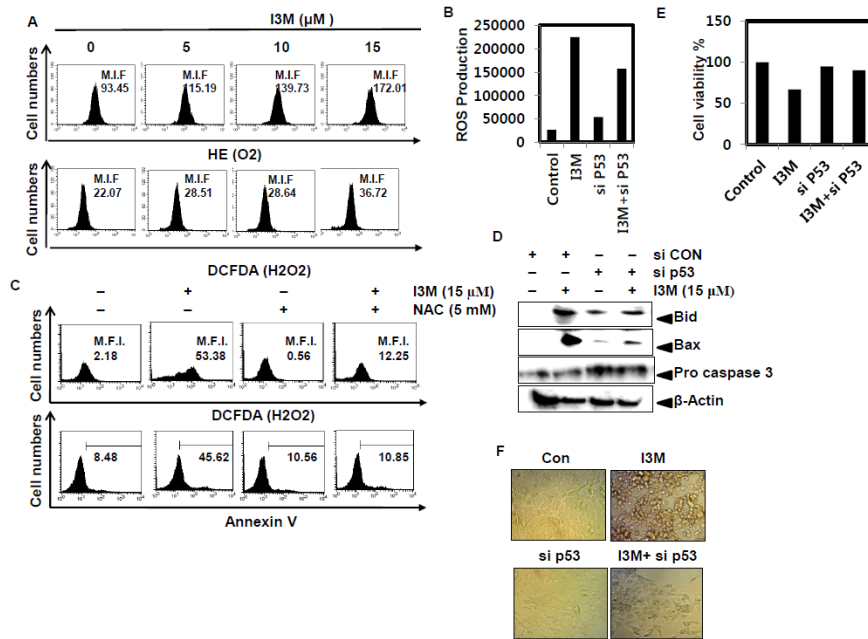
Fig. 38. I3M-mediated upregulation of p53 increases susceptibility to oxidative stress. (A) (p53$^{+/+}$) HCT-116 cells treated with indicated concentrations of I3M (0-15 μM) for 24 h and then stained with HE and DCFDA. Redox status was measured using flow cytometry. (B) Cells were transiently transfected with *p53* siRNA for 24 h and then treated with or without before treatment with 15 μM I3M for 24 h. ROS generation was analyzed by a fluorometer. (C and D) The cells were incubated with 5 mM NAC 1 h before 15 μM I3M treatment for 24 h. ROS generation and apoptotic cells were analyzed by flow cytometry. Cells were transiently transfected with *p53* siRNA for 24 h and then treated with or without before treatment with 15 μM I3M for 24 h. (D) Cells were harvested and the indicated proteins were detected by western blot analysis. β-actin was used as a loading control. (E) Cell viability was determined using an MTT assay. (F) The morphology of cells treated with or without I3M was examined under light microscopy (×400).

148

6.3.6. I3M enhances the expression of TRAIL in p53$^{+/+}$ HCT-116 cells

TRAIL was shown to be able to induce apoptosis in a variety of cancer cells, raising hopes that TRAIL may have therapeutic potential as an anti-cancer agent. Because, our flow cytometry data shown that treatment of I3M for 2 h, followed by treatment with pan caspase inhibitor Z-VAD fmk, remarkably attenuated I3M-induced sub G1 cell population (Fig. 39A). Particularly, MTT assay indicated I3M-increased cell death significantly reduced with the pretreatment of Z-VAD fmk (Fig. 39B). Since limited data are available about TRAIL expression we were widespread interest to investigate the TRAIL expression in p53$^{+/+}$ HCT-116 cells. To confirm the TRAIL expression in p53$^{+/+}$ HCT-116 cells, whole cell lysates were analyzed by flow cytometry. Compared with the untreated control one I3M treatment induced the TRAIL expression in time dependent manner (Fig. 39C). Consequently, dose-dependent treatment of I3M enhanced the TRAIL protein expression as induced mean fluorescence intensity (MFI) as 15.89, 17.87, 19.63, and 22.77 in untreated group, 0, 5, 10, and 15 μM I3M treatment groups, respectively (Fig. 39D). Furthermore, western blot analysis shown dose dependently treatment of I3M induced TRAIL protein expression (Fig. 39E). It is known that TRAIL activates apoptosis through the binding of distinct death receptors DR4 and DR5. We therefore performed a western blot analysis cells with the treatment of DR5 blocking antibody. I3M treatment group up-regulated TRAIL protein expression level, in contrast 10 ng/ml treatment of DR5 blocking antibody attenuated I3M-induced protein expression level of TRAIL (Fig. 39F). These results suggest that I3M enhances the expression of TRAIL thereby induced the apoptosis in p53$^{+/+}$ HCT-116 cells.
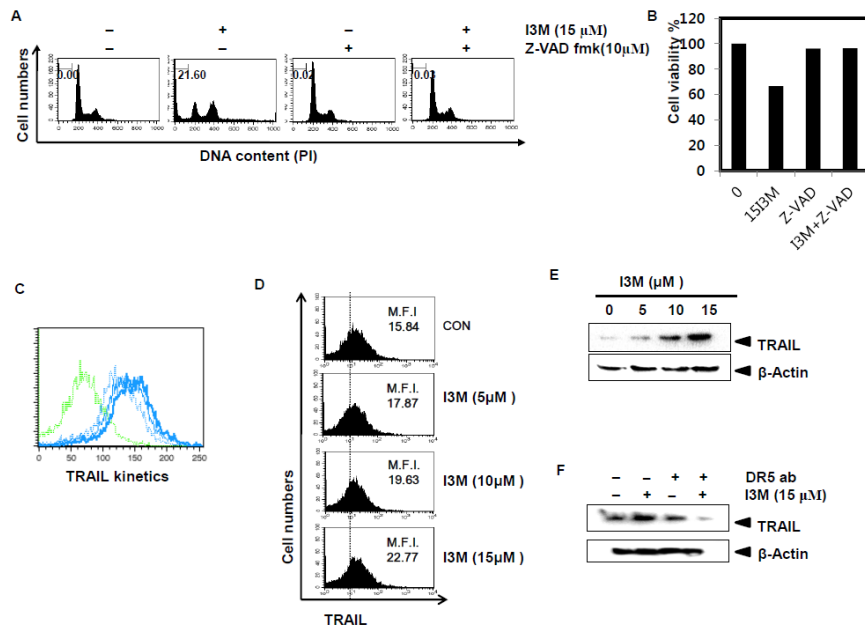
Fig. 39. I3M upregulates TRAIL expression in (p53$^{+/+}$) HCT-116 cells. Cells were seeded at a density of 1×10^5 cells/ml and incubated with the indicated concentration of I3M (15 μM) 2 h before treatment with *Z-VAD*-FMK (25 μM) for 24 h. (A) The percentage of apoptotic cells were analyzed by flow cytometry. Percentages of apoptotic cells are represented in each panel. Data in the figure represent percentages of each apoptotic cell populations in cell cycle distribution. (B) Cell viability was determined using an MTT assay. (C and D) Cells were seeded at 2×10^5 cells/ml and incubated with 15 μM I3M for indicated time (0-24 h) and/or cells were incubated with indicated concentrations of I3M (0-15 μM) for 24 h. Flow cytometry was conducted to analyze the expression level of TRAIL. (E) Cells were seeded at 2×10^5 cells/ml and incubated with indicated concentration of I3M (0-15 μM) for 24 h and/or (F) cells were incubated with 15 μM I3M for 24 h with or without DR5-specific blocking chimera antibody. Equal amount of cell lysates was resolved on SDS–polyacrylamide gels, transferred to nitrocellulose membranes, and probed with antibodies against TRAIL. β-actin was used as a loading control.

150

6.3.7. Treatment of TRAIL synergistically enhanced I3M-induced DR5 expression

We postulated that I3M induced DR5 expression through a CHOP-dependent mechanism. To further evaluate the above fact, cells were subjected to expression of protein analysis through western blot. We found that compared with the untreated control group, combined-treatment of I3M and TRAIL synergistically enhanced DR5 expression in p53$^{+/+}$ HCT-116 cells (Fig. 40A).   In this study, we also examined that I3M did not affect DR4 surface expression at the transcriptional level (data not shown). Many scientists have reported that the DR5 signaling pathway is more prominently involved in TRAIL-induced apoptosis in malignant liver cell lines than DR4 (Zhang et al., 2005). To confirm the functional role of DR5 induced by I3M in the sensitization of TRAIL-induced apoptosis, we examined the effect of a DR5-specific blocking chimera antibody on I3M/TRAIL-induced apoptosis. Concentration dependent manner addition of a DR5 specific blocking antibody significantly blocked I3M/TRAIL-induced reduction of cell growth (Fig. 40B). To further confirmation of above results next cells were treated with siRNA DR5 and transfection efficacy was analyzed by western blot analysis. Compared with the control-transfected (CON siRNA), DR5 transient knockdown group markedly decreased the DR5 protein expression level (Fig. 40C). Similarly, treatment with siRNA DR5 in p53$^{+/+}$ HCT-116 cells decreased the cleavage of PARP induced by I3M/TRAIL (Fig. 40D). Further, combination treatment reduced protein level of pro caspase 8 was reduced by transfection of siRNA DR5. Nevertheless, we have evaluated the effects of a DR4-specific blocking chimeric antibody, which did not significantly block I3M/TRAIL-induced cell death p53$^{+/+}$ HCT-116 cells (data not shown). Therefore, these results support the hypothesis that I3M-induced DR5 upregulation is critical for caspase activation and induction of TRAIL sensitivity in p53$^{+/+}$ HCT-116 cells.
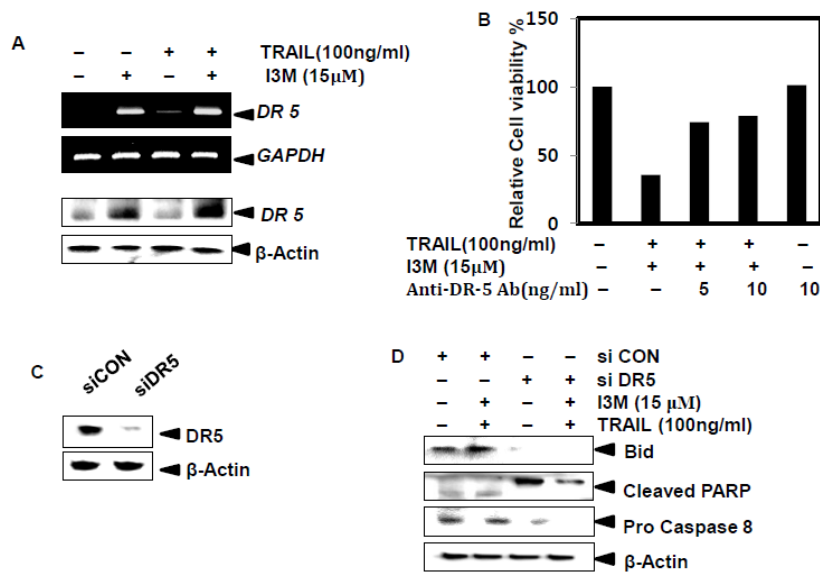
Fig. 40. Treatment of TRAIL synergistically enhanced I3M-induced DR5 expression in (p53$^{+/+}$) HCT-116 cells. (A) Cells were seeded at a density of 1×10^5 cells/ml and incubated with the indicated concentration of I3M (15 μM) 2 h before treatment with TRAIL (100 ng/ml). RT-PCR and western blot analyses of DR5 was performed at 6 h and 24 h, respectively. (B) Cells were pretreated with 15 μM I3M and 100 ng/ml TRAIL for 24 h with or without DR5-specific blocking chimera antibody or DR5 siRNA. Cellular viability was measured by an MTT assay. (C) Cells were transiently transfected with *DR5* siRNA for 24 h. The transfection efficiency was assayed by western blot analysis. (D) Cells were transiently transfected with *DR5* siRNA for 24 h and then cells were pretreated with 15 μM I3M and 100 ng/ml TRAIL for 24 h. Cells were harvested and the indicated proteins were detected by Western blot analysis. β-Actin was used as a loading control.

6.3.8. Treatment of TRAIL more sensitize I3M-mediated apoptosis

152

Previous our data was shown treatment of I3M alone reduced the cell viability as 60% in p53$^{+/+}$ HCT-116 cells. Despite the widespread interest on whether treatment of TRAIL could synergistically enhance the I3M-upregulates apoptosis. Therefore, to facilitate examine this matter we treated p53$^{+/+}$ HCT-116 cells with or without I3M or TRAIL. Interestingly, combination treatment of I3M (15 μM) and TRAIL (100 ng/ml) decreased viability of cells nearly as 30% (Fig. 41A). Moreover, the morphology changes of p53$^{+/+}$ HCT-116 cells were observed in Fig. 41B. Compared to the untreated control group, formation of apoptotic bodies were appeared in the I3M and TRAIL combination treatment group (Fig. 41B). Next, to determine the effect of caspase activation on I3M/TRAIL-induced apoptosis, we compared the effects of I3M/TRAIL on apoptosis induction in the absence and presence of z-VAD-fmk. The accumulation of sub-G$_1$ phase cell populations significantly up-regulated by I3M/TRAIL-combination treatment as nearly as 48.49% whereas I3M alone treatment it's indicated as 16.20% (Fig. 41C, upper panel). Pre-treatment with z-VAD-fmk significantly blocked the accumulation of sub-G1phase cell populations (Fig. 41C, upper panel). Furthermore, we detected that treatment of p53$^{+/+}$ HCT-116 cells with a combination of I3M and TRAIL for 24 h significantly increased the annexin-V positive cell population, but treatment with I3M or TRAIL alone significantly did not (Fig. 41C, lower panel). Although resistance to TRAIL in some cell types occurred, because of the reduced the release of second mitochondria-derived activator of caspases (Smac/Diablo) from the mitochondria to the cytosol (Zhang et al., 2005). Therefore, apoptotic events in the mitochondria were evaluated by measuring the mitochondrial membrane potential using DiOC6. Marked reduction in the mitochondrial membrane potential was observed in cells treated with I3M and TRAIL (Fig. 41D). Additionally, this process was accompanied by the release of cytochrome *c* from the

153

mitochondria into the cytosol (Fig. 41E). Further, combination treatment of I3M and TRAIL reduced the anti-apoptotic protein Bcl-2 expression and increased the cleaved PARP in cytosol compartment (Fig. 41F). Taken together, these results suggest that treatment of TRAIL effectively induced I3M-mediated apoptosis in p53$^{+/+}$ HCT-116 cells.
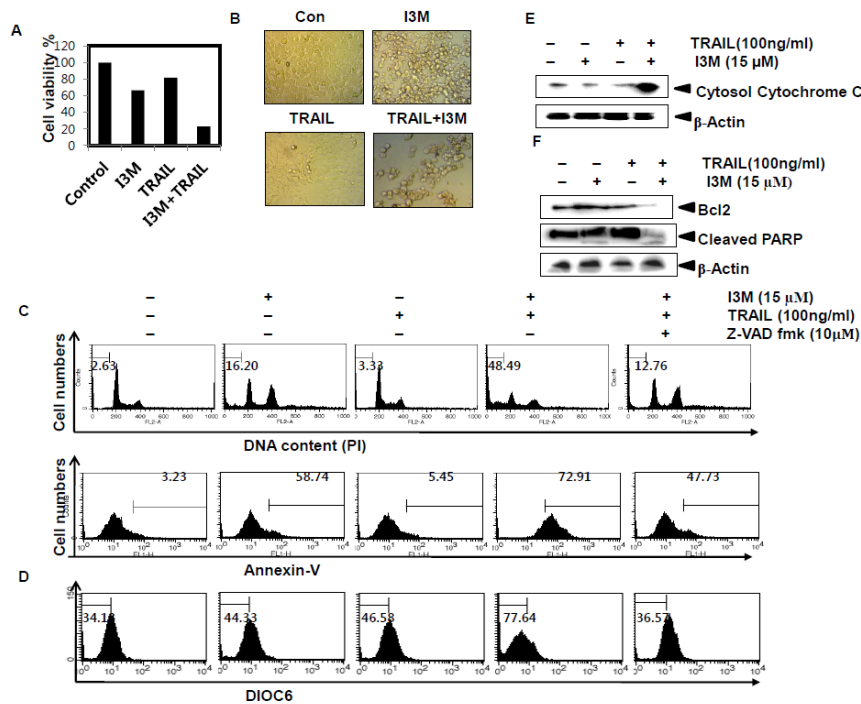
Fig. 41. Treatment of TRAIL more sensitize I3M-mediated apoptosis in (p53$^{+/+}$) HCT-116 cells. in (p53$^{+/+}$) HCT-116 cells were treated with 15 μM I3M and with or without 100 ng/ml TRAIL for 24 h. (A) Cell viability was tested by the MTT assay. (B) The morphology of cells treated with or without I3M was examined under light microscopy (×400). Cells were seeded at a density of 1×10^5 cells/ml and incubated with the indicated concentration of I3M (15 μM) 2 h before treatment with Z-VAD-FMK (25 μM) for 24 h. (C) The percentage of apoptotic cells were analyzed by flow cytometry. Percentages of apoptotic cells are represented in each panel. Data in the figure represent percentages of each apoptotic cell populations in cell cycle distribution. In a parallel experiment, the percentage of apoptosis was analyzed by flow

cytometry after staining with annexin V. Cell populations for annexin V$^+$ are shown in each panel. (E and F) Cells were treated with 15 μM I3M and with or without 100 ng/ml TRAIL for 24 h. Cells were harvested and the indicated proteins were detected by western blot analysis. β-actin was used as a loading control.

6.4. Discussion

I3M has been reported to have a broad spectrum of anti-cancer functions in many human cancer cells (Kim et al., 2007). Previous studies have demonstrated that I3M is a promising anti-cancer agent based on the capability of selectively induce apoptotic cell death in a wide spectrum of human cancer cells with minimal toxicity on normal cells and potentiates to arrest tumor growth in rat model *in vivo* (Kim et al., 2007). However, the molecular mechanisms underlying the apoptotic cell death induced by I3M has not been fully elucidated. In this study we provide convincing evidence demonstrating that I3M-induced apoptosis via TRAIL-sensitization engage the CHOP and DR5. Further, we have shown that expression of DR5 depends on the p53 status in HCT-116 colon carcinoma cells.

Tumor necrosis factor-related apoptosis-inducing ligand or Apo2 ligand (TRAIL/Apo2L) is a member of the tumor necrosis factor (TNF) family of ligands capable of initiating apoptosis through binding of its death receptors (Kim et al., 2012). TRAIL selectively induces apoptosis of a variety of tumor cells and transformed cells, but not normal cells, and therefore has garnered intense interest as a promising agent for cancer therapy (Kim et al., 2012). To date, few studies have examined the distribution pattern of TRAIL in human tissues. Recent study

155

reported that expression of TRAIL in human hepatocytes, bile duct epithelium, colon, germ and leydig cells (Spierings et al., 2004). Another past research was shown that TRAIL is expressed in activated T cells with a CD4$^+$ and a CD8$^+$ phenotype (Mariani and Krammer, 1998). Therefore, we examined whether treatment of I3M induce the expression of TRAIL in p53$^{+/+}$ HCT-116 cells. Interestingly, our data shown I3M treatment significantly induce the TRAIL expression in concentration and time dependent manner. Further, this study has shown that combination treatment of I3M and TRAIL synergistically enhanced apoptosis than in I3M-alone treatment.

Specifically, past studies have demonstrated the functional importance of the oncogenic Ras in modulating TRAIL-induced apoptosis in RAS-transformed cells (Drosopoulos et al., 2005). The oncogenic Ras protein controls the cellular proliferation, differentiation in cancers and other pathological processes (Fernández-Medarde et al., 2011). There are three closely related Ras family members, encoded by distinct genes on different chromosomes the K-Ras, H-Ras and N-Ras, and the vast majority of cancerous mutations are found in K-Ras (Drosopoulos et al., 2005). Besides, aberrant Ras activation up-regulates the expression of TRAIL receptors, thereby induced the TRAIL sensitization. Therefore, to investigate the functional mechanism of Ras to induce TRAIL- mediated apoptosis, next we examined the Ras expression in both p53$^{+/+}$ and p53$^{-/-}$ HCT-116 cells by I3M. Recent studies have established a biochemical link between oncogenic Ras and tumor suppressor p53 signaling. The ability of *Ras* to activate *p53* has been extensively studied in past decades (Lin et al., 2001). On the other hand, several studies have been reported about the oncogenic Ras directly modulates by p53 gene. It has been noted that oncogenic Ras activates by p53 through activation of MAPK and PI3K/Akt signaling pathway (Fang et al., 2001). More importantly Deguin-Chambon *et al* have

156

also reported that c-Ha-Ras gene directly transactivation by p53 either overexpressed or activated in response to a cellular stress (Deguin-Chambon et al., 2000). The endogenous c-Ha-Ras gene expression is positively regulated by wt p53 protein in human transformed cell lines (Deguin-Chambon et al., 2000). Despite, our data was shown opposing effect according to the above facts. Oncogenic Ras expression was upregulated in p53$^{-/-}$ HCT-116 cells while decreased the Ras expression in p53$^{+/+}$ HCT-116 cells treated with I3M in time and dose dependent manner. Eventhough Ras expression was upregulated in p53$^{-/-}$ HCT-116 cells since there was no significant effect of cell viability we determined that apoptosis occurred via TRAIL sensitization independent of oncogenic Ras.

Therefore, next we focused on alternative signal transduction pathways which are mediated by p53. Much has been learned about the TRAIL receptor DR5 expression mediated through p53 as DR5 is downstream target of p53 (Xiaowen and Yi., 2012). OCI-AML3 and U937 leukemia cells treated with triptolide for 48 h enhanced both p53 and DR5 expression level (Carter et al., 2008). Apoptosis augmented by TRAIL-sensitization mediated via expression of DR5 in p53 dependent manner in human hepatocellular carcinoma cells (Wang et al., 2009). Consequently, treatment of I3M induced DR5 expression in p53$^{+/+}$ HCT-116 cells. Aside from the induction of DR5 expression in p53$^{+/+}$ HCT-116 cells by I3M, p53$^{-/-}$ HCT-116 cells was found to did not change the expression of DR5 (data not shown). Therefore, I3M regulate the extrinsic apoptosis pathway through the induction of DR5 via p53. Since p53 can activates the intrinsic pathway of cellular apoptosis by targeting several p53-regulated apoptotic target genes further studies needed to evaluate the efficacy of I3M- mediated apoptosis in colon cancer cells.

It is well known that DR5 expression regulate at the transcriptional level through binding of CHOP to promoter region of the DR5 gene (Liu et al., 2012). CHOP is primarily regulated at the transcriptional level and is one of most induced genes activated by ER stress. As such, ER stress inducers such as thapsigargin and tunicamycin potentiate to enhance DR5 expression via CHOP and sensitize tumor cells to TRAIL-induced cell death, thus CHOP may be a good target for new anticancer agents (Shiraishi et al., 2015 and Yamaguchi 2004). In this study we have shown the induction of CHOP expression by I3M both in m-RNA and protein level. Moreover, further researches are needed to investigate the effect of ER stress on the expression of DR5 in colon cancer cells. Nevertheless, our data was shown that siRNA transfection of p53 remarkably reduced the I3M-induced CHOP expression in p53$^{+/+}$ HCT-116 cells. However, because of insufficient data to elucidate the functional relationship between p53 and CHOP, further studies are essential to investigate the above fact.

Though it is generally recognized that oxidative stress is associated with p53- dependent apoptosis, a clear understanding of the mechanisms of the interactions between oxidative stress and p53 is still exclusive. Therefore, next we have reported interaction among p53 and oxidative stress with I3M treatment. According to our data, treatment of I3M induced intracellular superoxide anion and hydrogen peroxide levels by indicating increased ROS production in p53$^{+/+}$ HCT-116 cells. More interestingly, that I3M induced-ROS production in p53$^{+/+}$ HCT-116 cells did not change in p53$^{-/-}$ HCT-116 cells (data not shown). Therefore, it was specified that interrelationship between p53 and oxidative stress. Hussain *et al* was reported that p53 enhanced the upregulation of redox-controlling genes, such as MnSOD and GPx thereby induced the oxidative stress in doxorubicin treated TK6 cells with WT p53 (Hussain et al., 2004). In addition, another report has illustrated that transactivation of p53 is

acquired to induce ROS production by engaging the mitochondrial branch of the apoptotic machinery (Ott et al., 2007). Specially, p53 can regulate the genes which have an impact on cellular oxidative stress (Ott et al., 2007). Similar to the above results our data also indicated the knockdown of p53 attenuated I3M-induced ROS production in $p53^{+/+}$ HCT-116 cells. Further, siRNA treatment with p53 enhanced I3M-reduced cell viability and pro-caspase 3 protein expression level while decreasing I3M-induced Bid and Bax expression levels. Aside p53 regulate the oxidative stress, it was also found to oxidative stress regulate the p53. It has suggested ROS can regulate p53 through many signaling pathways. Nevertheless, ROS can lead to p53 activation in leukemia cells (Karawajew et al., 2005) and normal lymphocytes and stabilization of p53 during hypoxia condition in MCF-7 human breast cancer cells (Chandel et al., 2000). Thus, NAC treated $p53^{+/+}$ HCT-116 cells were shown remarkably reduced I3M-induced annexin V positive cells by confirming the ROS regulate p53 activation. Hence, above facts indicates how oxidative stress influence the activation of cell death, which might be used for therapeutic intervention in colon cancers.

6.5. Conclusion

Taken together, we showed that I3M potently enhances TRAIL-induced apoptosis by upregulating DR5 expression via activating p53. Furthermore, we have demonstrated that TRAIL-sensitization independent of oncogenic Ras expression. We suggest that relationship between p53 and oxidative stress indirectly regulate I3M/TRAIL induced apoptosis in $p53^{+/+}$ HCT-116 cells.

Chapter 7

I3M suppresses NLRP3 & NLRP1 inflammasomes activation in BV2 microglia cells; Involvement of ROS dependent autophagy

Abstract

Indirubin is the active ingredient of the traditional Chinese medicine *Dang Gui Long Hui Wan*, a mixture of plants, was reported used as an anti-leukemic, anti-inflammatory, and detoxification treatment. Nevertheless, the anti-inflammatory properties of Indirubin-3-monoxime (I3M) occurred via inflammasomes components against LPS- and ATP-stimulated responses have not yet been studied. In this study, we elucidated whether I3M has the ability to attenuate the expression of pro-inflammatory cytokine IL-1β by suppression of inflammasomes activity in BV2 microglial cells. Moreover, we have shown the relation between reactive oxygen species (ROS) and autophagy process in regulation of inflammasomes activation. I3M has the ability to attenuate the expression of IL-1β and caspase-1 in LPS- and ATP-stimulated BV2 microglial cells. Pretreatment of caspase-1 inhibitor significantly decreased the expression levels of LPS- and ATP-induced caspase-1 and IL-1β genes suggests IL-1β expression is associated with activation of caspase-1. Furthermore, we found that I3M suppresses LPS- and ATP-induced NLRP1 and NLRP3 inflammasomes expression in BV2 microglial cells. The protein expression levels of Beclin-1 and Atg7 was attenuated by I3M treatment where as an autophagy inhibitor, 3-Methyladenine (3-MA) suppressed the LPS- and ATP-induced Beclin-1, and Atg7 protein level. Fluorometric analysis showed that approximately 30% of the relative fluorescence intensity of DCFDA was increased in response to LPS and ATP. The LPS- and ATP-enhanced Beclin-1 and Atg7 protein notably decreased with the treatment of NAC and GSH, therefore these results indicate that LPS- and ATP-enhanced autophagy process regulate via ROS production in BV2 microglial cells. Taken together our results demonstrated that the I3M is a potent inhibitor of LPS-and ATP-induced caspase-1 activation and IL-1β secretion by suppression of NLRP1, NLRP3 inflammasomes,

ROS production and autophagy process. Considering above facts, I3M may be useful as an anticancer agent to treat various inflammatory diseases.

Key words; inflammasomes; reactive oxygen species; IL-1β; autophagy

7.1. Introduction

Microglia are the resident macrophages of the Central Nervous System (CNS) which are primary cells that regulate the inflammatory responses. Activated microglia play an important role during initiation and development of inflammatory responses by secreting pro- and anti-inflammatory cytokines such as IL-18 and IL-1β (Kaushik et al., 2012). IL-1β is an endogenous pyrogen, also one form of IL-1, perform many of the functions and bind to the IL-1 receptor (IL-1R) (Duque and Descoteaux., 2014). Together IL-1β and IL-18 belongs to the IL-1 cytokine superfamily promote the various innate immune responses associated with inflammation and autoimmunity. IL-1β produced as an inactive 31 kDa precursor, known as pro-IL-1β, in response to molecular motifs presence on the pathogens called 'pathogen associated molecular patterns' (PAMPs) (Eigenbrod et al., 2016). The Increased production of IL-1β involved in a development of different autoinflammatory syndromes, most notably the monogenic conditions referred to as CAPS, due to mutations in the inflammasome receptor NLRP3 which triggers processing of IL-1β. Nonetheless, IL-1β has been associated with severe inflammatory disorders, such as chronic infantile neurologic, Muckle-Wells syndrome, cutaneous and articular syndrome/neonatal onset multisystem inflammatory disease, and gout (Church et al., 2008).

The IL-1β and IL-18 are synthesized as inactive precursors (pro-IL1 β and pro-IL-18) that

accumulate within monocytes and macrophages. The secretion of IL-1β and IL-18 must be stimulated by pathogen associated molecular patterns (PAMPs) or damage associated molecular patterns (DAMPs) (Castejon and Brough., 2011). PAMP referred to as small molecular motifs conserved within a class of microbes that are recognized by cells of the innate immune system. Since PAMPs produced the first signal that induces the generation of pro-IL1 β and pro-IL-18, a second signal in the form of DAMPs normally necessitate to enhances inflammasome complex formation, caspase-1 activation, secretion of cytokines and their precursor cleavage (Lamkanfi and Dixit., 2014).

Inflammasomes are a group of intracellular molecular complexes that sense and respond to injury and infections. Recent advances have highly increased the comprehension of the macromolecular activation of inflammasomes, respond to large range of PAMPs, derived from invading pathogens and DAMPs, such as resulting due to endogenous stress (Lamkanfi and Dixit., 2014). Inflammasomes activation promotes the caspase-1 activation and the proteolytic cleavage of pro-IL-1β and pro-IL-18 converts their active forms (Sollberger et al., 2014). The inflammasome complexes are derived by three components; a nucleotide binding and oligomerization domain (NOD)-like receptor (NLR), ASC (apoptosis-associated speck-like protein containing a caspase recruitment domain), and pro-caspase-1. Upon activation, NLR protein binds the inflammasome adaptor protein ASC, which interacts with caspase-1 promotes to its activation. The active caspase-1 is a cysteine-dependent protease that induces the maturation of proinflammatory cytokines IL1 β and IL-18 (Latz et al., 2013). Several distinct inflammasomes have currently been described, among them NLRP1, (CARD7, NAC, CLR17.1 or DEFCAP) and NLRP3 (PYCARD, CASP1, CASP4, or CASP5) well characterized canonical inflammasomes recognized thus far (Davis et al., 2011). Several

stimuli activate the NLRP3 including extracellular ATP, reactive oxygen species, cholesterol, crystals of monosodium urate, K^+ efflux, environmental particles and nanoparticles, etc. Inflammasome activation is essential for host defense to pathogens but recent research have also investigated a role for the inflammasomes in the pathogenesis of several inflammatory diseases such as rheumatoid arthritis, multiple sclerosis, Alzheimer's disease, Parkinson's disease, inflammatory bowel disease, and atherosclerosis (Guo et al., 2016). This inappropriate inflammasome activity has been incriminated in the pathogenesis of many inflammatory diseases, therapeutics should be carried out targeting inflammasomes is one of the best approach.

Autophagy is an important "self-eating" process by which cytoplasmic compartments such as organelles and protein aggregates are broken down and recycled via the lysosomal apparatus and required for maintaining intracellular homeostasis (Kaur and Debnath., 2015). Autophagy occurs constitutively under normal physiological conditions but may be up-regulated by various factors, including nutrient stress, hormonal regulation and environmental stressors such as heat stress, hypoxia, ER stress and accumulation of reactive oxygen species (ROS) (Hale et al., 2013). Nevertheless, autophagy emerging as a process of significant importance in starvation adaptation, cell death and development, anti-aging, tumor growth retardation, as well as regulation of innate immunity and inflammation (Zhang et al., 2014).

Indirubin is the active ingredient in the ancient herbal remedy, *Danggui Longhui Wan*, which comprises 11 plant ingredients was reported used as an anti-leukemic, anti-inflammatory, and detoxification treatment. Indirubin originates from the root of herbal plant *Isatis indigotica*, *Strobilanthes cusia*, and *Polygonum tinctorium*, has been used to treat inflammatory-based diseases. Several indirubin analogues, such as N-methyl isoindigo,

164

5-chloro-indirubin and indirubin-3'-monoxime (I3M), have been synthesized by various molecular substitution of the parental indirubin with improved selectivity, solubility, and bioavailability (Damiens et al., 2001 and Blažević et al., 2015). Nevertheless, several studies have been shown the anti-inflammatory activity or immunomodulatory effects of different derivatives of indirubin (Kwok et al., 2016 and Kim et al., 2012). However, the effect of inflammasomes activation by I3M was not characterized so far. Therefore, main objective of the current study was to determine whether I3M can modulate inflammasome activation in microglial cells. We evaluated that I3M attenuates IL-1β secretion and activation of caspase-1 in BV2 microglial cells. The suppression of IL-1β and caspase-1 activation is associated with down regulation of NLRP1 and NLRP3 inflammasomes. Moreover, LPS- and ATP-induced autophagy are suppressed by I3M and our data indicates this autophagy process dependent on ROS production.

7.2. Materials and method

7.2.1. Reagents and antibodies

Antibodies against Atg-7 and SQSTM1/p62 and Beclin-1 were obtained from Thermo Scientific (Thermo Fisher Scientific). Antibodies against NLRP1, NLRP3, Caspase 1, IL-1β and P2X7 were obtained from Santa Cruz Biotechnology (Santa Cruz, CA). ATP, LPS and 3-(4,5-dimethylthiazol-2-yl)-2,5-diphenyl-tetrazolium bromide (MTT) were obtained from Sigma Chemical Co. (St. Louise, MO). The antibody against β-actin was purchased from Cell Signaling (Beverly, MA). Peroxidase-labeled goat anti-rabbit immunoglobulin was obtained from Thermo Scientific. Dulbecco's modified Eagle's medium (DMEM) and fetal bovine

serum (FBS) were purchased from WelGENE Inc. (Daegu, Republic of Korea). Glutathione (GSH) and *N*-acetyl-L-cysteine (NAC) were purchased from Sigma. Other chemicals were purchased as Sigma grades.

7.2.2. Cell culture and cytotoxicity

BV2 microglial cells were cultured in DMEM medium in supplemented with 5% FBS and 1% Penicillin-Streptomycin (WelGENE). Cells were maintained at 37℃ in 5% CO2 level. The cells were tested periodically and resulted negative for mycoplasma contamination using the MycoAlert Mycoplasma Detection Kit (Lonza, Rockland, ME). Viability of cells were assessed using a commercial MTT-based assay. This assay detects viable cells based on the generation of the purple formazan in viable cells. BV2 cells were incubated with the indicated concentrations (0-5 uM) of I3M, followed by treatment with LPS (400 ng/ml) for 1 h and ATP (1.0mM) for 1 h. After 24 h, MTT (5 mg/ml) were added to each well, and the plates were incubated at 37°C for 45 min. The precipitate of each wells were dissolved with 700 μl DMSO. Absorbance was monitoring the signal at 540 nm using a microplate reader (Thermo Electron Corporation, Marietta, OH, USA).

7.2.3. Measurement of the IL-1β production

BV2 microglial cells were seeded at 1×10^5 cells/ml in 24 well plates. The cells were pre-incubated with I3M at the indicated concentration for 1h followed by treatment with LPS (400 ng/ml) for 1 h and ATP (1.0 mM) for 1 h. Secreted IL-1β was measured in cell culture supernatants using commercially-available ELIASA kits following the instructions provided by the manufacturers.

166

7.2.4. Western blot analysis

Cellular proteins were isolated from the cells using PRO-PREP protein extraction solution (iNtRON Biotechnologu, Sungnam Republic of Korea). After treatment with various concentrations of I3M, prior treatment with LPS and ATP, cells were collected, washed once with 1X PBS and gently lysed for 1 h in ice-cold PRO-PREP solution. Lysates were centrifuged 15,000 rpm at 4°C for 20 min to obtain the supernatants. Protein concentrations of the supernatants were measured using the Bio-Rad protein assay kit (Bio-Rad, Hercules, CA). The protein samples were separated on SDS-polyacrylamides gels and transferred to nitrocellulose membranes (GE Healthcare Bio-Sciences coporation, NJ, USA). The detection of specific proteins was carried out with an ECL western blotting kit (Amersham) according to the recommended procedure.

7.2.5. Isolation of total RNA and RT-PCR

Total RNA was extracted from BV2 cells using the Easy-Blue reagent (iNtRON Biotechnology, Sungnam, Republic of Korea). One microgram of RNA was reverse-transcribed using moloney murine leukemia virus reverse transcriptase (Bioneer, Daejeon, Republic of Korea). Following the manufacturer′s protocol (One-Step RT-PCR Premix; Daejeon, Republic of Korea), RT-PCR was conducted. The *NLRP3* sense primer 5′-ATT ACC CGC CCG AGA AAG G-3′ and the anti-sense primer 5′-TCG CAG CAA AGA TCC ACA CAG-3′ were used to amplify mouse *NLRP3* mRNA. The *P2X7R* sense primer 5′-GAC AAA CAA AGT CAC CCG GAT-3′ and the anti-sense primer 5′-GCG TCA CCA AAG CAA AGC TAA T-3′, Caspase 1 sense primer 5′-CTG ACT GGG ACC CTC AAG-3′ and the anti-sense primer 5′-CCT CTT

167

CAG AGT CTC TTA CTG-3′, IL1β sense primer 5′-GCC CAT CCT CTG TGA CTC AT-3′ and the anti-sense primer 5′-AGG CCA CAG GTA TTT TGT CG-3′ were used to amplify mouse P2X7R, caspase-1, and IL-1β mRNA, respectively. For *glyceraldehyde-3-phosphate dehydrogenase* (*GAPDH*), the sense primer 5′-CCA CCC ATG GCA AAT TCC ATG GCA-3′ and the anti-sense primer 5′-TCT AGA CGG CAG GTC AGG TCC ACC-3′ were used. The following PCR conditions were applied: *GAPDH*, 28 cycles of denaturation at 94°C for 30 s, annealing at 58°C for 30 s and extended at 72°C for 30 s; *NLRP3*, 31 cycles of denaturation at 94°C for 30 s, annealing at 57°C for 30 s and extended at 72°C for 30 s; *Caspase 1*, 33 cycles of denaturation at 94°C for 30 s, annealing at 57°C for 30 s and extended at 72°C for 30 s; *IL1β*, 32 cycles of denaturation at 94°C for 30 s, annealing at 57°C for 30 s and extended at 72°C for 30 s. *GAPDH* was used as an internal control.

7.2.6. *Measurement of ROS*

BV2 microglial cells were seeded on 24-well plate at a density of 1×10^5 cells/ml and preincubated with fluorescence dye 6-carboxy-2′,7′-dichlorofluorescein diacetate (H$_2$DCFDA, Molecular Probes, Eugene, OR) for 1 h and then treated the indicated concentrations of I3M, NAC and GSH, 1 h before stimulation with ATP (1.0 mM) and LPS (400 ng/ml) for 24 h. Using triton, cells were lysed and the sample was centrifuged and supernatant was analyzed for ROS production using GLOMAX luminometer (Promega).

7.2.7. *Flow cytometric analysis*

Flow cytometer was used to analyze the Atg-7, Beclin-1expression level. Cells grown overnight were treated with I3M for 24 h in complete media. Cells were trypsinized, washed

once with PBS, fixed with ice-cold 70% ethanol for overnight and immunostained with a rabbit anti-Atg7, Beclin-1antibodies followed by a FITC-conjugated goat anti-rabbit antibody. The Atg7 and Beclin-1 expression levels were analyzed using a fluorescence-activated cell sorting cater-plus flow cytometry.

7.2.8. *Statistical analysis*

All values are expressed as means ± SEM. The data were derived from at least three independent experiments. Multiple group comparison was performed by one-way ANOVA test. The images were visualized with Chemi-Smart 2000 (Vilber Lourmat, Cedex, France). Images were captured using Chemi-Capt (Vilber Lourmat) and transported into Adobe Photoshop (version 8.0). Values of $P < 0.05$ were considered to be statistically significant.

7.3. Results

7.3.1. *Effect of I3M on viability of BV2 microglial cells*

To address the cytotoxic effect of I3M in BV2 microglial cells, we first pre-treated the cells with the various concentrations of I3M for 1 h, then with LPS (400 ng/ml) for 1 h and with ATP (1.0 mM) for 24 h. Viability was determined by the metabolic reduction of a tetrazolium salt to a formazan dye using MTT assay. No cytotoxicity was observed with I3M at a concentration up to 2.5 μM of regardless of the presence of LPS and ATP; however, significant cytotoxicity was observed with 5 μM I3M (Fig. 42A). Therefore, the sub-toxic concentrations (≤ 0.9 μM) were used in subsequent experiments. The cell morphology was observed by light microscopy also showed that no apoptotic cell death was observed for 0.9 μM I3M, compared

to the results for the positive H_2O_2-treated group (Fig. 42B). Collectively, these results indicate low doses of I3M do not influence the viability of BV2 microglial cells, regardless of the presence of LPS and ATP.
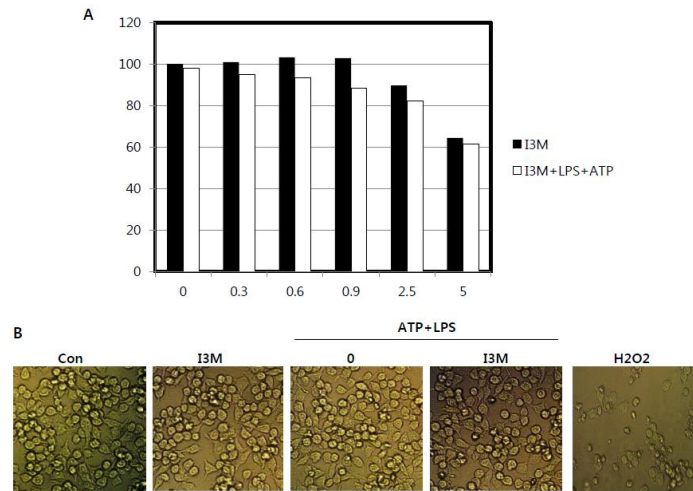
Fig. 42. Effects of I3M on the viability of BV2 microglial cells. (A) Cells were seeded at 1×10^5 cells/ml and incubated with the indicated concentrations of I3M 1 h before treatment with LPS (400 ng/ml) and ATP (1.0 mM) for 24 h. Cell viability was determined by an MTT assay. (B) The morphology of cells was examined under light microscopy ($\times 400$). H_2O_2 treated group serve as a positive control group.

7.3.2. Effects of I3M on inflammasomes activation in BV2 microglial cells

Among the inflammasomes components, NLRP1 and NLRP3 inflammasomes have been broadly studied and respond to a wide range of pathogen-associated molecular patterns (PAMP) or damage--associated molecular patterns (DAMP). In this study we examine the potency of I3M on the regulatory effect of NLRP1 and NLRP3 inflammasomes activation.   RT-PCR analysis showed that pretreatment with I3M significantly decreased LPS- and ATP-induced

170

expression of NLRP1 and NLRP3 inflammasomes in a dose-dependent manner at 6 h (Fig. 43A). Consistent with the RT-PCR data on NLRP1 and NLRP3 inflammasomes expression, western blot analysis also showed that I3M downregulated LPS- and ATP-induced NLRP1 and NLRP3 inflammasomes expression (Fig. 43B). These results confirm that I3M suppresses LPS- and ATP-induced NLRP1 and NLRP3 inflammasomes expression in BV2 microglial cells.
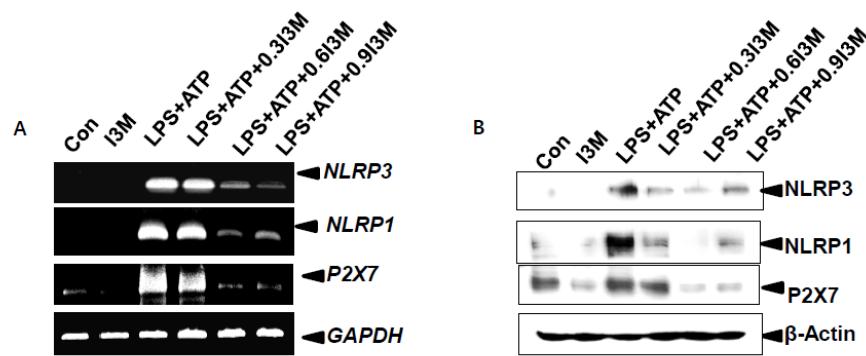
Fig. 43. Effects of I3M on inflammasomes activation in BV2 microglial cells. (A) Cells were seeded as density as 1×10^5 cells/ml then exposure to I3M for 1 h prior to stimulation with LPS and ATP for 6 h. (A) Total RNA was isolated and RT-PCR analysis of NLRP1, NLRP3 and P2X2 was performed. (B) In a parallel experiment, cells were treated with I3M for 1 h prior to stimulation with LPS and ATP, cytosolic protein lysates were prepared at 24 h, subjected to SDS-PAGE, and immunoblotted using specific antibodies against NLRP1, NLRP3 and P2X2. GAPDH and β-Actin were used as internal controls for RT-PCR and western blot analyses respectively.

7.3.3. Effect of I3M on IL-1β activation in BV2 microglial cells

171

Since it is reported that activation of inflammasomes trigger the release bioactive IL-1β from its pro form. Therefore, we next examine the effect of I3M on IL-1β secretion and particular gene expression, BV2 microglial cells were pretreated with various concentrations of I3M for 1 h, followed by stimulation with LPS and ATP with 1 h interval. The level of IL-1β secreted in the culture supernatants of treated maicroglial cells were analyzed by using ELISA. The dose dependent manner pre-treatment of cells with I3M remarkably reduced ATP- and LPS-enhanced the level of IL-1β secretion (Fig. 44A). Both RT-PCR and western blot analysis were conducted to determine the inhibitory effects of I3M on the expression of IL-1β mRNA and protein level. RT-PCR analysis showed that treatment with LPS plus ATP significantly enhanced the expression of IL-1β mRNA level at 6 h (Fig. 44B). Western blot analysis also showed that IL-1β protein level was correlated at 24 h with the levels of the corresponding IL-1β mRNA level. The expression of IL-1β mRNA and protein was concentration-dependently attenuated by pretreatment with I3M for 1 h (Fig. 44B and 44C). These data suggest that I3M downregulates ATP enhanced LPS-induced IL-1β expression.
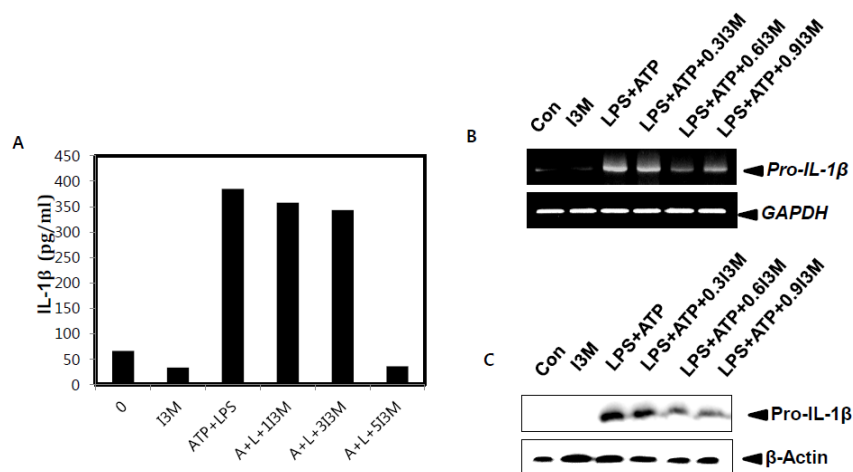

Fig. 44. Effect of I3M on IL-1β activation in BV2 microglial cells. BV2 microglial cells were seeded at 2×10^5 cells/ml and incubated with the indicated concentrations of I3M 1 h before

treatment with 400 ng/ml LPS and another 1 h prior to treatment with ATP (1.0 mM) for 24 h (A and C) or 6 h (B). (A) IL-1β production was determined by ELISA according to the manufacturer's instructions. (B) RT-PCR analysis of IL-1β was performed from total RNA isolated at 6 h. (C) In a parallel experiment, an equal amount of cell lysates at 24 h was resolved on SDS-polyacrylamide gels, transferred to nitrocellulose membranes, and probed with specific antibody against IL-1β. GAPDH and β-Actin were used as internal controls for RT-PCR and western blot analyses respectively.

7.3.4. Effects of I3M on caspase-1 expression

Activated inflammasomes serve as a platform for activation of caspase-1. To examine whether I3M affects caspase-1 expression, BV2 microglial cells pre-treated with different concentrations of I3M for 1 h, prior to LPS and ATP treatments. As shown in Fig. 4A, dose dependent manner exposure to I3M remarkably increased the LPS- and ATP-reduced pro-caspase-1 m-RNA expression level (Fig. 45A). Nevertheless, the expression of caspase-1 further analyzed in protein level by western blot analysis. Similar to the RT-PCR analysis, the expression levels of pro-caspase-1 protein were markedly down regulated in the presence of LPS and ATP. However, the expression levels of pro-caspase-1 were consistently upregulated with increasing concentrations of I3M (Fig. 45B). In order to that, the active form of caspase-1 decreased in I3M treated group compared with the LPS and ATP treated group. Moreover, to detect the ability of I3M to reduce IL-1β expression is associated with decreased expression and activation of caspase-1, using a caspase-1 inhibitor evaluate the expression levels of caspase-1 and IL-1β mRNA and protein levels. As expected, caspase-1 inhibitor significantly decreased the expression levels of LPS- and ATP-induced caspase-1 and IL-1β genes (Fig.

제주대학교 중앙도서관
JEJU NATIONAL UNIVERSITY LIBRARY

45C). Additionally, western blot data indicated that LPS- and ATP-induced caspase-1 and IL-1β protein expression remarkably attenuated by I3M (Fig. 45D). These data indicated that I3M supresses LPS- and ATP-induced caspase-1 expression and expression of IL-1β depends on the caspase-1.
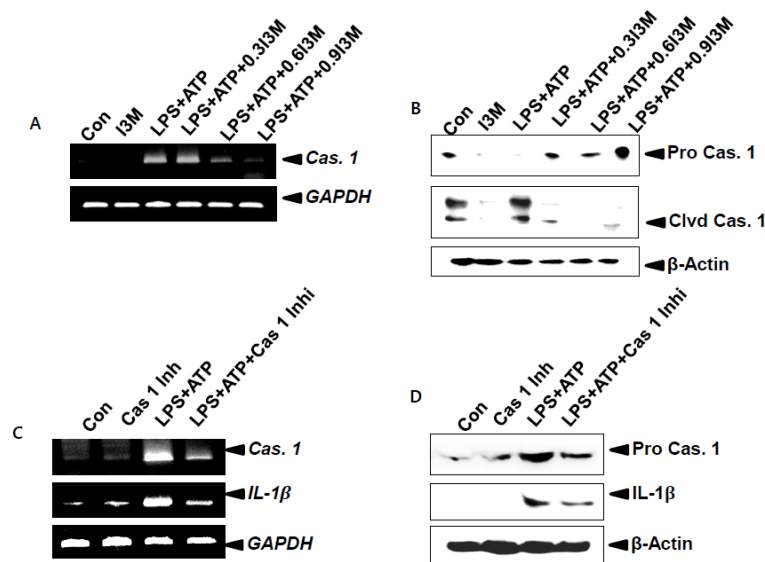
Fig. 45. Effects of I3M on caspase-1 expression. Cells were seeded at 2×10^5 cells/ml and incubated with the indicated concentrations of I3M 1 h before LPS (400 ng/ml) and ATP (1.0 mM) treatment for 24 h or 6 h. Total RNA was isolated at 6 h and RT-PCR analysis of *caspase-1* was performed. (B) In a parallel experiment, expression of caspase-1 was measured by Western blot analysis in cytosol compartment. The cells were incubated with 5 μM of caspase-1 inhibitor 1 h before treatment with 400 ng/ml LPS and 1.0 mM ATP. (C) After 6 h incubation, the total RNA was isolated and RT-PCR analyses of caspase-1 and IL-1β expression were performed. (D) Equal amount of cell lysates were resolved on SDS–polyacrylamide gels, transferred to nitrocellulose membranes, and probed with antibodies against caspase-1 and IL-1β. GAPDH and β-actin were used as internal controls for RT-PCR

174

and western blot analyses, respectively.

7.3.5. Effects of I3M on LPS- and ATP-induced autophagy process

To elucidate the involvement of autophagy in the I3M reduced inflammasome activation, next we perform the western blot analysis to detect the expression levels of proteins which regulate the autophagy process. Treatment of I3M significantly reduced the LPS- and ATP-induced protein expression levels of Beclin-1 and Atg7 (Fig. 46A). To further confirmation of above results then we used an autophagy inhibitor, 3-Methyladenine (3-MA). The combined treatment of LPS and ATP sharply enhanced the Beclin-1, and Atg-7 protein expression levels. However, exposure to both I3M as well as 3MA suppressed the LPS- and ATP-induced Beclin-1, and Atg-7 protein level (Fig. 46B). Flow cytometry analysis further shown LPS- and ATP-enhanced Atg-7 expression significantly decreased by the pretreatment of 3-MA and I3M (Fig. 46C). Moreover, ELISA assay shown that LPS- and ATP-increased IL-1β secreation comparatively down regulated with the treatment of I3M and 3-MA (Fig. 46D). Theses data indicates I3M potent to down regulate LPS- and ATP-induced autophagy process in BV2 microglial cells.
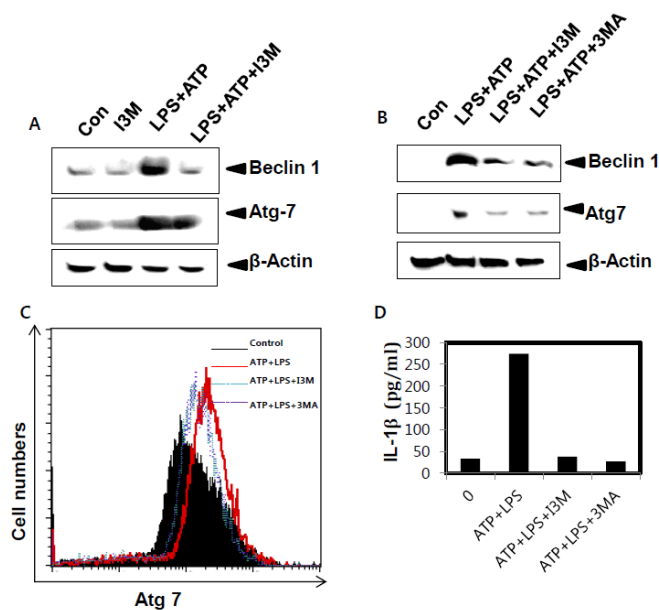
Fig. 46. Effects of I3M on LPS- and ATP-induced autophagy process. BV2 microglial cells were seeded at 2×10^5 cells/ml and incubated with the indicated concentrations of I3M 1 h before LPS (400 ng/ml) and ATP (1.0 mM) treatment for 24 h. (A) Cell lysates were prepared at 24 h and western blot analysis was performed using antibodies specific for Beclin-1 and Atg-7. Cells were treated with indicated concentration of I3M (0.9 μM) and 300 μM of 3-methyladenine (3-MA) in the absence or presence of LPS (400 ng/ml) and ATP (1.0 mM) for 24 h. (B) Equal amount of cell lysates were resolved on SDS–polyacrylamide gels, transferred to nitrocellulose membranes, and probed with antibodies against Beclin-1 and Atg-7. (C) Cells were fixed, permeabilized, and stained with Atg-7 monoclonal antibody. The monoclonal antibody was detected using an antimouse secondary antibody conjugated with Alexa Fluor® 488. Flow cytometry was conducted to analyze the expression level of Atg-7. (D) IL-1β production was determined by ELISA according to the manufacturer's instructions. β-Actin was used as an internal control for western blot analysis.

7.3.6. LPS- and ATP-induced autophagy regulates via ROS

Past researches have shown the link between ROS and autophagy process. Thus, we first detect the ROS production in BV2 microglial cells 24 h after treated with I3M and ROS inhibitors NAC and GSH prior to stimulation with LPS and ATP. Fluorometric analysis showed that approximately 30% of the relative fluorescence intensity of DCFDA was increased in response to LPS and ATP. I3M down regulated LPS- and ATP-induced relative intensity corresponding to treatment with NAC and GSH (Fig. 47A). The flow cytometric data indicated that combine treatment of LPS- and ATP-upregulated Beclin-1 expression level comparatively decreased pretreatment of NAC and GSH (Fig. 47B). In a parallel experiment we conducted western blot analysis to detect the protein expressions of Beclin-1 and Atg-7. The LPS- and ATP-enhanced Beclin-1 and Atg-7 protein notably decreased with the treatment of NAC and GSH (Fig. 47C). Taken together, these results indicate that LPS- and ATP-enhanced autophagy process regulate via ROS production in BV2 microglial cells.
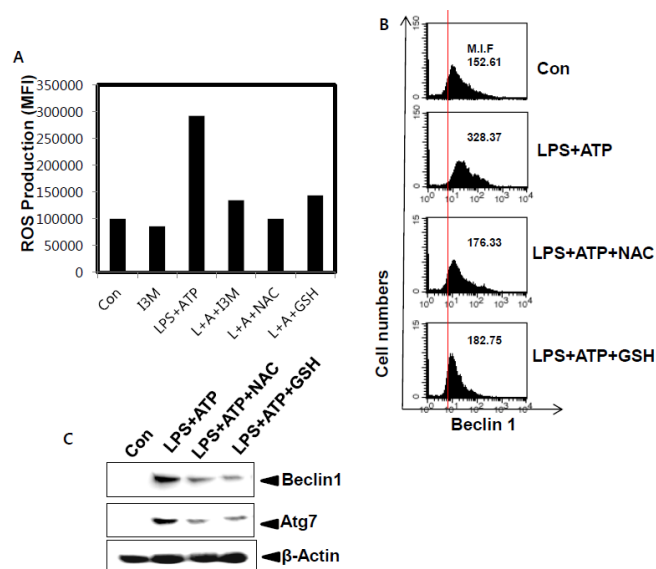
Fig. 47. Effect of ROS on LPS- and ATP-induced autophagy in BV2 microglial cells. BV2

177

microglial cells were pretreated with 0.9 μM I3M, 5 mM NAC, and 2.5 mM GSH 1 h before stimulation with 400 ng/ml LPS and 1.0 mM ATP for 24 h. (A) Relative production of ROS generation were analyzed by fluorometry after staining with DCFDA. (B) Cells were fixed, permeabilized, and stained with Beclin-1 monoclonal antibody. The monoclonal antibody was detected using an antimouse secondary antibody conjugated with Alexa Fluor® 488. Flow cytometry was conducted to analyze the expression level of Beclin-1. An equal amount of cell lysates was isolated at 24 h, resolved on SDS-polyacrylamide gels, transferred to nitrocellulose membranes, and probed with antibodies against Beclin-1 and Atg-7. β-Actin was used as an internal control for western blot analysis.

7.4. Discussion

Inflammation is a protective immune response, tightly regulated by the host, relies on recognition of evolutionarily conserved innate immune system in response to harmful stimuli, such as pathogens, damaged cells or irritants (Delvaeye and Conway., 2009). Insufficient inflammation commonly leads to a greater susceptibly, on the other hand excessive inflammation can cause chronic or systemic inflammatory diseases (LaRock and Nizet., 2015). Inflammation mediated by the inflammasome and recent advances have greatly expanded our understanding of the macromolecular activation of inflammasomes. In the onset of inflammatory disease, inflammasomes play either causative or functional roles, and also inflammatory reactions to infectious agents may be exaggerated (Lukens and Kanneganti., 2014). Activation of inflammasomes leads to number of autoinflammatory and autoimmune diseases, including Alzheimer's disease, Parkinson's disease, and multiple sclerosis like

neurodegenerative diseases and type II diabetes, atherosclerosis like metabolic disorders (Lukens and Kanneganti., 2014). Therefore, it has been thought that inhibition of inflammasomes activation would be beneficial for inhibition of inflammatory diseases.

I3M, an indirubin analogue exhibits different biological properties, such as chemopreventive, antiangiogenic, and neuropreventive activities. A previous study has shown that I3M inhibits the production of nitric oxide (NO) and prostaglandin E2 (PGE$_2$), interleukin (IL)-1β and IL-6 in LPS-induced RAW264.7 macrophage cells (Kim et al., 2012). In the present study, we reported the potential of I3M to down regulation of inflammasomes activity and inhibition of IL-1β and caspase-1 activity in BV2 microglial cells.

Cumulative studies indicated that inflammasomes is participate in IL-1β secretion, hence we examined whether the decreased levels of IL-1β secretion in LPS- and ATP-stimulated cells were result of particular inflammasomes components. However, the activation of inflammasomes involves in protease caspase-1 activation, which is in turn modulate the activation as well as cleavage of IL-1β and mature cytokines secretion (Gurung et al., 2015). According to the present results, I3M down regulated the IL-1β and caspase-1 protein and m-RNA level in LPS- and ATP-induced BV2 microglial cells. We observed that the LPS- and ATP-induced down regulation of production of IL-1β by I3M is due to the suppression of NLRP1 and NLRP3 inflammasomes and caspase-1 activation. Similar to present study, several studies have been indicated the correlation among inflammasomes components, NLRP1 and NLRP3 in activation of IL-1β via caspase-1 (Kaushal et al., 2015 and Huang et al., 2014).

ROS are indispensable second messengers in innate and adaptive immune cells and excessive ROS production occurred in immune cells may be lead to hyperactivation of

179

inflammatory responses, resulting in tissue damage and pathology (Schieber et al., 2014). Nevertheless, ROS play a crucial role as intracellular mediators of inflammasomes activation. ROS can be promoted the activation of inflammasomes through P2X7R activation stimulate by ATP (Carta et al., 2015). Previously, Udumula *et al*. reported the antioxidant effect of I3M in rat cardiac myocytes (Udumula et al., 2016). Our data also demonstrated that pretreatment of I3M significantly inhibits ATP-induced P2X7R expression at protein and m-RNA level. Further, our experiment shown that ATP-stimulated ROS production is down regulates by exposure to I3M. In addition, in response to elevated ROS autophagy pathway can be activated, thus it may influence to activation of inflammasomes and related cytokines production. Past research have revealed the relation in between ROS and autophagy however, understanding of the mechanisms of ROS-enhanced autophagy related to activation of inflammasomes pathway may useful to treat inflammatory deseases. In this regard, Zhang *et al*. indicated NLRP3 inflammasome activation via autophagy cause to lung inflammatory injury in pulmonary macrophages (Zhang et al., 2014). Our study also shown that I3M reduce LPS- and ATP-induced autophagy process via ROS. Pretreatment of ROS inhibitors NAC and GSH suppressed the expression of autophagy related protein expression similar to the I3M treatment group by confirming ROS is involve to regulates the autophagy process in microglial cells.

In summary, this current study demonstrated that the I3M is a potent inhibitor of LPS-and ATP-induced caspase-1 activation and IL-1β secretion in BV2 microglial cells. The suppression of caspase-1 activity and IL-1β secretion by I3M is linked with attenuation of P2X7 expression, NLRP1, NLRP3 inflammasomes, ROS production and autophagy process. Considering above facts, I3M may be useful as an anti-inflammatory agent to treat various inflammatory diseases. However, further experiments are essential to determine the effect of

I3M *in vivo*.

7.5. Conclusion

I3M inhibits LPS-and ATP-induced caspase-1 activation and IL-1β secretion in BV2 microglial cells. The attenuation of caspase-1 activity and IL-1β secretion by I3M is associated with attenuation of P2X7 expression, NLRP1, NLRP3 inflammasomes, ROS production and autophagy process. I3M possesses potential anti-inflammatory activities in neuronal disorders induced by aberrant microglia.

References

Abbas, T., and Dutta, A., 2009. p21 in cancer: intricate networks and multiple activities. Nat. Rev. Cancer 9, 400-14.

Abed, D.A., Goldstein, M., Albanyan, H., Jin, H., Hu, L., 2015. Discovery of direct inhibitors of Keap1–Nrf2 protein–protein interaction as potential therapeutic and preventive agents. Acta Pharm. Sin. B. 5, 285-99.

Aglund, K., Rauvala, M., Puistola, U., Angström, T., Turpeenniemi-Hujanen, T., Zackrisson, B., et al., 2004. Gelatinases A and B (MMP-2 and MMP-9) in endometrial cancer-MMP-9 correlates to the grade and the stage. Gynecol. Oncol. 94, 699-704.

Ahn, M.Y., Kim, T.H., Kwon, S.M., Yoon, H.E., Kim, H.S., Kim, J.I., et al., 2015. 5-Nitro-5'-hydroxy-indirubin-3'-oxime (AGM130), an indirubin-3'-oxime derivative, inhibits tumor growth by inducing apoptosis against non-small cell lung cancer *in vitro* and *in vivo*. Eur. J. Pharm. Sci. 79, 122-31.

Aroui, S., Najlaoui, F., Chtourou, Y., Meunier, A.C., Laajimi, A., Kenani, A., Fetoui, H., 2016. Naringin inhibits the invasion and migration of human glioblastoma cell via downregulation of MMP-2 and MMP-9 expression and inactivation of p38 signaling pathway. Tumour Biol. 37, 3831-9.

Bae, S., Ha, T.S., Yoon, Y., Lee, J., Cha, H.J., Yoo, H., Choe, T.B., Li, S., Shon, I., Kim, J.Y., Kim, C.S., Jin, H.O., Lee, H.C., Park, I.C., Kim, C.S., Jin, Y.W., Ahn, S.K., 2008. Genome-wide screening and identification of novel proteolytic cleavage targets of caspase-8 and -10 *in vitro*. Int. J. Mol. Med. 21, 381-6.

Bal-Price, A., and Brown, G.C., 2000. Nitric-oxide-induced necrosis and apoptosis in PC12 cells mediated by mitochondria. J. Neurochem. 75, 1455-64.

Baraz, R., Cisterne, A., Saunders, P.O., Hewson, J., Thien, M., Weiss, J., Basnett, J., Bradstock, K.F., Bendall, L.J., 2014. mTOR inhibition by everolimus in childhood acute lymphoblastic leukemia induces caspase-independent cell death. PLoS One 9, e102494.

Bedal, K.B., Grässel, S., Oefner, P.J., Reinders, J., Reichert, T.E., Bauer, R., 2014. Collagen XVI induces expression of MMP9 via modulation of AP-1 transcription factors and facilitates invasion of oral squamous cell carcinoma. PLoS One 9, e86777.

Benbernou, N., Esnault, S., Galibert, F., 2013. Activation of SRE and AP1 by olfactory receptors via the MAPK and Rho dependent pathways. Cell Signal. 25, 1486-97.

Berger, A., Quast, S.A., Plötz, M., Hein, M., Kunz, M., Langer, P., Eberle, J., 2011. Sensitization of melanoma cells for death ligand-induced apoptosis by an indirubin derivative—Enhancement of both extrinsic and intrinsic apoptosis pathways. Biochemical Pharmacol. 81, 71-81.

Biswas, C., Shah, N., Muthu, M., La, P., Fernando, A.P., Sengupta, S., Yang, G., Dennery, P.A., 2014. Nuclear Heme Oxygenase-1 (HO-1) Modulates subcellular distribution and activation of Nrf2, impacting metabolic and anti-oxidant defenses. J. Biol. Chem. 289, 26882-94.

Blažević, T., Heiss, E.H., Atanasov, A.G., Breuss, J.M., Dirsch, V.M., Uhrin, P., 2015. Indirubin and indirubin derivatives for counteracting poliferative diseases. Evid. Based Complement. Alternat. Med. 2015, 654098.

Bonavida, B., and Garban, H., 2015. Nitric oxide-mediated sensitization of resistant tumor cells to apoptosis by chemo-immunotherapeutics. Redox Biol. 6, 486-94.

Bonnans, C., Chou, J., Werb, Z., 2014. Remodelling the extracellular matrix in development and disease. Nat. Rev. Mol. Cell Biol. 15, 786-801.

Broecker-Preuss, M., Becher-Boveleth, N., Gall, S., Rehmann, K., Schenke, S., Mann, K., 2015. Induction of atypical cell death in thyroid carcinoma cells by the indirubin derivative 7-bromoindirubin-3'-oxime (7BIO). Cancer Cell Int.15, 97.

Braig, S., Bischoff, F., Abhari, B.A., Meijer, L., Fulda, L., Skaltsounis, L., Vollmar, A.M., 2014. The pleiotropic profile of the indirubin derivative 6BIO overcomes TRAIL resistance in cancer. Biochem. Pharmacol. 91, 157-67.

Broecker-Preuss, M., Becher-Boveleth, N., Gall, S., Rehmann, K., Schenke, S., Mann, K., 2015. Induction of atypical cell death in thyroid carcinoma cells by the indirubin derivative 7-bromoindirubin-3'-oxime (7BIO). Cancer Cell Int.15, 97.

Bröker, L.E., Kruyt, F.A.E., Giaccone, G., 2005. Cell death independent of caspases: A review. Clin. Cancer Res. 11, 3155.

Brown, D.I., and Griendling., K.K., 2015. Regulation of Signal Transduction by Reactive Oxygen Species in the Cardiovascular System. Circ. Res. 116, 531-49.

Carta, S., Penco, F., Lavieri, R., Martini, A., Dinarello, C.A., Rubartelli, A., 2015. Cell stress increases ATP release in NLRP3 inflammasome-mediated autoinflammatory diseases, resulting in cytokine imbalance. Proc. Natl. Acad. Sci. USA 112, 2835-40.

Castejon, G.L., and Brough, D., 2011. Understanding the mechanism of IL-1β secretion. Cytokine Growth Factor Rev. 22, 189-95.

Chaudhari, N., Talwar, P., Parimisetty, A., d'Hellencourt, C.L., Ravanan, P., 2014. A Molecular web: Endoplasmic reticulum stress, inflammation, and oxidative stress. Front. Cell Neurosci. 8, 213.

Church, L.D., Cook, G.P., McDermott, M.F., 2008. Primer: inflammasomes and interleukin 1beta in inflammatory disorders. Nat. Clin. Prac. Rheumatol. 4, 34-42.

Circu, M.L., and Aw, T.Y., 2010. Reactive oxygen species, cellular redox systems, and apoptosis. Free Radic. Biol. Med. 48, 749-62.

Damiens, E., Baratte, B., Marie, D., Eisenbrand, G., Meijer, L., 2001. Anti-mitotic properties of indirubin-3'-monoxime, a CDK/GSK-3 inhibitor: induction of endoreplication following prophase arrest. Oncogene 20, 3786-97.

Davis, B.K., Wen, H., Ting, J.P.Y., 2011. The Inflammasome NLRs in immunity, fnflammation, and associated diseases. Annu. Rev. Immunol. 29, 707-35.

Delvaeye, M., and Conway, E.M., 2009. Coagulation and innate immune responses: can we view them separately? Blood 114, 2367-74.

de Oliveira Barros, E.G., Palumbo, A. Jr., Mello, P.L., de Mattos, R.M., da Silva, J.H., Pontes, B., et al., 2014. The reciprocal interactions between astrocytes and prostate cancer cells represent an early event associated with brain metastasis. Clin. Exp. Metastasis 31, 461-74.

Dilshara, M.G., Lee, K.T., Choi, Y.H., Moon, D.O., Lee, H.J., Yun, S.G., et al., 2014. Potential chemoprevention of LPS-stimulated nitric oxide and prostaglandin E2production by α-L-rhanopyranosyl-(1→6)-β-D-glucopyranosyl-3-indolecarbonate in BV2 microglial cells through suppression of the ROS/PI3K/Akt/NFκB pathway. Neurochem. Int. 67, 39-45.

Dilshara, M.G., Lee, K.T., Jayasooriya, R.G.P.T., Kang, C.H., Park, S.R., et al., 2014. Downregulation of NO and PGE$_2$ in LPS-stimulated BV2 microglial cells by *trans*-isoferulic acid via suppression of PI3K/Akt-dependent NF-κB and activation of Nrf2-mediated HO-1. Int. Immunopharmacol. 18, 203-11.

Dilshara, M.G., Lee, K.T., Lee, C.M., Choi, Y.H., Lee, H.J., Choi, I.W., Kim, G.Y., 2015. New compound, 5-*O*-isoferuloyl-2-deoxy-D-ribono-γ-lacton from *Clematis mandshurica*: Anti-inflammatory effects in lipopolysaccharide-stimulated BV2 microglial cells. Int. Immunopharmacol. 24, 14-23.

Ding, X., Pan, H., Li, J., Zhong, Q., Chen, X., Dry, S.M., Wang, C.Y., 2013. Epigenetic Activation of AP-1 promotes squamous cell carcinoma metastasis. Sci. Signal. 6, ra28.1–13.

Duque, G.A., and Descoteaux, A., 2014. Macrophage cytokines: involvement in immunity and infectious diseases. Front. Immunol. 5, 491.

Eigenbrod, T., Bode, K.A., Dalpke, A.H., 2016. Early inhibition of IL-1β expression by IFN-γ is mediated by impaired binding of NF-κB to the IL-1β promoter but is independent of nitric oxide. J. Immunol. 190, 6533-41.

Elmore, S., 2007. Apoptosis: A review of programmed cell death. Toxicol. Pathol. 35, 495-516.

Espinosa-Diez, C., Miguel, V., Mennerich, D., Kietzmann, T., Sánchez-Pérez, P., Cadenas, S.,

Lamas, S., 2015. Antioxidant responses and cellular adjustments to oxidative stress. Redox Biol. 6, 183-97.

Evellin, S., Galvagni, F., Zippo, A., Neri, F., Orlandini, M., Incarnato, D., Dettori, D, Neubauer, S., et al., 2013. FOSL1 controls the assembly of endothelial cells into capillary tubes by direct repression of αv and β3 integrin transcription. Mol. Cell Biol. 33, 1198-209.

Ferrando, M., Gueron, G., Elguero, B., Giudice, J., Salles, A., Leskow, F.C., Erijman, E.A.J., 2011. Heme oxygenase 1 (HO-1) challenges the angiogenic switch in prostate cancer. Angiogenesis 14, 467-79.

Ferreiro, E., Baldeiras, I., Ferreira, I.L., Costa, R.O., Rego, A.C., Pereira, C.F., Oliveira, C.R., 2012. Mitochondrial- and endoplasmic reticulum-associated oxidative stress in Alzheimer's disease: From pathogenesis to biomarkers. Int. J. Cell Biol. 2012, 735206.

Fitzgerald, A.L., Osman, A.A., Xie, T.X., Patel, A., Skinner, H., Sandulache, V., Myers, J.N., 2015. Reactive oxygen species and $p21^{Waf1/Cip1}$ are both essential for p53-mediated senescence of head and neck cancer cells. Cell Death Dis. 6, e1678.

Fulda, S., 2010. Evasion of apoptosis as a cellular stress response in cancer. Int. J. Cell Biol. 2010, ID 370835.

Gandaglia, G., Abdollah, F., Schiffmann, J., Trudeau, V., Shariat, S.F., Kim, S.P., et al., 2014. Distribution of metastatic sites in patients with prostate cancer: a population-based analysis. The Prostate 74, 210-6.

Gandin, V., Pellei, M., Tisato, F., Porchia, M., Santini, C., Marzano, C., 2012. A novel copper

complex induces paraptosis in colon cancer cells via the activation of ER stress signaling. J. Cell Mol. Med. 16, 142-51.

García-Becerra, R., Santos, N., Díaz, L., Camacho, J., 2013. Mechanism of resistance to endocrine therapy in breast cancer: Focus on signaling pathways, miRNAs and genetically based resistance. Int. J. Mol. Sci. 14, 108-45.

González, R., José López-Grueso, M., Muntané, J., Bárcena, J.A., Padilla, C.A., 2015. Redox regulation of metabolic and signaling pathways by thioredoxin and glutaredoxin in NOS-3 overexpressing hepatoblastoma cells. Redox. Biol. 6, 122-34.

Görlach, A., Bettram, K.M., Hudecova, O., Krizanova, O., 2015. Calcium and ROS: A mutual interplay. 6, 260-71.

Gotoh and Mori., 2006. Nitric oxide and endoplasmic reticulum stress. Arterioscler Thromb. Vasc. Biol. 26, 1439-46.

Guicciardi, M.E., Malhi, H., Mott, J.L., Gores, G.J., 2013. Apoptosis and necrosis in the liver. Compr. Physiol. 3, 977-1010.

Guo, H., Callaway, J.B., Ting, J.P.Y., 2016. Inflammasomes: Mechanism of Action, Role in Disease, and Therapeutics. Nat. Med. 21, 677-87.

Gurung, P., Li, B., Malireddi, R.K.S., Lamkanfi, M., Geiger, T.L., Kanneganti, T.D., 2015. Chronic TLR stimulation controls NLRP3 inflammasome activation through IL-10 mediated regulation of NLRP3 expression and caspase-8 activation. Sci. Rep. 5, 14488.

Hale, A.N., Ledbetter, D.J., Gawriluk, T.R., Rucker, E.B., 2013. Autophagy; regulation and role

in development. Autophagy 9, 951-72.

Haupt, S., Berger, M., Goldberg, Z., Haupt, Y., 2003. Apoptosis-the p53 network. J. Cell Sci. 116, 4077-85.

Herszényi, L., Barabás, L., Hritz, I., István, G., Tulassay, Z., 2014. Impact of proteolytic enzymes in colorectal cancer development and progression. World J. Gastroenterol. 20, 13246-57.

He, H., Feng, Y.S., Zang, L.H., Liu, W.W., Ding, L.Q., Chen, L.X., Kang, N., et al., 2014. Nitric oxide induces apoptosis and autophagy; autophagy down-regulates NO synthesis in physalin A-treated A375-S2 human melanoma cells. Food Chem. Toxicol. 71, 128-35.

Horie, R., Watanabe, M., Okamura, T., Taira, M., Shoda, M., Motoji, T., et al., 2006. DHMEQ, a new NF-κB inhibitor, induces apoptosis and enhances fludarabine effects on chronic lymphocytic leukemia cells. Leukemia 20, 800-6.

Hsieh, H.J., Liu, C.A., Huang, B., Tseng, A.H., Wang, D.L., 2014. Shear-induced endothelial mechanotransduction: the interplay between reactive oxygen species (ROS) and nitric oxide (NO) and the pathophysiological implications. J. Biomed. Sci. 21, 3.

Huang, S., Hill, R.D., Wally, O.S., Dionisio, G., Ayele, B.T., Jami, S.K., Stasolla, C., 2014. Hemoglobin control of cell survival/death decision regulates *in vitro* plant embroyogenesis. Plant Physiol. 65, 810-25.

Huang, T.T., Wu, S.P., Chong, K.Y., Ojcius, D.M., Ko, Y. F., Wu, Y.H., et al., 2014. The medicinal fungus *Antrodia cinnamomea* suppresses inflammation by inhibiting the NLRP3 inflammasome. J. Ethnopharmacol. 155, 154-64.

189

Huang, Y., Yu, J., Wan, F., Zhang, W., Yang, H., Wang, L., Qi, H., et al., 2014. Panaxatriol saponins attenuated oxygen-glucose deprivation injury in PC12 cells via activation of PI3K/Akt andNrf2 signaling pathway. Oxid. Med. Cell Longev. 2014, Article ID 978034, 11 pages.

Indran, I.R., Tufo, G., Pervaiz, S., Brenner, C., 2011. Recent advances in apoptosis, mitochondria and drug resistance in cancer cells. Biochim. Biophys. Acta 1807, 735-45.

Jambrina, E., Alonso, R., Alcalde, M., Rodŕiguez, M.C., Serrano, A., Marťinez-A, C., Sancho, J.C., Izquierdo, M., 2003. Calcium influx through receptor operated channel induces mitochondria triggered paraptotic cell death. J. Biol. Chem. 278, 14134-45.

Jaramillo, M.C., and Zhang, D.D., 2013. The emerging role of the Nrf2–Keap1 signaling pathway in cancer. Genes Dev. 27, 2179-91.

Jayasooriya, R.G.P.T., Dilshara, M.G., Choi, Y.H., Moon, S.K., Kim, W.J., Kim, G.Y., 2014. Tianeptine sodium salt suppresses TNF-α-induced expression of matrix metalloproteinase-9 in human carcinoma cells via suppression of the PI3K/Akt-mediated NF-κB pathway. Environ. Toxicol. Pharmacol. 38, 502-9.

Jia, D., Wang, S., Zhang, B., Fang, F., 2015. Paraptosis triggers mitochondrial pathway-mediated apoptosis in Alzheimer's disease. Exp. Ther. Med. 10, 804-8.

Jung, K.A., Choi, B.H., Nam, C.W., Song, M., Kim, S.T., Lee, J.Y., Kwak, M.K., 2013. Identification of aldo-keto reductases as NRF2-target marker genes in human cells. Toxicol. Lett. 218, 39-49.

Kaiser, H.E., and Nasir, A., 2008. Selected Aspects of Cancer Progression: Metastasis,

Apoptosis and Immune Response. Springer Science and Business Media 106.

Kameswaran, T.R. and Ramanibai, R., 2009. Indirubin-3-monooxime induced cell cycle arrest and apoptosis in Hep-2 human laryngeal carcinoma cells. Biomed. Pharmacother. 63, 146-54.

Kapral, M., Wawszczyk, J., Sośnicki, S., Weglarz, L., 2015. Down regulation of inducible nitric oxide synthase expression by inositol hexaphosphate in human colon cancer cells. Acta Pol. Pharm. 72, 705-11.

Kaur, J., and Debnath, J., 2015. Autophagy at the crossroads of catabolism and anabolism. Nat. Rev. Mol. Cell Biol. 16, 461-72.

Kaushal, V, Dye, R., Pakavathkumar, P., Foveau, B., Flores, J., Hyman, B., et al., 2015. Neuronal NLRP1 inflammasome activation of Caspase-1 coordinately regulates inflammatory interleukin-1-beta production and axonal degeneration-associated Caspase-6 activation. Cell Death Differ. 22, 1676-86.

Kaushik, D.K., Gupta, M., Kumawat, K.L., Basu, A., 2012. NLRP3 inflammasome: key mediator of neuroinflammation in murine Japanese encephalitis. PLoS One 7, e32270.

Keller, S.A., Schattner, E.J., Cesarman, E., 2000. Inhibition of NF-κB induces apoptosis apoptosis of KSHV-infected primary effusion lymphoma cells. Blood 96, 2537-42.

Kim, M.H., Choi, Y.Y., Yang, G., Cho, I.H., Nam, D., Yang, W.M., 2013. Indirubin, a purple 3,2-bisindole, inhibited allergic contact dermatitis via regulating T helper (Th)-mediated immune system in DNCB-induced model. J. Ethnopharmacol. 145, 214-9.

Kim, S.A., Kim, Y.C., Kim, S.W., Lee, S.H., Min, J.J., Ahn, S.G. Yoon, J.H., 2007. Antitumor activity of novel indirubin derivatives in rat tumor model. Clin. Cancer Res. 13, 253–9.

Kim, W.S., Lee, M.J., Kim, D.H., Lee, J.E., Kim, J.I., Kim, Y.C., et al., 2013. 5'-OH-5-nitro-Indirubin oxime (AGM130), an indirubin derivative, induces apoptosis of imatinib-resistant chronic myeloid leukemia cells. Leuk. Res. 37, 427-33.

Kim, J.K., and Park, G.M., 2012. Indirubin-3-monoxime exhibits anti-inflammatory properties by down-regulating NF-κB and JNK signaling pathways in lipopolysaccharide-treated RAW264.7 cells. Inflamm. Res. 61, 319-25.

Kim, J.K., Shin, E.K., Kang, Y.H., Park, J.H., 2011. Indirubin-3'-monoxime, a derivative of a chinese antileukemia medicine, inhibits angiogenesis. J. Cell Biochem. 112, 1384-91.

Kirichok, Y., Krapivinsky, G., Clapham, D.E., 2004. The mitochondrial channel uniporter is a highly selective ion channel. Nature 427, 360-4.

Knockaert, M., Blonder, M., Bach, S., Leost, M., Elbi, C., Hager, G.L., et al., 2004. Independent action on cyclin-dependent kinases and aryl hydrocarbon receptor mediate the antiproliferative effects of indirubins. Oncogene 23, 4400-12.

Kolluru, G.K., Shen, X., Kevil, C.G., 2013. A tale of two gases: NO and H_2S foes or friends for life? Redox Biol. 1, 313-8.

Koul, H.K., Pal, M., Koul, S., 2013. Role of p38 MAP kinase signal transduction in solid tumors. Genes Cancer 4, 342-59.

Kovac, S., Angelova, P.R., Holmström, K.M., Zhang, Y., Kostova, A.T.D., Abramov, A.Y., 2015. Nrf2 regulates ROS production by mitochondria and NADPH oxidase. Biochim Biophys. Acta 1850, 794-801.

Krämer, S., Crauwels, P., Bohn, R., Radzimski, C., Szaszák, M., Klinger, M., Rupp, J., et al., 2015. AP-1 transcription factor serves as a molecular switch between *Chlamydia pneumoniae* replication and persistence. Infect. Immun. 83, 2651-60.

Kritsanida, M., Magiatis, P., Skalsounis, A.L., Peng, Y., Li, P., Wennogle, L.P., 2009. Synthesis and antiproliferative activity of 7-Azaindirubin-3′-oxime, a 7-Aza isotere of the natural indirubin pharmacophore. J. Nat. Prod. 72, 2199-202.

Kwok, H.H., Poon, P.Y., Fok, S.P., Yue, P.Y.K., Mak, N.K., Chan, M.C.W., Peiris, J.S.M., Wong, R.N.S., 2016. Anti-inflammatory effects of indirubin derivatives on influenza A virus-infected human pulmonary microvascular endothelial cells. Sci. Rep. 6, 18941.

Lamkanfi, M., Dixit, V.M., 2014. Mechanisms and functions of inflammasomes. Cell 157, 1013-22.

LaRock, C.N., and Nizet, V., 2015. Inflammasome/IL-1β Responses to Streptococcal Pathogens. Front Immunol. 6, 518.

Latz, E., Xiao, T.S., Stutz, A., 2013. Activation and regulation of the inflammasomes. Nat. Rev. Immunol. 13, 10.

Lee, J.J., Han, J.H., Jung, S.H., Lee, S.G., Kim, I.S., Cuong, N.M., et al., 2014. Antiplatelet action of indirubin-3'-monooxime through suppression of glycoprotein VI-mediated signal transduction: A possible role for ERK signaling in platelets. Vascul. Pharmacol. 63, 182-92.

Lee, M.Y., Liu, Y.W., Chen, M.H., Wu, J.Y., Ho, H.Y., Wang, Q.F., Chuang, J.J., 2013. Indirubin-3-monooxime promotes autophagic and apoptotic death in human acute lymphoblastic leukemia cells and K562 human chronic myelogenous leukemia cells. Oncol. Rep. 29, 2072-78.

Lee, J.W., Moon, M.J., Min, H.Y., Chung, H.J., Park, E.J., Park, H.J., Hong, J.Y., et al., 2005. Induction of apoptosis by a novel indirubin-5-nitro-3'-monooxime, a CDK inhibitor, in human lung cancer cells. Bioorg. Med. Chem. Lett. 15, 3948-52.

Liao, X.M., and Leung, K.N., 2013. Indirubin-3'-oxime induces mitochondrial dysfunction and triggers growth inhibition and cell cycle arrest in human neuroblastoma cells. Oncol. Rep. 29, 371-9.

Liu, K.P., Luo, F., Xie, S.M., Tang, L.J., Chen, M.X., Wu, X.F., et al., 2012. Glycogen synthase kinase 3β inhibitor (2'Z,3'E)-6-bromo-indirubin- 3'-oxime enhances drug resistance to 5-fluorouracil chemotherapy in colon cancer cells. Clin. J. Cancer Res. 24, 116-23.

Liu, J.J., Lin, X.J., Yang, X.J., Zhou, L., He, S., Zhuang, S., Yang, J., 2014. A novel AP-1/miR-101 regulatory feedback loop and its implication in the migration and invasion of hepatoma cells. Nucleic Acids Res. 42, 12041-51.

Li, X., Liang, Q., Liu, W., Zhang, N., Xu, L., Zhang, X., Zhang, J., et al., 2016. Ras association domain family member 10 suppresses gastric cancer growth by cooperating with GSTP1 to regulate JNK/c-Jun/AP-1 pathway. Oncogene 35, 2453-64.

Lucas, D.M., Still, P.C., Pérez, L.B., Grever, M.R., Kinghorn, A.D., 2011. Potential of plant-derived natural products in the treatment of leukemia and lymphoma. Curr. Drug Targets 11,

812-22.

Löffek, S., Schilling, O., Franzke, C.W., 2011. Biological role of matrix metalloproteinases: a critical balance. Eur. Respir. J. 38, 191-208.

Lo, W.Y., and Chang, N.W., 2013. An indirubin derivative, indirubin-3'-monoxime suppresses oral cancer tumorigenesis through the downregulation of surviving. PLoS One 8, e70198.

Lukens, J.R., and Kanneganti, T.D., 2014. Beyond canonical inflammasomes: emerging pathways in IL-1-mediated autoinflammatory disease. Semin. Immunopathol. 36, 595-609.

Lv, H., Ren, H., Wang, L., Chen, W., Ci, X., 2015. Lico A enhances Nrf2-mediated defense mechanisms against t-BHP-induced oxidative stress and cell death via Akt and ERK activation in RAW 264.7 cells. Oxid. Med. Cell Longev. 2015, 709845.

Ma., 2013. Role of Nrf2 in Oxidative Stress and Toxicity. Annu. Rev. Pharmacol. Toxicol. 53, 401-26.

Maltese, W.A., and Overmeyer, J.H., 2014. Nonapoptotic cell death associated with vacuolization of macropinosome and endosome compartments. Am. J. Pathol. 184, 1630-42.

Masgras, I., Carrera, S., de Verdier, P.J., Brennan, P., Majid, A., Makhtar, W., Tulchinsky, E., Jones, G.D.D., et al., 2012. Reactive oxygen species and mitochondrial sensitivity to oxidative stress determine induction of cancer cell death. J. Biol. Chem. 287, 9845-54.

Meares, G.P., Hughes, K.J., Naatz, A., Papa, F.R., Urano, F., Hansen, P.A., Benveniste, E.N., et al., 2011. IRE1-dependent activation of AMPK in response to nitric oxide. Mol. Cell Biol. 31, 4286-97.

Merchant, A.A., Singh, A., Matsui, W., Biswal, S., 2011. The redox-sensitive transcription factor Nrf2 regulates murine hematopoietic stem cell survival independently of ROS levels. Blood 118, 6572-9.

Minn, A.J., Kang, Y., Serganova, I., Gupta, G.P., Giri, D.D., Doubrovin, M., et al., 2004. Distinct organ-specific metastatic potential of individual breast cancer cells and primary tumors. J. Clin. Inves. 115, 44-55.

Murphy, S.H., Suzuki, K., Downes, M., Welch, G.L., Jesus, P.D., Miraglia, L.J., et al., 2011.Tumor suppressor protein (p)53, is a regulator of NF-κB repression by the glucocorticoid receptor. Proc. Natl. Acad. Sci. USA 108, 17117-22.

Nahrevanian, H., 2009. Involvement of nitric oxide and its up/down stream molecules in the immunity against parasitic infections. Braz. J. Infect. Dis. 13, 440-8.

Nam, S., Wen, W., Schroeder, A., Hermann, A., Yu, H., Cheng, X., Merz, K.H., Eisenbrand, G., Li, H., Yuan, Y.C., Jove, R., 2013. Dual inhibition of Janus and Src family kinases by novel indirubin derivative blocks constitutively-activated Stat3 signaling associated with apoptosis of human pancreatic cancer cells. Mol. Oncol. 7, 369-78.

Nicolaou, K.A., Liapis, V., Evdokiou, A., Constantinou, C., Magiatis, P., Skaltsounis, A.L., Koumas, L., et al., 2012. Induction of discrete apoptotic pathways by bromo-substituted indirubin deravatives in invasive breast cancer cells. Biochem. Biophys. Res. Commun. 425, 76-82.

Orrenius, S., Nicotera, P., Zhivotovsky, B., 2011. Cell death mechanisms and their implications in toxicology. Toxicol. Sci. 119, 3-19.

Parker, N.H., Donninger, H., Birrer, M.J., Leaner, V.D., 2013. p21-activated kinase 3 (PAK3) is an AP-1 regulated gene contributing to actin organisation and migration of transformed fibroblasts. PLoS One 8, e66892.

Park, C.M., Cho, C.W., Song, Y.S., 2014. TOP 1 and 2, polysaccharides from *Taraxacum officinale*, inhibit NFκB-mediated inflammation and accelerate Nrf2-induced antioxidative potential through the modulation of PI3K-Akt signaling pathway in RAW 264.7 cells. Food Chem. Toxicol. 66, 56-64.

Park, S.Y., Jin, M.L., Kim, Y.H., Lee, S.J., Park, G., 2014. Sanguinarine inhibits invasiveness and the MMP-9 and COX-2 expression in TPA-induced breast cancer cells by inducing HO-1 expression. Oncol. Rep. 31, 497-504.

Patergnani, S., Suski, J.M., Agnoletto, C., Bononi, A., Bonora, M., De Marchi, E., Giorgi, C., et al., 2011. Calcium signaling around mitochondria associated membranes (MAMs). Cell Commun. Signal 9, 19.

Paulkumar, K., Arunachalam, R., Kameswaran, R., Ramanibai, R., Annadurai, G., 2010. Anti-cancer effect of indirubin-3'-monoxime for human laryngeal carcinoma. Int. J. Cancer Res. 6, 27-34.

Paul, M.K, Bisht, B., Darmawan, D.O., Chiou, R., Ha, V.L., Wallace, W.D., et al., 2014. Dynamic changes in intracellular ROS levels regulate airway basal stem cell homeostasis through Nrf2-dependent Notch signaling. Cell Stem Cell 15, 199-214.

Perabo, F.G.E., Frössler, C., Landwehrs, G., Schmidt, D.H., Rücker, A.V., Wirger, A., Müller,

S.C., 2006. Indirubin-3′-monoxime, a CDK inhibitor induces growth inhibition and apoptosis-independent up-regulation of survivin in transitional cell cancer. Anticancer Res. 26, 2129-35.

Perabo, F.G., Landwehrs, G., Frössler, C., Schmidt, D.H., Müeller., S.C., 2011. Antiproliferative and apoptosis inducing effects of indirubin-3'-monoxime in renal cell cancer cells. Urol. Oncol. 29, 815-20.

Piccolo, M.T., and Crispi, S., 2012. The dual role played by p21 may influence the apoptotic or anti-apoptotic fate in cancer. J. Can. Res. Updates 1, 189-202.

Preuss, M.B., Booveleth, N.B., Gall, S., Rehmann, K., Schenke, S., Mann, K., 2015. Induction of atypical cell death in thyroid carcinoma cells by the indirubin derivative 7-bromoindirubin-3′-oxime (7BIO). Cancer Cell Int. 15, 97.

Qin, Z., Voorhees, J., Fisher, G.J., Quan, T., 2014. Age-associated reduction of cellular spreading/mechanical force up-regulates matrix metalloproteinase-1 expression and collagen fibril fragmentation via c-Jun/AP-1 in human dermal fibroblasts. Aging Cell 13, 1028-37.

Ravichandran, K., Pal, A., Ravichandran, R., 2010. Effect of indirubin-3-monoxime against lung cancer as evaluated by histological and transmission electron microscopic studies. Microsc. Res. Tech. 73, 1053-8.

Rivest, P., Renaud, M., Sanderson, J.T., 2011. Proliferative and androgenic effects of indirubin derivatives in LNCaP human prostate cancer cells at sub-apoptotic concentrations. Chem. Biol. Interact. 189, 177-85.

Rojpibulstit, P., Kittisenachai, S., Puthong, S., Manochantr, S., Gamnarai, P., Jitrapakdee, S., Roytrakul, S., 2014. Hep88 mAb-initiated paraptosis-like PCD pathway in hepatocellular

carcinoma cell line through the binding of mortalin (HSPA9) and alpha-enolase. Cancer Cell Int. 14, 69.

Romagnoli, A., Aguiari, P., De Stefani, D., Leo, S., Marchi, S., Rimessi, A., Zecchini, E., et al., 2007. Endoplasmic reticulum/mitochondria calcium cross talk. Novartis Found Symp. 287, 122-31.

Sahu, U., Sidhar, H., Ghate, P.S., Advirao, G.M., Raghavan, S., Giri, R.K., 2013. A Novel Anticancer agent, 8-methoxypyrimido[4′,5′:4,5]thieno(2,3-b) quinoline-4(3H)-one induces Neuro 2A neuroblastoma cell death through p53-dependent, caspase-dependent and -independent apoptotic pathways. PLoS One 8, e66430.

Saldarriaga, O.A., Travi, B.L., Choudhury, G.G., Melby, P.C., 2012. Identification of hamster inducible nitric oxide synthase (*iNOS*) promoter sequences that influence basal and inducible *iNOS* expression. J. Leukoc. Biol. 92, 205-18.

Sano, R., and Reed, J.C., 2013. ER stress-induced cell death mechanisms. Biochim. Biophys. Acta 12, 3460-70.

Satoh, H., Moriguchi, T., Takai, J., Ebina, M., Yamamoto, M., 2013. Nrf2 prevents initiation but accelerates progression through theKras signaling pathway during lung carcinogenesis. Cancer Res. 73, 4158.

Schieber, M., and Chandel, N.S., 2014. ROS function in redox signaling and oxidative stress. Curr. Biol. 24, R453-62.

Sekhon, B.S., 2010. Matrix metalloproteinases-an overview. Res. Rep. Biol. 1, 1-20.

Sharma, P.S., Sharma, R., Tyagi, T., 2011.VEGF/VEGFR pathway inhibitors as anti-angiogenic agents present and future. Curr. Cancer Drug Targets 11, 624-53.

Shaulian, E., and Karin, M., 2001. AP-1 in cell proliferation and survival. Oncogene 20, 2390-400.

Shin, J.W., Ohnishi, K., Murakami, A., Lee, J.S., Kundu, J.K., Na, H.K., Ohigashi, H., et al., 2011. Zerumbone induces heme oxygenase-1 expression in mouse skin and cultured murine epidermal cells through activation of Nrf2. Cancer Prev. Res. 4, 860-70.

Shi, R.Z., Hu, X.L., Peng, H.W., 2012. The cytotoxicity of indirubin derivative PHII-7 against human breast cancer MCF-7 cells and its mechanisms. Zhongguo Zhong Xi Yi Jie He Za Zhi 32, 1521-5.

Shi, R., Li, W., Zhang, Y., Peng, H., Xie, Y., Fan, D., Liu, X., Xiong, D., 2011. A novel indirubin derivative PHII-7 potentiates adriamycin cytotoxicity via inhibiting P-glycoprotein expression in human breast cancer MCF-7/ADR cells. Eur. J. Pharmacol. 669, 38-44.

Shi, J., Shen, H.M., 2008. Critical role of Bid and Bax in indirubin-3'-monoxime-induced apoptosis in human cancer cells. Biochem. Pharmacol. 75, 1729-42.

Snyder, C.M., Shroff, E.H., Liu, J., Chandel., N.S., 2009. Nitric Oxide Induces Cell Death by Regulating Anti-Apoptotic BCL-2 Family Members. PLoS One 4, e7059.

Sollberger, G., Strittmatter, G.E., Garstkiewicz, M., Sand, J., Beer, H.D., 2014. Caspase-1: The inflammasome and beyond. J. Innate Immun. 20, 115-25.

Suzanne, M., and Steller., H., 2013. Shaping organisms with apoptosis. Cell Death Differ. 20,

669-75.

Tasheva, S.M., Obis, E., Tamarit, J., Ros, J., 2013. Apoptotic cell death and altered calcium homeostasis caused by frataxin depletion in dorsal root ganglia neurons can be prevented by BH4 domain of Bcl-XL protein. Hum. Mol. Genet. 23, 1829-41.

Thakur, V.S., Amin, A.R.M.R., Paul, R.K., Gupta, K., Hastak, K., Agarwal, M.K., et al., 2010. p53-Dependent p21-mediated growth arrest pre-empts and protects HCT116 cells from PUMA-mediated apoptosis induced by EGCG. Cancer Lett. 296, 225-32.

Thomas, M.P., Liu, X., Whangbo, J., McCrossan, G., Sanborn, K.B., Basar, E., Walch, M., Lieberman, J., 2015. Apoptosis triggers specific, rapid, and global mRNA decay with 3′ uridylated intermediates degraded by DIS3L2. Cell Rep. 11, 1079-89.

Udumula, M. P., Medapi, B., Dhar, I., Bhat, A., Desai, K., Sriram, D., Dhar, A., 2016. The small molecule indirubin-3'-oxime inhibits protein kinase R: Antiapoptotic and antioxidant effect in rat cardiac myocytes. Pharmacology 97, 25-30.

Um, H.C., Jang, J.H., Kim, D.H., Lee, C., Surh, Y.J., 2011. Nitric oxide activates Nrf2 through S-nitrosylation of Keap1 in PC12 cells. Nitric Oxide 25, 161-8.

Vanini, F., Kashfi, K., Nath, N., 2015. The dual role of Inos in cancer. Redox Biol. 6, 334-43.

Varela, A.T., Gomas, A.P., Simões, A.M., Teodoro, J.S., Duarte, F.V., 2008. Indirubin-3′-oxime impairs mitochondrial oxidative phosphorylation and prevents mitochondrial permeability transition induction. Toxicol. Appl. Pharmacol. 233, 179-85.

Voccoli, V., Tonazzini, I., Signore, G., Caleo, M., Cecchini, M., 2014. Role of extracellular calcium and mitochondrial oxygen species in psychosine-induced oligodendrocyte cell death.

Cell Death Dis. 5, e1529.

Webster, G.A., and Perkins, N.D., 1999. Transcriptional cross talk between NF-κB and p53. Mol. Cell Biol. 19, 3485-95.

Wang, W.B., Feng, L.X., Yue, Q.X., Wu, W.Y., Guan, S.H., Jiang, B.H., Yang, M., Liu, X., Guo, D.A., 2012. Paraptosis accompanied by autophagy and apoptosis was induced by celastrol, a natural compound with influence on proteasome, ER stress and Hsp90. J. Cell Physiol. 227, 2196-206.

Wang, G.W., Lv, C., Shi, Z.R., Zeng, R.T., Dong, X.Y., Zhang, W.D., Liu, R.H., Shan, L., et al., 2014. Abieslactone induces cell cycle arrest and apoptosis in human hepatocellular carcinomas through the mitochondrial pathway and the generation of reactive oxygen species. PLoS One 9, e115151.

Wang, Y., Li, X., Wang, L., Ding, P., Zhang, Y., Han, W., Ma, D., et al., 2003. An alternative form of paraptosis-like cell death, triggered by TAJ/TROY and enhanced by PDCD5 overexpression. J. Cell Sci. 117, 1525-32.

Wang, Y., Xu, K., Zhang, H., Zhao, J., Zhu, X., Wang, Y., Wu, R., 2014. Retinal ganglion cell death is triggered by paraptosis via reactive oxygen species production: A brief literature review presenting a novel hypothesis in glaucoma pathology. Mol. Med. Rep. 10, 1179-83.

Wang, Y., Zhu, X., Yang, Z., Zhao, X., 2013. Honokiol induces caspase-independent paraptosis via reactive oxygen species production that is accompanied by apoptosis in leukemia cells. Biochem. Biophys. Res. Commun. 430, 876-82.

Wei, T., Kang, Q., Ma, B., Gao, S., Li, X., Liu, Y., 2014. Activation of autophagy and paraptosis

in retinal ganglion cells after retinal ischemia and reperfusion injury in rats. Exp. Ther. Med. 9, 476-82.

Wei, Y.F., Su, J., Deng, Z.L., Zhu, C., Yuan, L., Lu, Z.J., Zhu, Q.Y., 2015. Indirubin inhibits the proliferation of prostate cancer PC-3 cells. Zhonghua Nan Ke Xue 21, 788-91.

Wei, T., Kang, Q., Ma, B., Gao, S., Li, X., Liu, Y., 2015. Activation of autophagy and paraptosis in retinal ganglion cells after retinal ischemia and reperfusion injury in rats. Exp. Ther. Med. 9, 476-82.

Williams, S.P., Nowicki, M.O., Liu, F., Press, R., Godlewski, J., Rasoul, M.A., Kaur, B., et al., 2011. Indirubins decrease glioma invasion by blocking migratory phenotypes in both the tumor and stromal endothelial cell compartments. Cancer Res. 71, 5374-80.

Xia, Y., Lian, S., Khoi, P.N., Yoon, H.J., Joo, Y.E., Chay, K.O., Kim, K.K., 2015. Chrysin inhibits tumor promoter-induced MMP-9 expression by blocking AP-1 via suppression of ERK and JNK pathways in gastric cancer cells. PLoS One 10, e0124007.

Yoon, M.J., Kang, Y.J., Lee, J.A., Kim, I.Y., Kim, M.A., Lee, Y.S., Park, J.H., et al., 2014. Stronger proteasomal inhibition and higher CHOP induction are responsible for more effective induction of paraptosis by dimethoxycurcumin than curcumin. Cell Death Dis. 5, e1112.

Yoon, M.J., Lee, A.R., Jeong, S.A., Kim, Y.S., Kim, J.Y., Kwon, Y.J., Choi, K.S., 2014. Release of Ca2+ from the endoplasmic reticulum and its subsequent influx into mitochondria trigger celastrol-induced paraptosis in cancer cells. Oncotarget 5, 6816-31.

Yoon, M.J., Kang, Y.J., Lee, J.A., Kim, I.Y., Kim, M.A., Lee, Y.S., Park, J.H., et al., 2014. Stronger proteasomal inhibition and higher CHOP induction are responsible for more effective

induction of paraptosis by dimethoxycurcumin than curcumin. Cell Death Dis. 5, e1112.

Yoon, M.J., Kim, E.H., Lim, J.H., Kwon, T.K., Choi, K.S., 2010. Superoxide anion and proteasomal dysfunction contribute to curcumin-induced paraptosis of malignant breast cancer cells. Free Radic. Biol. Med. 48, 713-26.

Yoon, J.H., Kim, S.A., Kim, J.I., Park, J.H., Ahn, S.G., Yoon, J.H., 2010. Inhibition of invasion and migration of salivary gland adenocarcimona cells by 5'-nitro-indirubinoxime (5'-NIO). Head Neck 32, 619-25.

Yoon, M.J., Kim, E.H., Kwon, T.K., Park, S.A., Choi, K.S., 2012. Simultaneous mitochondrial Ca^{2+} overload and proteasomal inhibition are responsible for the induction of paraptosis in malignant breast cancer cells. Cancer Lett. 24, 197-209.

Yoon, M.J., Kim, E.H., Lim, J.H., Kwon, T.K., Choi, K.S., 2010. Superoxide anion and proteasomal dysfunction contribute to curcumin-induced paraptosis of malignant breast cancer cells. Free Radic. Biol. Med. 48, 713-26.

Zhang, K., Chen, D., Jiao, X., Zhang, S., Liu, X., Cao, J., Wu, L., Wang, D., 2011. Slug enhances invasion ability of pancreatic cancer cells through upregulation of matrix metalloproteinase-9 and actin cytoskeleton remodeling. Lab. Invest. 91, 426-38.

Yoon, M.J., Kang, Y.J., Lee, J.A., Kim, I.Y., Kim, M.A., Lee, Y.S., Park, J.H., et al., 2014. Stronger proteasomal inhibition and higher CHOP induction are responsible for more effective induction of paraptosis by dimethoxycurcumin than curcumin. Cell Death Dis. 5, e1112.

Zhang, A., Ning, B., Sun, N., Wei, J., Ju, X., 2015. Indirubin increases CD4^{+} CD25^{+} Foxp3^{+} regulatory T cells to prevent immune thrombocytopenia in mice. PLoS One 10, e0142634.

Zhang, Y., Liu, G., Dull, R.O., Schwartz, D.E., Hu, G., 2014. Autophagy in pulmonary macrophages mediates lung inflammatory injury via NLRP3 inflammasome activation during mechanical ventilation. Am. J. Physiol. Lung Cell Mol. Physiol. 307, L173-85.

Zhang, C., Su, Z.Y., Khor, T.O., Shu, L., Kong, A.N.T., 2013. Sulforaphane enhances Nrf2 expression in prostate cancer TRAMP C1cells through epigenetic regulation. Biochem. Pharmacol. 85, 1398-404.

Zhang, YY., Du, Z., Zhuang, Z., Wang, Y., Wang, F., Liu, S., Wang, H., et al., 2015. E804 induces growth arrest, differentiation and apoptosis of glioblastoma cells by blocking Stat3 signaling. J. Neurooncol. 125, 265-75.

Zhang, L., Wang, K., Lei, Y., Li, Q., Nice, E.C., Huang, C. 2015. Redox signaling: Potential arbitrator of autophagy an apoptosis in therapeutic response. Free Radic. Biol. Med. 89, 452-65.

Zhou, Y., Ye, L., Zheng, B., Zhu, S., Shi, H., Zhang, H., Wang, Z., Wei, X., et al., 2016. Phenylbutyrate prevents disruption of blood-spinal cord barrier by inhibiting endoplasmic reticulum stress after spinal cord injury. Am. J. Transl. Res. 8, 1864-75.

Zhu, X., Jiao, Q., Zhang, C., Zuo, X., Xiao, X., Liang, Y., Nan, J., 2012. Electropolymerization of graphene and 5-[o-(4-bromine amyloxy) phenyl]-10,15,20-triphenylporphrin (o-BrPETPP) composite film electrode for the electrocatalytic oxidation of indirubin. J. Electroanl. Chem. 681, 133-8.

Zong, W.X., and Thompson, C.B., 2006. Necrotic death as a cell fate. Genes Dev. 20, 1-45.

Zou, Y., Wang, R., Guo, H., Dong, M., 2015. Phytoestrogen β-ecdysterone protects PC12 cells

against MPP[+]-induced neurotoxicity in vitro: Involvement of PI3K-Nrf2-regulated pathway. Toxicol. Sci. 147, 28-38.

Acknowledgments

Creating a PhD thesis is not an individual experience; rather it takes place in a social context and includes several persons, whom I would like to thank sincerely. The most important acknowledgment of gratitude I wish to express my advisor Professor Gi-Young Kim, you have been a tremendous mentor for me. I would like to thank you for encouraging my research and for allowing me to grow as a research scientist. It has been a greatly enriching experience to me to work under his authoritative guidance. Your advice on both research as well as on my career has been priceless.

I would like to extend my gratitude to all of the staff members in department of Marine Life Sciences in Jeju National University, Prof. Choon-bok song, Prof. Moon-Soo Heo, Prof. Jehee Lee, Prof. Kyeong-Jun Lee, Prof. Kwang-Sik Choi, Prof. You-Jin Jeon, Prof, In-Kyu Yeo, Prof. Joon-Bom Lee, Prof. Young Dong Lee, Prof. Jung Suk-Geun, Prof. Seungheon Lee, Prof. Sang-Rul Park for their support towards the successful completion of my studies in Jeju National University. For me, it is a proud privilege and a matter of honor to offer my overwhelming gratitude to Professor Moon-Soo, Professor Seungheon Lee, Professor Sang-Rul Park and Kil Nam Kim, for being the members of supervising committee in my thesis. Many thanks also go to my lab members Chang-Hee Kang, Sang-Hyuck Kang, Hee-Ju Kim for being enthusiastic with my research. Words cannot express how grateful I am to inspiring parents, my mother G.D.L. Premakanthi, father M. Pemachandra and my soul mates, dear sisters Dilini Dilhara and Achini Dilthara and to my beloved grandparents for all of the sacrifices that you've made on my behalf. At the end I would like express appreciation to my beloved husband Dr. R.G.P.T. Jayasooriya who spent every second with and was always my support in the moments when there was no one to answer my queries. I also many thanks to

my loving son Sanru Methsith for bearing all of sorrows and seclusion because of my departure. I also express my gratitude to the Sri Lankans and all other colleagues who support me to success my work. All of your continued support and urging after moving to JNU is deeply appreciate.